Carl Böck, BSc.

ECG Signal Analysis based on the Wavelet Transform

MASTER'S THESIS

to achieve the university degree of

Diplom-Ingenieur

Master's degree programme: Telematics

submitted to

Graz University of Technology

Supervisor

Univ.-Prof. DI Dr. Gernot Kubin

Signal Processing and Speech Communication Laboratory

Univ.-Prof. DI Dr. Mario Huemer
Institute of Signal Processing - JKU Linz

Graz, December 2015

AFFIDAVIT

I declare that I have authored this thesis independently, that I have not used other than the declared sources/resources, and that I have explicitly indicated all material which has been quoted either literally or by content from the sources used. The text document uploaded to TUGRAZonline is identical to the present master's thesis dissertation.

Graz, _____   _____
                    Date   Signature

Abstract

MOTIVATION: The electrocardiogram (ECG) is a well-established and easy to obtain physiological signal of remarkable diagnostic power. It bears a wide spectrum of information about a patient's condition thereby accessing the normal as well as the pathophysiological individual state. Within the last decades, clinical studies revealed that even the subtle changes of the ECG's morphology carry important information for ECG analysis and disease detection.

OBJECTIVE: Within this work the wavelet transform (WT) is investigated regarding its suitability to analyze the ECG, like it is proposed as a promising approach in current medical research. Special focus is placed on the detection of minimal changes in the ECG.

METHODS: The theory behind the ECG and the WT was briefly reviewed and potential applications for using the WT to analyze the ECG were identified and summarized. For verifying new developed evaluation methods, it is inevitable to start with well-known test signals. For that reason a graphical ECG generator capable of producing individually adapted heart cycle morphologies was developed within this thesis. Additionally, for performing ECG beat segmentation and subsequently extracting useful clinical parameters, an algorithm based on the WT was implemented. This algorithm was evaluated on artificial data, provided by the graphical ECG generator, as well as on real patient data. In the latter case the automatically extracted ECG parameters were compared to those extracted manually by experts.

RESULTS: The results showed that the algorithm is able to detect subtle changes in the ECG for synthetic data. Evaluation on real patient data illustrated that the chosen method is reliable and well suited for the extraction of meaningful clinical parameters.

CONCLUSION: A first version of a framework for ECG analysis, mainly consisting of an artificial beat generator and of a beat segmentation algorithm, has been developed. This thesis is seen as a foundation for future research in the fields of ECG analysis within a newly built up cooperation of the Johannes Kepler University and the general hospital in Linz.

KEYWORDS: Wavelet transform, ECG beat generator, ECG beat segmentation, ECG signal analysis

Kurzfassung

MOTIVATION: Das Elektrokardiogramm (EKG) ist ein bewährtes und einfach messbares Biosignal mit enormer diagnostischer Aussagekraft. Es beinhaltet ein breites Spektrum an Information über den Zustand eines Patienten sowohl in physiologischer als auch in pathologischer Hinsicht. Innerhalb der letzten Jahrzehnte wurde durch klinische Studien gezeigt, dass sogar geringfügige Änderungen im EKG sehr hilfreich für die Analyse und Interpretation des EKGs sein können.

ZIEL: Diese Arbeit befasst sich mit der Wavelet-Transformation (WT) in Bezug auf deren Eignung zur EKG Analyse. Spezieller Fokus liegt dabei auf der Detektion von geringfügigen Änderungen im EKG.

METHODEN: Die Theorie hinter dem Biosignal EKG und der WT wurde aufgearbeitet und potentielle Anwendungsgebiete der WT im Bereich der EKG Signalanalyse wurden identifiziert und zusammengefasst. Zur Bewertung von neu entwickelten EKG Analysemethoden, ist es von großem Vorteil mit genau definierbaren Testsignalen zu arbeiten. Daher wurde im Zuge dieser Arbeit ein graphischer EKG Generator implementiert. Dieser erlaubt die Generierung von individuell modellierten und genau parametrisierbaren Herzschlägen. Zusätzlich wurde ein auf der WT basierender Algorithmus zur automatisierten Segmentierung von Herzschlägen implementiert. Daraus können klinisch wertvolle Parameter abgeleitet werden. Der Algorithmus wurde einerseits mithilfe künstlich generierter Herzschläge und andererseits mit realen Patientendaten getestet. Für Letztere wurden die automatisiert extrahierten klinischen Parameter mit Expertenmarkern, welche manuell gesetzt wurden, verglichen.

ERGEBNISSE: Anhand von synthetisch generierter Herzschläge konnte gezeigt werden, dass sich der Algorithmus zur Detektion von geringfügigen Änderungen im EKG eignet. Die Evaluierung mithilfe realer Patientendaten belegte, dass der Algorithmus eine zuverlässige Segmentierung des EKGs im klinischen Alltag ermöglicht.

SCHLUSSFOLGERUNG: Ein erstes Grundgerüst, bestehend aus einem EKG Generator und dem Algorithmus zur automatisierten Segmentierung von Herzschlägen wurde bereitgestellt. Der Autor sieht diese Arbeit als Fundament für zukünftige Forschung im Bereich der EKG Signalanalyse innerhalb einer neu entstandenen Kooperation zwischen der Johannes Kepler Universität und dem Allgemeinen Krankenhaus der Stadt Linz.

SCHLAGWÖRTER: Wavelet-Transformation, EKG Generator, EKG Segmentierung, EKG Signalanalyse

Contents

Contents

1. Introduction

1.1. Motivation

Demographic development shows a steady increase of elderly people in Austria. In 2040 almost every sixth person will be 75 years or older [1]. This trend correlates with the prevalence of age-related diseases, as for instance cardiovascular diseases. It is more likely for patients belonging to this age group to need intensive care. However, commonly used diagnostic tools are limited regarding extraction, evaluation and visualization of important information hidden in physiological signals.

In spring 2014 two departments of Linz General Hospital (AKh Linz GmbH) entered into cooperation with the Institute of Signal Processing belonging to Johannes Kepler University. In this way a close collaboration between the Department of Anesthesia and Operative Care, the Department for Biomedical Engineering and the Institute of Signal Processing has evolved. This interdisciplinary partnership combines the strengths of signal processing with medical expert knowledge.

The development of innovative methods for the analysis and diagnosis of cardiovascular diseases of intensive care patients is a main goal of the cooperation, resulting in an optimized "best practice" in health care especially for the aging population.

As a first step, clinically useful parameters of the Electrocardiogram (ECG), like amplitudes or time intervals between single waves, should be extracted (Figure 1.1). Many medical diagnoses are based on the evaluation of these so called characteristic points. For instance, two important time intervals are the PR and the QT interval, which have a significant influence on a patient's state of health [2]. However, minimal alternations of amplitudes and intervals between waves over time are hard to detect by simple visual inspection. Additionally, interval measurements carried out by specialized
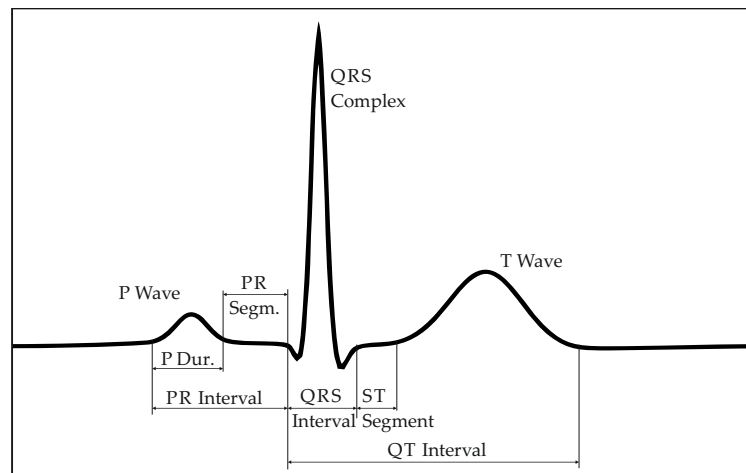
Figure 1.1.: Standard segmentation of the ECG.

ECG analysts are extremely time-consuming and error-prone due to individual interpretations of the experts. Unfortunately ECG monitors of the AKh Linz GmbH do not support an automated extraction of ECG characteristic points. As a result, researcher of AKh Linz GmbH need a reliable method for performing this task.

According to literature (e.g. [3,4]), the wavelet transform (WT) is a very promising approach for detecting ECG characteristic points. Through its ability to decompose signals into well localized basis functions, the WT is suited to distinguish ECG waves from noise [3]. Hence, it is worth investigating this technique for the extraction of ECG time intervals and amplitudes. A possible scenario for automatically evaluating detected characteristic points is shown in Figure 1.2. The recorded ECG of Patient X should be investigated before and after a certain event, as for instance a medication. For that reason mean and standard deviation of the extracted characteristic points are compared in order to check if one or more of these parameters changed significantly. In a next step one could analyze alternations and localized abnormalities in the morphology[1] of single ECG segments, like the QRS complex, the P wave or the ST segment.

Furthermore, since it is a main goal of this cooperation to investigate the suitability of the WT for a further analysis of the ECG, e.g. for extracting

---

[1]Describes the shape and structure of the ECG.
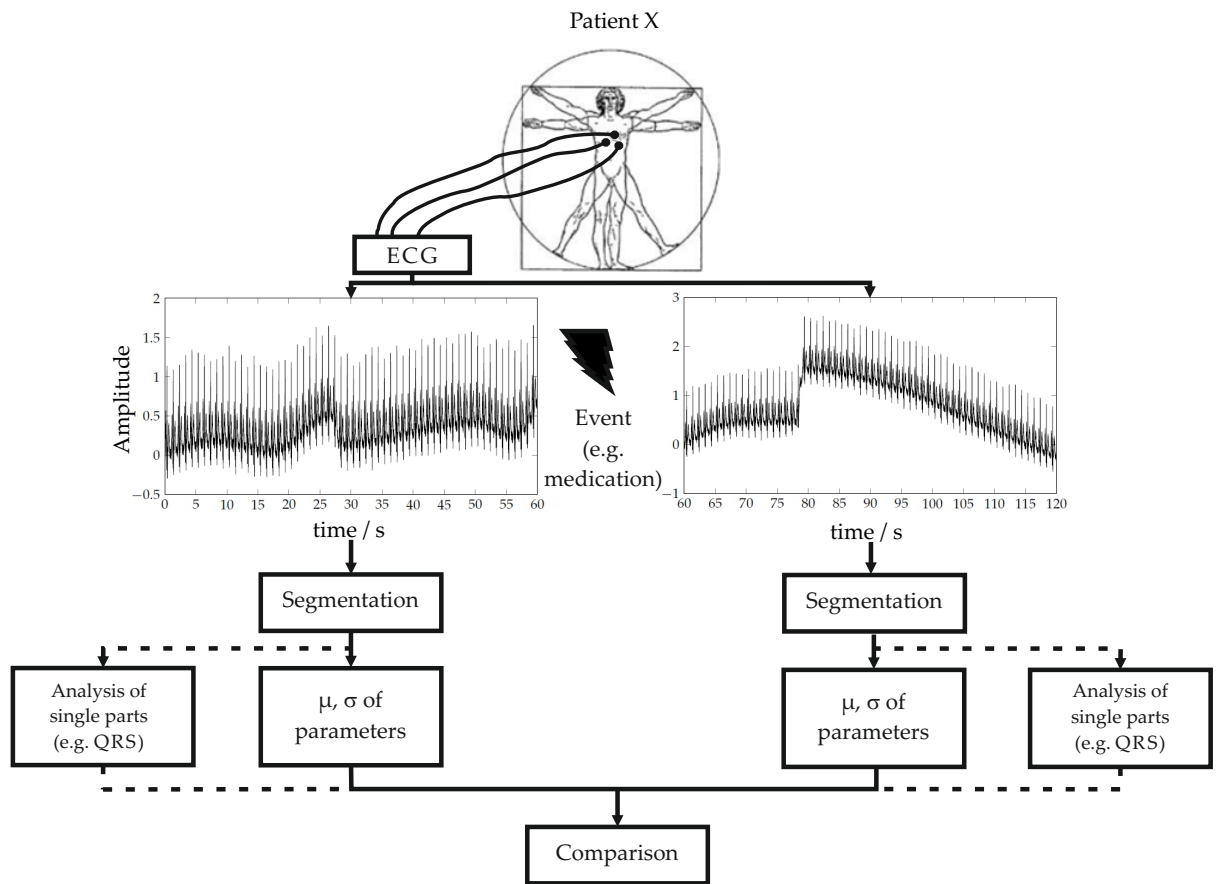
Figure 1.2.: Automatic evaluation of ECG characteristic points.

hidden information, the thesis includes a compact and intuitive description of the WT theory. On the one hand, this is motivated by giving physicians an idea about the principles and power of the WT and on the other hand by providing a solid foundation for future project staff in order to minimize the period of familiarization.

1.2. Objectives

- Preparation of the theory behind the WT.
- Overview of techniques based on the WT used for analyzing the ECG.
- Implementation of an algorithm for automated extraction of ECG characteristic points.
- Development of a graphical ECG generator to verify the implemented algorithm.
- Correct functionality of the algorithm for ECG beat segmentation is proved for artificially generated beats and for real data provided by Physionet[2] [5,6] and by AKh Linz GmbH in the course of the project "Herzfrequenzvariabilität und EKG Morphologie bei Intensivpatienten".

1.3. Outline and Contributions

This thesis deals with the development of a system for automatic extraction of meaningful clinical features from the ECG using the WT.
The work consists of 5 chapters:

Chapter 2 provides the theoretical background of the ECG and the WT. Section 2.1 focuses on the emergence of a cardiac cycle. By the end of this section it should be clear why the single waves of a heart cycle occur and what they stand for. Section 2.2 provides the theoretical background of the continuous as well as the discrete WT.
In **Chapter 3** different ECG analyzing techniques are presented. Furthermore, this chapter deals with the methods chosen for achieving the objectives defined in Section 1.2. Starting with the description of an ECG beat generator for creating meaningful test sets it continues with the method for extracting characteristic clinical features. Moreover data generation and techniques for evaluation of the implemented algorithms are discussed.
Chapter 4 presents the results obtained for automatic ECG feature extraction.
Chapter 5 concludes this thesis by discussing the results and identifying future research topics.

---

[2]http://physionet.org/physiobank/database/qtdb/

2. Theoretical Background

2.1. Electrocardiogram

This section gives an overview of the heart's electrophysiology, the generation of a single beat, of how the ECG is acquired, and of the most important parameters for ECG analysis.

2.1.1. The Electrophysiology of the Heart

The heart is basically a muscle divided into four chambers, the left and the right atria as well as the left and the right ventricles (Figure 2.1(a)). The right atrium collects used blood from the body and forwards it into the right ventricle, which pumps it into the lung. Similarly the left atrium receives blood from the lung and pumps it into the left ventricle, which consequently supplies the body with oxygen-rich blood.

This process can be tracked by the so called ECG which measures the electrical activity of the heart over time. The ECG signal is an electrical signal which is acquired at the body surface and reflects the total, time dependent activity of the heart. The transmission of potential changes throughout the heart's conduction system, and the subsequent contraction of the working myocardium can be measured between skin electrodes at the body surface in voltage over the time representing the well established ECG biosignal. [7,8]

Each activation of a heart muscle cell is caused by a distinct change of its initial electrical potential through a membrane bound ion in- and outward flux (depolarization). Therefore each activation of a single muscle fiber causes a potential change of the involved cells throughout the myocardium.

The activation and its depolarization is followed by the successive recovery of the initial ion concentration state between intracellular and extracellular space (repolarization).
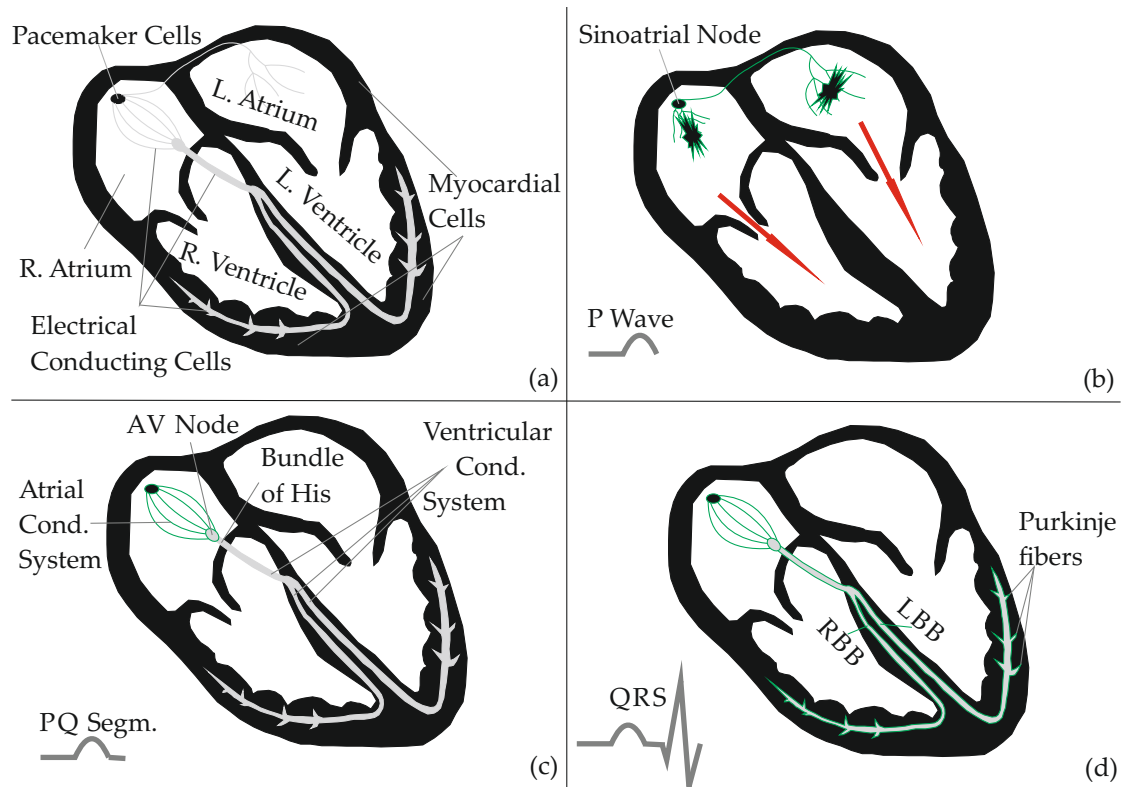
Figure 2.1.: Basic procedures during a heart cycle. (a) Overview of chambers and type of cells. (b) Atrial depolarization (P wave). (c) Origin of the PR segment (Delay due to the AV node). (d) Ventricular depolarization (QRS complex).

Cellular Electrophysiology: As can be seen in Figure 2.1(a) we distinguish between three main type of cardiac cells, pace maker cells, electrical conducting cells and myocardial cells. In their resting state cardiac cells are negatively charged. This means, that the potential inside of a cell is negative with respect to a surrounding fluid [9]. As already mentioned, cells can leave their resting state by a process called depolarization, resulting in a

positive potential. Analogously, repolarization describes the return to their original electrical state.

- **Pace maker cells:** Cells which are able to depolarize spontaneously and hence can initiate a heart cycle.
- **Electrical conducting cells:** These cells can be seen as hard wiring of the heart muscle and are there for conducting current rapidly and efficiently over longer distances. Depolarization is triggered by neighboring cells.
- **Myocardial cells:** Depolarization of myocardial cells leads to contraction of the cells. This means that parts of the heart muscle are contracted leading to a lowered volume within a specific chamber. Due to this, blood is displaced from the according chamber. Hence, contraction and following relaxation of myocardial cells are responsible for the transport of blood.

2.1.2. A Normal Heart Cycle

At a normal heart rate a cardiac cycle usually lasts about $0.8\,\text{s}$ and can be described by 5 consecutive waves, defined as P, Q, R, S and T wave. Sometimes the T wave is followed by a so called U wave. A possible reason for the appearance of an U wave are after-potentials (for further details see [10]). U waves, however, will not be considered explicitly throughout this thesis.

The distance between two consecutive R waves is called RR interval and can be used to determine the heart rate.

P Wave (Atrial Depolarization): Considering a normal heartbeat, the sinoatrial node (Figure 2.1(b)) fires spontaneously and initiates a heart beat. Myocardial cells of both atria depolarize causing atrial contraction. As a result, blood is transported to the ventricles through valves. Atrial depolarization and contraction is visible in the measured ECG, producing the so called P wave, while the spontaneous depolarization of the sinoatrial node cannot be tracked.

The valves separating the atria from the ventricles prevent the atrial myocardial cells from initiating depolarization of ventricular myocardial cells. Due to this fact, depolarization must be triggered somehow else. For that reason the depolarization wave travels from the sinoatrial node via the atrial conducting system, the atrioventricular (AV) node and the bundle of His to the ventricular conducting system (Figure 2.1(c)). The AV node plays a special role in this process by slowing down the depolarization wave and hence delaying the conduction. Due to this, in case of a normal healthy heartbeat, ventricular contraction does not start until atrial contraction is completed and all the blood from the atria is forwarded to the ventricles. This delay is manifested as PR segment in the ECG. [9]

Concluding, the P wave describes the excitation propagation in the atria. Usually it is positive and lasts about 110 ms. The PR interval, representing the atrioventricular conduction, typically lasts from 120 ms to 200 ms. Alternations of the P wave's typical shape as well as deviations of time intervals are significant indicators for pathology. [11]

QRS Complex (Ventricular Depolarization): The electrical conducting system of the ventricles is a little bit more complicated than that one of the atria. After the AV node and the bundle of His the conducting system splits up into the left and the right bundle branches (LBB, RBB), and finally ends up in Purkinje fibers, which are responsible for delivering the current to the myocardium (Figure 2.1(d)). Again, depolarization of myocardial cells lead to contraction of the cells and consecutive to contraction of the whole chambers. This results in displacement of the blood out of the ventricles. Furthermore, the left branch splits up into three fascicles (septal, left posterior and right posterior fascicles). Septal depolarization, for instance, represents the Q wave, which usually appears as small negative deflection in the ECG. Due to the complicated pathway, the QRS complex receives its complex shape. [9]

As a result the QRS complex describes the excitation propagation in the ventricles. Its usual width is about 100 ms. Pathological examples are abnormal broad (≥ 30 ms) or abnormal deep ($> \frac{1}{4} R_{\mathrm{magnitude}}$) Q waves. Also prolonged or deformed QRS complexes indicate abnormal excitation propagation in the ventricles. [11]

T Wave (Repolarization): After depolarization of a myocardial cell, it is not possible to stimulate this cell again for a certain amount of time, known as refractory period. Subsequently the initial ion concentration state between intracellular and extracellular space is restored (repolarization) and the cells can be activated again. The procedure of ventricular repolarization can be detected in the ECG and is manifested as the so called T wave. Extremely small and flat T waves are significant indicators for pathology. Repolarization of the atria cannot be detected since it is superimposed by the QRS complex. [9]

2.1.3. Recording the ECG

The ECG is measured by determining the potential difference between skin electrodes placed at the body surface. Depending on where these electrodes are placed and which potential differences are selected, we distinguish between different leads or derivations of the ECG. In the following these leads will be introduced very briefly, refer to [7–9] for further details.
As shown in Figure 2.2, one could imagine the overall electrical activity of the heart as a trajectory of a cardiac vector in a three-dimensional space. At any given moment all electrical forces induced by depolarization of single cells add up to one average force, representing the instantaneous cardiac vector. In order to receive the well known ECG pattern for a specific lead, this cardiac vector is projected onto one line of specific orientation (e.g. Lead II in Figure 2.2). Hence, the ECG of one lead represents the cardiac vector's magnitude, projected on a specific axes, over time. [2]
Figure 2.2 shows only the three standard limb leads, which are lead I, lead II and lead III. For lead I and lead II the negative electrode is placed on the right arm, while for lead III it is positioned on the left arm. The positive electrode is placed on the legs for leads II and III and on the left arm for lead I. The standard ECG consists of twelve leads, the six limb leads (I, II, III, aVF, aVL, aVR) and the six precordial leads (V1-V6). [9]
However, for instance, Lead II usually is best suited for detecting the PR interval and usually this lead should be sufficient for detecting arrhythmia [11]. Thus, for single lead considerations, Lead II is often preferred.
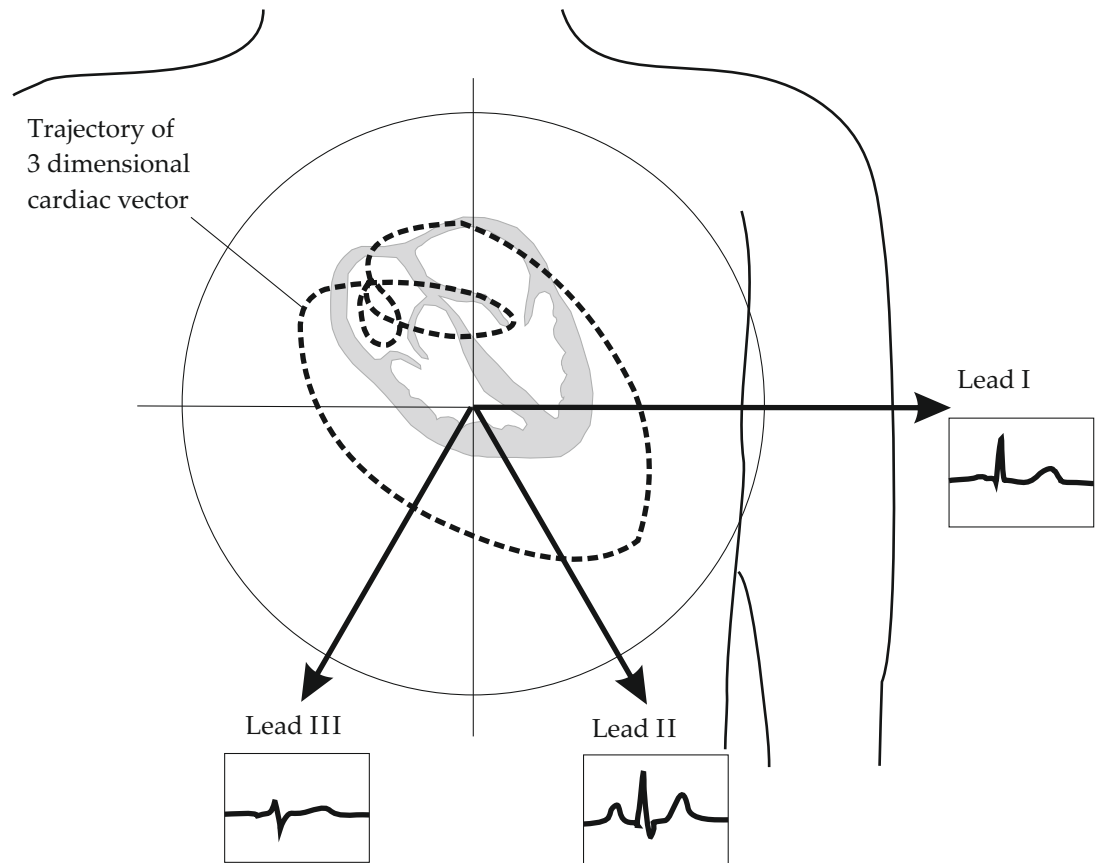
Figure 2.2.: Trajectory of the three dimensional cardiac vector and the three standard limb leads where it is projected on (inspired by [2]).

2.1.4. Parameters of the ECG

Concluding this section, the most important parameters of the ECG and their meaning are summarized in Table 2.1. Additionally, Table 2.2 shows typical Lead II ECG features for a healthy male adult. All of these features can be identified in Figure 1.1, except of the QTc interval. This parameter is introduced, since the QT interval strongly depends on the heart rate making it difficult to define a typical value. The QTc interval is obtained by dividing the QT interval by the square root of the RR interval.

P wave	Depolarization of both atria
PR interval	Time between the depolarization of the atria and the depolarization of the vetricles
QRS complex	Depolarization of the vetricles
ST interval	Time between the end of the ventricle depolarization and the beginning of the ventricle repolarization
T wave	Ventricular repolarization
QT interval	Measure of the total period of ventricular depolarization and repolarization

Table 2.1.: Overview of the fundamental parts building a cardiac cycle.

Feature	Normal Value	Normal Limit
P Width	110 ms	± 20 ms
P Amplitude	0.15 mV	± 0.05 mV
QRS Width	100 ms	± 20 ms
QRS Height	1.5 mV	± 0.5 mV
T Amplitude	0.3 mV	± 0.2 mV
PR Interval	160 ms	± 40 ms
QTc Interval	400 ms	± 40 ms

Table 2.2.: Typical Lead II ECG features for a healthy male adult (Source: [2]). Note: $QTc = \alpha QT$ where $\alpha = (RR)^{-\frac{1}{2}}$ and RR is the beat-to-beat interval in seconds.

2.2. Wavelet Transform

A fundamental goal of signal processing is to extract specific information from a given signal. For that reason signals are often transformed to different domains, expecting that the desired information can be read out easier [12]. One of these transformations is the so called wavelet transform (WT), which is introduced in the following. The subsequent sections present three major types of the WT, namely the continuous WT (CWT), the discrete WT (DWT) as well as the stationary discrete WT (SDWT). The aim of this section is to provide fundamental understandings of the concepts and to show how these three types differ. Explanations and graphics are mainly based on [12–15].

A Word about Wavelets

Wavelets are described by real- or complex-valued wave forms, which have a definite beginning and end as well as a mean value of zero (Figure 2.3). Simply said, the WT of a signal is obtained by comparing the input signal with dilated and shifted versions of the unstretched wavelet, the so called mother wavelet. Due to their limited duration, wavelets are able to deal simultaneously with time and frequency and hence are suited to describe events that start and stop, as it is the case for non-stationary signals.

2.2.1. Continuous Wavelet Transform

Definition of the CWT

The wavelet transform of the signal $x(t)$ is determined by calculating the inner product of $x(t)$ with dilated as well as shifted versions of a single function $\psi(t) \in L_2(\mathbb{R})^1$, defined as

$$W(b,a) = |a|^{-\frac{1}{2}} \int_{-\infty}^{\infty} x(t) \, \psi^* \left(\frac{t-b}{a} \right) dt. \tag{2.1}$$

The function $\psi(t)$ in its basic form is usually called mother wavelet or simply wavelet. The scaling factor a causes the dilation of the wavelet, while

---

[1] $L_2(\mathbb{R})$ is the set of complex valued functions which satisfy $\int_{-\infty}^{\infty} |f(t)|^2 \, dt < \infty$.
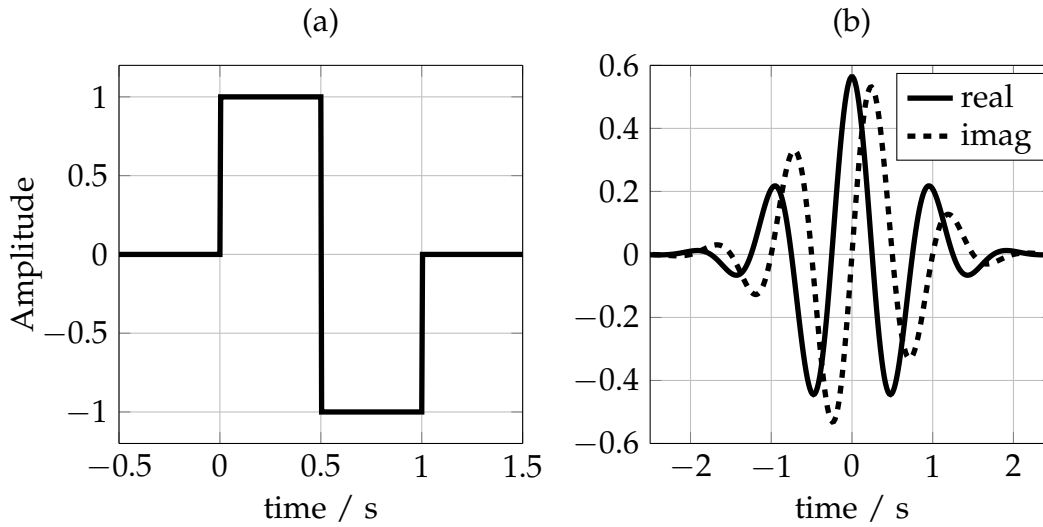
Figure 2.3.: Exemplary wavelets, (a) Real valued Haar wavelet and (b) Complex valued Morlet wavelet.

shifting is done by the translation parameter b. The factor $|a|^{-\frac{1}{2}}$ ensures that all functions $|a|^{-\frac{1}{2}}\psi(\frac{t}{a})$ have the same energy. [13]
It should be mentioned, that we also speak of a CWT even if it is implemented in digital signal processing (DSP) hardware, which only processes discrete signals. Due to sampling, the CWT cannot be exactly determined, however a good approximation can be obtained by choosing an appropriate sampling rate. As will be shown later, the WT corresponds to a band-pass analyis of a given input signal $x(t)$, whereas center frequency and bandwidth of the band-pass depend on the scaling factor a. For any specific scaling factor a we can express (3.1) as a convolution,

$$W(b,a) = |a|^{-\frac{1}{2}} \left(x(b) * h_a(b) \right) \tag{2.2}$$

where $h_a(b)$ represents the time reverse and complex conjugate of the wavelet function for a given a. Hence, for a specific a, the WT can be understood as a convolution of $x(t)$ with the scaled and mirrored wavelet [13].

Visualization and interpretation of the CWT

The outcome of (3.1) are wavelet coefficients, which are usually visualized via a so called scalogram. A scalogram is the counterpart of the spectrogram obtained when performing a short-time Fourier transform (STFT). Thus, for the CWT, we usually talk of a time-scale analysis instead of a time-frequency analysis as it is the case for the STFT. This is because the different wavelet coefficients are acquired by scaling the wavelet. The according frequency band for a specific scale a can be obtained by determining the center frequency and the bandwidth of the according band-pass.

Calculating the CWT of a short sequence

The following example, inspired by [14], demonstrates the working principle of the CWT by using the popular Haar wavelet, defined as

$$\psi(t) = \begin{cases} 1, & \text{if } 0 \leq t < \frac{1}{2} \\ -1, & \text{if } \frac{1}{2} \leq t < 1 \\ 0, & \text{otherwise} \end{cases} \tag{2.3}$$

and shown in Figure 2.3 (a). The Haar wavelet will be used for explanations throughout this chapter, since it fulfills all requirements for the CWT as well as the DWT. However, it should be mentioned that this wavelet is not of great importance in practice, because of its bad properties in the frequency domain. Nevertheless, due to its simple shape, the Haar wavelet is suited very well for explaining mechanisms, which can be applied on more complicated wavelets, e.g., on the complex Morlet wavelet (Figure 2.3 (b)).

Example: Given is a signal $x(t) = \sigma(t - 3) - \sigma(t - 6)$, where σ represents the step function. We want to determine the CWT based on the Haar wavelet for the scales $a = 1$ to 6, choosing the sampling frequency $f_s = 40 \, \text{Hz}$ in order to obtain a sufficiently good approximation of the CWT.
First, the signal $x(t)$ and the Haar wavelet are sampled, leading to the discrete sequence $x[n]$ as well as to discrete versions of the (dilated) wavelet functions shown in Table 2.3 (only integer scales are represented). Subsequently the CWT is calculated either by correlating the sequence $x[n]$ with the discretized wavelet functions or by convolving $x[n]$ with their time

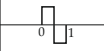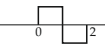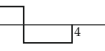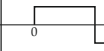| Scale	1	2	3	4	5	6
$\psi(t)$						

Table 2.3.: Wavelet functions $\psi(t)$ for the Haar wavelet filter (scales 1-6). Non-integer dilations are not represented in this table.

reverse[2]. Thus, the time-reverse of a discretized wavelet function defines its wavelet filter coefficients for a given a. The CWT can then be determined simply by filtering $x[n]$ with these wavelet filters. In order to ensure correct energy representation the result has to be divided by the square root of the scale.

Figure 2.4 shows the resulting scalogram when calculating the CWT of the sequence $x[n]$ for scales $a = 1$ to 6[3]. Bright spots indicate a high correlation at a specific scale and time instant. Maximum values occur at scale 6 and time instant 3 s as well as 6 s (the latter case is shown at the top to the right in Figure 2.4). It is obvious that the highest correlation occurs for this time-scale setting. Additionally at the top-left of Figure 2.4 the calculation for another specific time-scale combination is illustrated.

Requirements a wavelet needs to fulfill for the CWT

To be categorized as wavelet, a function basically has to satisfy the admissibility condition

$$C_\psi = \int_{-\infty}^{\infty} \frac{|\Psi(\omega)|^2}{|\omega|} \, d\omega < \infty, \tag{2.4}$$

where $\Psi(\omega)$ represents the Fourier transform of the wavelet $\psi(t)$. This condition has to be fulfilled in order to allow a flawless inverse WT (for more information see [13]). To satisfy (2.4)

$$\Psi(0) = \int_{-\infty}^{\infty} \psi(t) \, dt = 0 \tag{2.5}$$

---

[2]For complex valued wavelets we would also have to take the complex conjugate.
[3]High scales (representing low frequencies) are placed at the bottom of the y axis while low scales (representing high frequencies) are placed at the top.
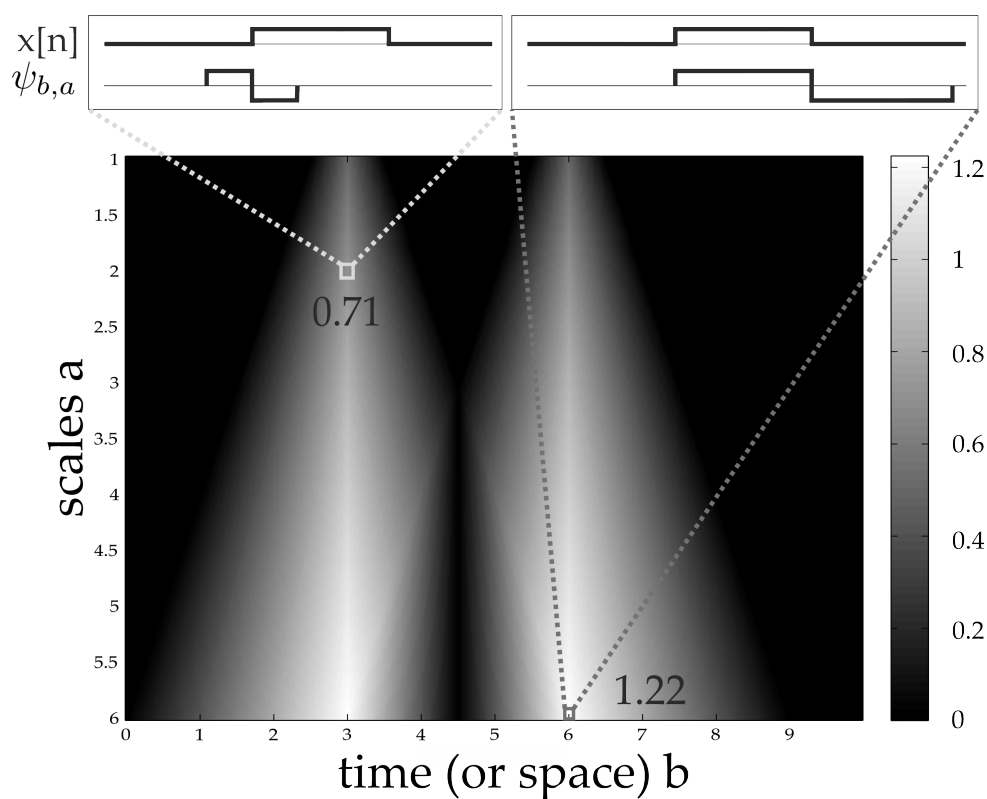
Figure 2.4.: CWT of a short sequence using the Haar wavelet.

has to hold and it can be shown that $|\Psi(\omega)|$ has to decrease significantly for $|\omega| \to \infty$ [12]. This means that the Fourier transform of $\psi(t)$ corresponds to a band-pass spectrum, whereas the center frequency and the bandwidth are determined by the scaling factor a.

Difference to the STFT

In the following, the difference of the CWT to the well known STFT is illustrated. For that reason a very popular and probably the most often used Wavelet for signal analysis is chosen. This so called complex Morlet wavelet[4], shown in Figure 2.3 (b), is a modulated Gaussian function, defined

---

[4]Interestingly this function only fulfills the admissibility condition approximately, but a proper choice of the parameters ω_0 and β allows the wavelet to be used in practice.

as

$$\psi(t) = e^{j\omega_0 t} e^{-\frac{\beta^2 t^2}{2}}. \tag{2.6}$$

The according WT of the signal $x(t)$,

$$W(b,a) = |a|^{-\frac{1}{2}} \int_{-\infty}^{\infty} x(t) \underbrace{e^{-\frac{\beta^2 (\frac{t-b}{a})^2}{2}}}_{*} \underbrace{e^{-j\omega_0 \frac{t-b}{a}}}_{**} dt,$$

*scaling the window via a

**scaling the frequency via a
$$\tag{2.7}$$

is very similar to the Gabor transform[5] of $x(t)$,

$$\begin{aligned} G(b,\omega) &= \int_{-\infty}^{\infty} x(t)\, w(t-b)\, e^{-j\omega t}\, dt \\ &= \int_{-\infty}^{\infty} x(t) \underbrace{e^{\frac{-\beta^2 (t-b)^2}{2}}}_{*} \underbrace{e^{-j\omega t}}_{**} dt. \end{aligned} \tag{2.8}$$

*fixed window size defined by β

**modulation with specific frequency

The evaluation of these two equations again corresponds to simple band-pass filtering (evaluated at a specific scale a, in case of the WT, and for a specific frequency ω, in case of the Gabor transform). To stay mathematically correct, we have to adapt (2.7), such that

$$W(b,a)\bigg|_{a=a_x} = \left(|a|^{-\frac{1}{2}} \int_{-\infty}^{\infty} x(t) \underbrace{e^{-\frac{\beta^2 (\frac{b-t}{a})^2}{2}} e^{j\omega_0 \frac{b-t}{a}}}_{h(b-t)} dt \right) \bigg|_{a=a_x}$$

$$= |a_x|^{-\frac{1}{2}} (x(b) * h(b))$$

---

[5]The Gabor transform of $x(t)$ is the STFT $of x(t)$ using a Gaussian window $w(t) = e^{-\frac{\beta^2 t^2}{2}}$.

and (2.8), such that

$$G(b,\omega)\Big|_{\omega=\omega_x} = \left(e^{-j\omega b} \int_{-\infty}^{\infty} x(t) \underbrace{e^{\frac{-\beta^2(b-t)^2}{2}} e^{j\omega(b-t)}}_{g(b-t)} dt \right) \Big|_{\omega=\omega_x}$$

$$= e^{-j\omega_x b} \left(x(b) * g(b) \right).$$

The factor $e^{-j\omega_x b}$ in the latter equation can be neglected for now, since it only influences the phase delay and we are just interested in the magnitude response in this case.

The resulting complex valued filters $g(t)$ and $h(t)$ are shown for two specific analysis frequencies at the top of Figure 2.5. We can observe that for the STFT only the frequency of the enclosed exponential function is changed, without changing the width of the window itself. Hence, the bandwidth of the according band-pass filters does not change and the time-frequency resolution is constant for all frequencies (Figure 2.5 (b),(c) - left). In contrast, for $h(t)$ both, the window and the frequency of the enclosed exponential function are scaled as shown on the right side of Figure 2.5 (a). Due to a shorter window length for higher frequencies, the time resolution of the WT increases as the frequency increases and vice versa. Fast transient changes in the signal usually correspond to high frequencies in the signal. Hence, the WT with its higher time resolution for high frequencies is in general better suited to detect such fast transient changes in the signal than the STFT. However, as can be observed on the right side of Figure 2.5 (b) and (c), the frequency resolution clearly decreases for increasing frequencies. Summing up, a very important difference of the STFT and the WT is the way they deal with the so called Gabor limit[6]. Which strategy is better suited depends on the application. The following example shows a scenario which emphasizes the advantages and disadvantages of the CWT and the STFT (inspired by [13]).

Example - CWT vs STFT: We want to analyze a signal sampled at $200\,\text{Hz}$ (Figure 2.6(a)). Basically it consists of 2 sinusoids at the frequencies 10 and

---

[6]This means that it is not possible to localize a signal precisely in both the time and the frequency domain.
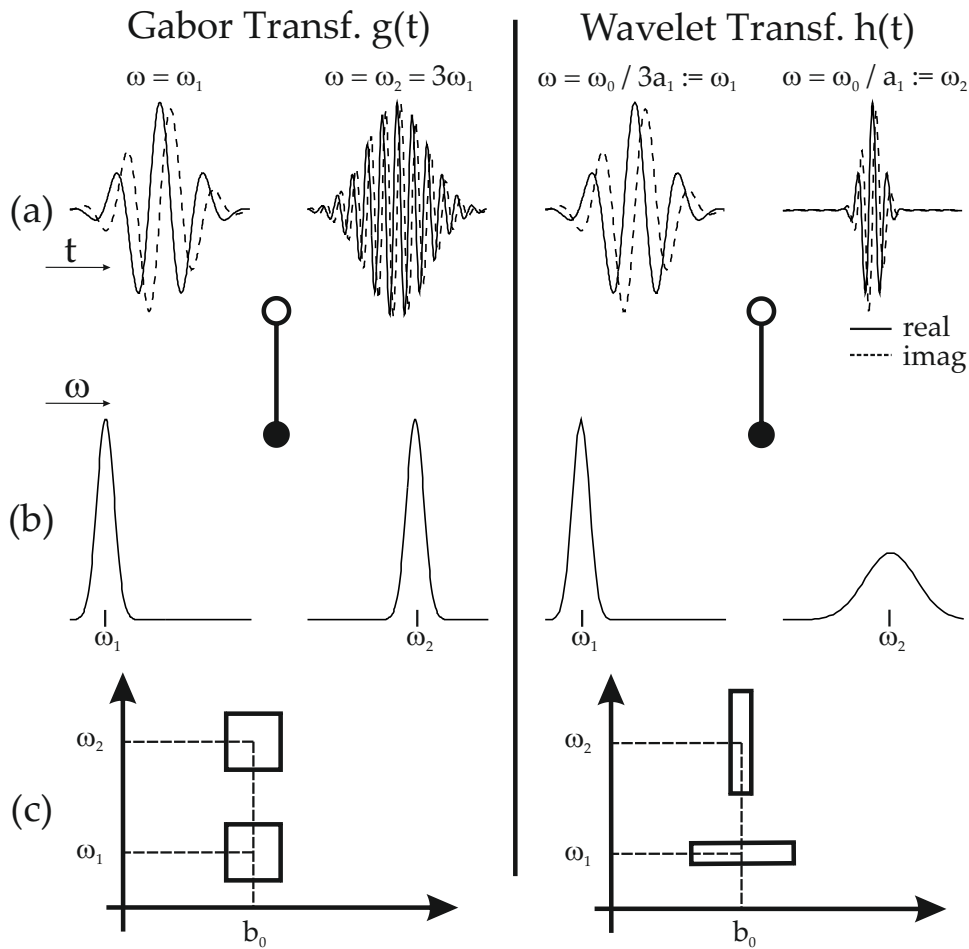
Figure 2.5.: Comparison of the Gabor transform and the WT. (a) Filters in time domain for lower and higher frequencies. (b) Filters in the frequency domain (magnitude response). (c) Illustration how the STFT and the WT deal with the Gabor limit.

20 Hz. Additionally two impulses occur at $t = 0.84\,\text{s}$ as well as $t = 0.94\,\text{s}$ and from $t = 1.4\,\text{s}$ to $2\,\text{s}$ another sinusoid at $70\,\text{Hz}$ is added. The analysis filters used for the WT and for the Gabor transform are obtained by sampling $h(t)$ and $g(t)$.

Figure 2.6 (b) shows the outcome of the WT. Both, the low-frequent sinusoids at 10 and 20 Hz, as well as the impulses can be detected. However,
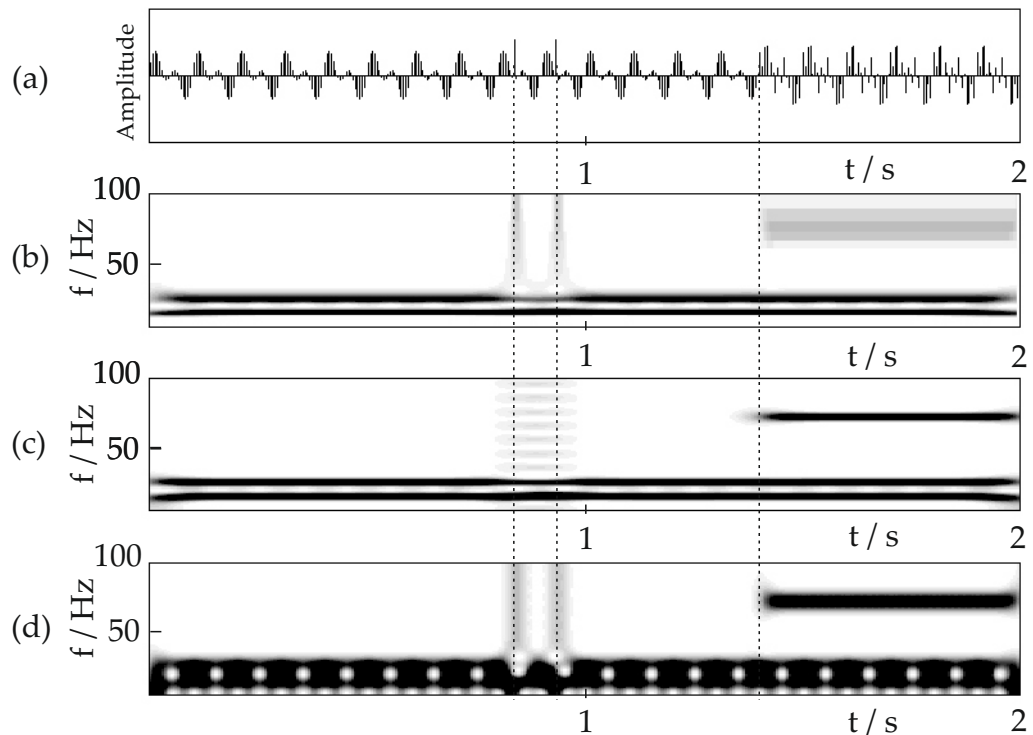
Figure 2.6.: Illustration of the characteristics of the WT and the STFT. (a) Sequence to investigate, (b) WT with Complex Morlet wavelet, (c) STFT with window length of 0.4 s and (d) STFT with window length of 0.15 s.

due to the bad frequency resolution for higher frequencies, we can only make a very imprecise estimate of the 70 Hz sine wave. The results of the STFT for two different window sizes are illustrated in Figure 2.6 (c) and (d). For the first case, using a window length of 0.4 s, all three frequencies are easily distinguishable. Unfortunately due to the wider window it is not possible to locate the two peaks. In contrast, for a window length of 0.15 s (Figure 2.6 (d)) the two peaks can be located, but we are not able to differ between the 10 and 20 Hz frequencies anymore.

In addition to the difference how the two transformations deal with the uncertainty principle, another important distinction can be observed. While the STFT is limited to sinusoidal analyzing functions, for the WT we can use any shape we want as long as it satisfies the admissibility condition [16].

2.2.2. Discrete Wavelet Transform and Multiresolution Analysis

Due to the fact that the information carried by CWT-coefficients is extremely redundant[7], one could think of evaluating the transformation integral only for a subset of scales a_m and translations $b_{m,n}$. This means that the time-scale plane is sub-sampled for certain scales and time points. However, the transformation should still be invertible, leading to restrictions for the sampling points and the wavelets themselves. Although there exist different ways how to sub-sample the time-scale plane, the name DWT is usually reserved for a specific setting [15]:

- As shown in Figure 2.7 the time-scale plane is only evaluated for dyadic scales a_m and sampling points $b_{m,n}$,

$$a_m = 2^m, \quad b_{m,n} = a_m nT = 2^m nT, \quad m, n \in \mathbb{Z}, \ T = \frac{1}{f_s}. \quad (2.9)$$

- Wavelets are restricted to functions which form an orthonormal basis (ONB) for the space of interest, which is $L_2(\mathbb{R})$ for our considerations.
- The wavelet used for analysis must be of compact support, i.e., it is only non-zero for a specific interval.
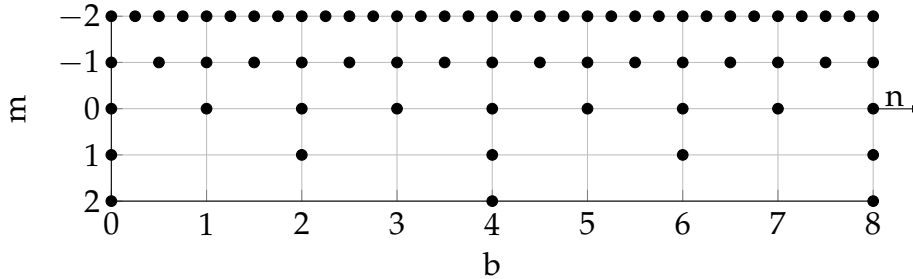

Figure 2.7.: Dyadic sampling of the time-scale plane

For this setting the DWT can be calculated very efficiently via a specific filterbank, which will be introduced later. Furthermore, the wavelet coef-

---

[7]In general there are one or two orders of magnitude more calculated wavelet coefficients than samples of the signal being analyzed [16].

ficients carry zero redundancy, what makes this type of transformation especially interesting for signal compression.

Generation of orthonormal wavelets

The mathematical framework to generate orthonormal basis functions is provided by the Multi-Resolution-Analysis (MRA) and was introduced by Mallat in 1989 [17,18]. Assuming that our signal of interest $x(t)$ is defined in $L_2(\mathbb{R})$, we want to dived $L_2(\mathbb{R})$ into a sequence of nested spaces

$$0 \subset \cdots \subset V_2 \subset V_1 \subset V_0 \subset V_{-1} \subset V_{-2} \cdots \subset L_2(\mathbb{R})$$

building a ladder of resolutions of the space $L_2(\mathbb{R})$. For a large scale ($m >>$), V_m would therefore be a coarse representation of $L_2(\mathbb{R})$, while a small scale approximates $L_2(\mathbb{R})$ with a finer resolution.

First, a so called scaling function $\phi_{m,n}(t)$ is defined, which, together with its integer translations forms an ONB for a specific subspace V_m. As we do have dyadic sampling, $\phi_{m,n}(t)$ can be defined as

$$\begin{aligned}
\phi_{m,n}(t) &= |a_m|^{-\frac{1}{2}} \phi(\frac{t - b_{m,n}}{a_m}) \\
&= 2^{-\frac{m}{2}} \phi(\frac{t}{2^m} - nT).
\end{aligned} \tag{2.10}$$

In case of the Haar wavelet this scaling function would simply be a boxcar function, defined as

$$\phi_{0,0}(t) = \begin{cases} 1, & \text{if } 0 \leq t < 1 \\ 0, & \text{otherwise.} \end{cases} \tag{2.11}$$

For now, we want to take a look at V_0, which does not differ in its properties from other subspaces, but makes explanations a bit easier. The projection of an arbitrary signal $x(t) \in L_2(\mathbb{R})$ onto the subspace V_0 can therefore be described via a linear combination of $\phi_{0,n}(t)$. The according projection coefficients are calculated by building the inner product,

$$c_{0,n} = \left\langle \mathbf{x}, \boldsymbol{\phi}_{0,n} \right\rangle = \int_{-\infty}^{\infty} x(t) \, \phi_{0,n}^*(t) \, dt. \tag{2.12}$$

Hence, projection of $x(t)$ onto the subspace V_0 is stated as

$$x_0(t) = \sum_{n\in\mathbb{Z}} c_{0,n}\,\phi_{0,n}(t) = \sum_{n\in\mathbb{Z}} \left\langle \boldsymbol{\phi}_{0,n}, \mathbf{x} \right\rangle \phi_{0,n}(t) \qquad (2.13)$$

and after inserting (2.10), where we set $T = 1$ for simplicity, as

$$x_0(t) = \sum_{n\in\mathbb{Z}} \langle \phi(t-n), x(t) \rangle\, \phi(t-n). \qquad (2.14)$$

For the Haar wavelet this corresponds to a simple step-approximation as shown in Figure 2.8 (a), (b).

In order to obtain an MRA, every subspace must be related to V_0 in a consistent way. This is realized via the dyadic dilation and translation of the scaling function. Projection onto subspace V_{-1} is subsequently defined as

$$x_{-1}(t) = \sum_{n\in\mathbb{Z}} 2\,\langle \phi(2t-n), x(t) \rangle\, \phi(2t-n) \qquad (2.15)$$

and shown for the Haar Wavelet in Figure 2.8 (b).

Hence, we observe, that $\{\phi_{0,n}\}_{n\in\mathbb{Z}}$ builds an ONB for V_0, while $\{\phi_{-1,n}\}_{n\in\mathbb{Z}}$ provides an ONB for V_{-1}. Additionally, V_0 is a subspace of V_{-1} since it is possible to describe any function in V_0 via a linear combination of $\{\phi_{-1,n}\}_{n\in\mathbb{Z}}$. For our example we would simply express the coarser step approximation $x_0(t)$ through a linear combination of $\phi_{-1,n}$. This means, that the scaling functions indeed build an ONB for a specific dilation m, but they are linearly dependent for different spaces.

We want to find out, whether it is possible to complete $\{\phi_{0,n}\}_{n\in\mathbb{Z}}$ (lower resolution) to an ONB of V_{-1} (higher resolution). In case of the Haar wavelet this can be illustrated very nicely by subtracting $x_0(t)$ from $x_{-1}(t)$ or in other words by finding the function which needs to be added to $x_0(t)$ in order to receive $x_{-1}(t)$. The result, shown in Figure 2.8 (d), is a linear combination of the well known Haar mother wavelet and its integer translations and can be defined as

$$y_0(t) = \sum_{n\in\mathbb{Z}} d_{0,n}\,\psi_{0,n}(t). \qquad (2.16)$$

Such a linear combination of orthonormal functions spans a subspace W_m similar to V_m. One can show that this subspace fulfills the following properties:
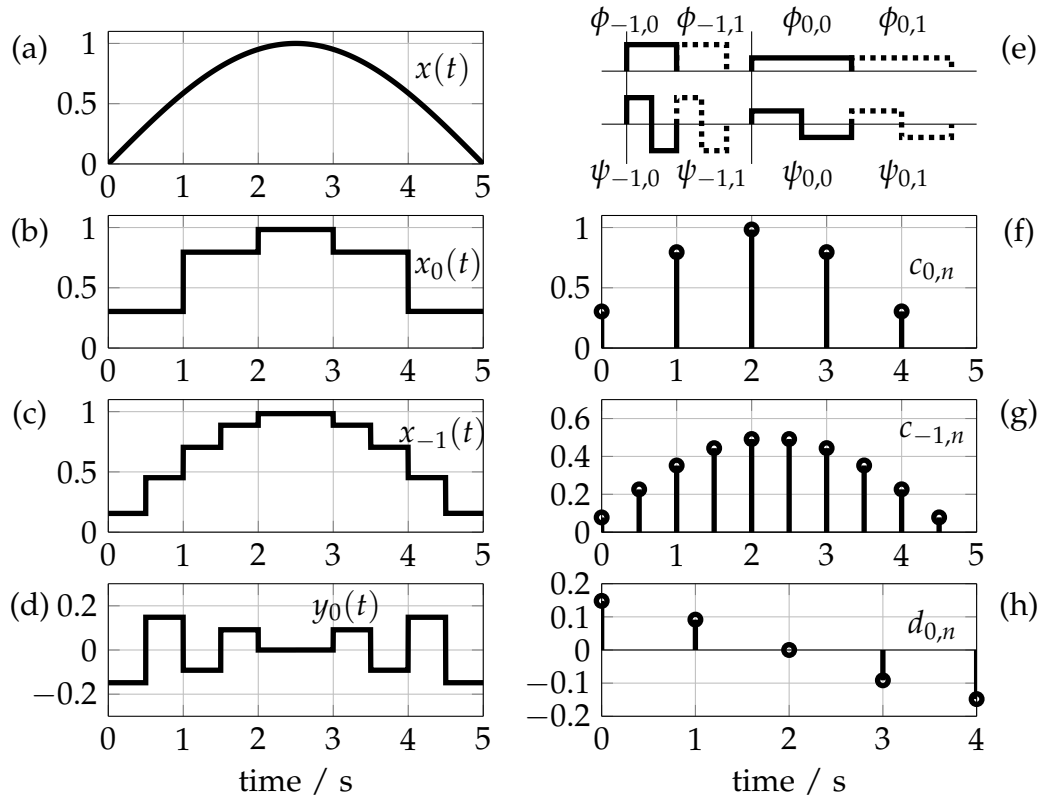
Figure 2.8.: MRA for the Haar wavelet.

- A wavelet function $\psi_{m,n}(t)$ of the subspace W_m and its integer translations are orthonormal, stated as

$$\langle \psi_{m,k}, \psi_{m,l} \rangle = \delta_{k,l}. \tag{2.17}$$

This is easy to verify for the Haar wavelet since the translations do not overlap, as shown in Figure 2.8 (e).

- The wavelet functions of different spaces W_m, $m \in \mathbb{Z}$ are orthonormal as well, defined as

$$\langle \psi_{i,k}, \psi_{j,l} \rangle = \delta_{i,j}\delta_{k,l}. \tag{2.18}$$

This is illustrated exemplary in Figure 2.8 (e) for the Haar wavelet.

Finally, we conclude that $\{\phi_{0,n}\}_{n \in \mathbb{Z}}$ can be completed to an ONB of V_{-1} by adding the wavelet subspace W_0 spanned by $\{\psi_{0,n}\}_{n \in \mathbb{Z}}$. For our example

(Figure 2.8) this can be illustrated by adding up $x_0(t) \epsilon V_0$ and $y_0(t) \epsilon W_0$ to receive $x_{-1}(t) \epsilon V_{-1}$,

$$
\begin{aligned}
x_{-1}(t) &= x_0(t) + y_0(t) \\
&= \sum_{n \epsilon \mathbb{Z}} c_{0,n} \, \phi_{0,n}(t) + \sum_{n \epsilon \mathbb{Z}} d_{0,n} \, \psi_{0,n}(t).
\end{aligned} \tag{2.19}
$$

Formally this is defined as the orthogonal or direct sum of subspace V_0 and W_0,

$$
V_{-1} = V_0 \oplus W_0 \quad \text{and} \quad V_0 \perp W_0, \tag{2.20}
$$

or more general,

$$
V_m = V_{m+1} \oplus W_{m+1} \quad \text{and} \quad V_{m+1} \perp W_{m+1} \tag{2.21}
$$

We can observe that W_m extracts the details (higher frequent part) and V_m the approximation (lower frequent part) of a specific subspace (cmp. Figure 2.8). Equation 2.21 can be easily extended to

$$
V_m = V_{m+N} \oplus W_{m+N} \oplus W_{m+N-1} \oplus \cdots \oplus W_{m+1}, \tag{2.22}
$$

i.e., we can form an orthonormal basis expansion for a signal $x(t) \epsilon L_2(\mathbb{R})$. Hence, a signal $x(t)$ can be represented by the series expansion

$$
x(t) = \underbrace{\sum_{n \epsilon \mathbb{Z}} c_{m_0,n} \, \phi_{m_0,n}(t)}_{\text{approximation } x_{m_0}(t)} + \underbrace{\sum_{m=-\infty}^{m_0} \sum_{n \epsilon \mathbb{Z}} d_{m,n} \, \psi_{m,n}(t)}_{\text{detail } y_m(t)}, \tag{2.23}
$$

where $c_{m_0,n}$ are the approximation coefficients of an arbitrary space V_{m_0} and $d_{m,n}$ are the wavelet (detail) coefficients of the spaces $W_{-\infty \cdots m_0}$.

To sum up, the MRA theory provides the mathematical foundation to generate orthonormal wavelets. Once a valid scaling function ϕ for an MRA is defined, the according wavelet function ψ can be determined based on the MRA theory. However, in general this is not that easy as it was for the Haar wavelet. There exist different strategies to find and define new wavelets fulfilling the requirements mentioned above, but this is beyond the scope of this thesis. The interested reader is referred to [13,15,19].

Efficient implementation of the DWT

For DSP implementations the signal is sampled with a specific sampling frequency f_s. In practice these samples are determined to be the approximation coefficients at scale $m = 0$, i.e. we assume that the discretized signal $x[n]$ is equal to the projection of $x(t)$ onto subspace V_0[8]. Thus, the sequence of approximation coefficients at scale $m = 0$ ($c_0[n]$) is the most accurate representation of our signal. Wavelet coefficients of this scale are implicitly assumed to be zero.

The DWT can then be determined very efficiently via a filter-bank implementation (Figure 2.9,) which is known as Mallat's Algorithm [22]. The filter-bank consists of a decomposition (or analysis) bank and a reconstruction (or synthesis) bank. In case of orthonormality, the reconstruction filters H' and L' are given by the time-reverse of the decomposition filters H and L. The algorithm is especially of interest for DSP-implementations, since we only have to deal with finite impulse response filters and down-sampling by the factor 2.
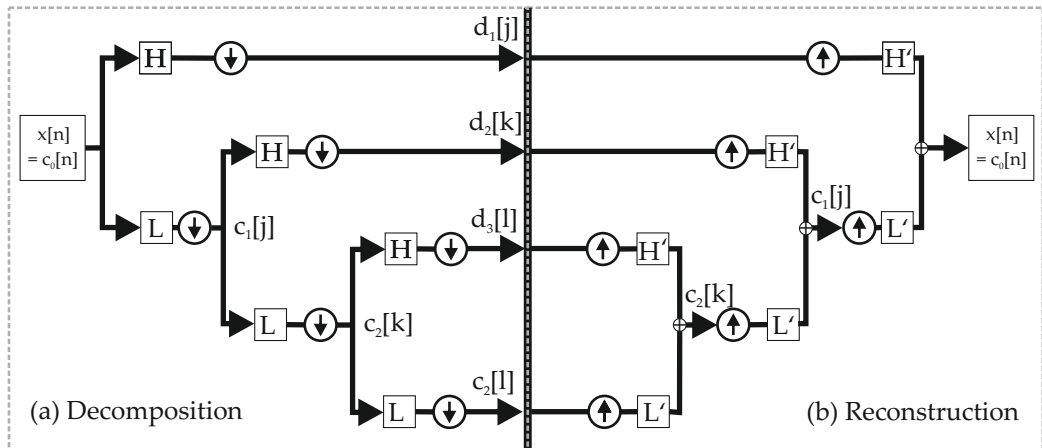

Figure 2.9.: 3-level fast wavelet transform (Mallat's Algorithm).

---

[8]This is actually not correct and therefore called "wavelet crime". For further discussion see [20] and [21].

Biorthogonal Wavelets
Except for trivial cases as the Haar wavelet, the phase responses of the decomposition and reconstruction filters introduced in the previous paragraph, are generally non-linear. This is due to the fact that orthogonality and symmetric filters exclude each other in most cases [23]. However, it is desirable to perform an MRA with linear phase filters or more generally with a non-orthogonal filter-bank.
One can show that this is possible by introducing the function systems $\tilde{\psi}_{0,n}(t)$ and $\tilde{\phi}_{0,n}(t)$, which define the reconstruction filter bank. In general decomposition and reconstruction filters do not have the same coefficients anymore. In case that the conditions

$$\langle \psi_{i,k}, \tilde{\psi}_{j,l} \rangle = \delta_{i,j}\delta_{k,l} \tag{2.24}$$

and

$$\langle \phi_{i,k}, \tilde{\phi}_{j,l} \rangle = \delta_{i,j}\delta_{k,l} \tag{2.25}$$

are met, an MRA as done for orthonormal wavelets can be carried out coming along with the drawback that the subspaces W_m are not orthogonal anymore. However decomposition and reconstruction filters can be designed to be symmetrically now, what is desired in many applications [14].

2.2.3. Stationary Discrete Wavelet Transform

Due to the dyadic down-sampling, which is performed for calculating DWT coefficients, the DWT clearly lacks translation invariance [16]. Translation invariance means that shifting the input signal $x[n]$ by an arbitrary amount of samples simply leads to a shift of the output by the same amount of samples. However, dyadic down-sampling of an exemplary sequence $x[n]$ leads to a different result than for the case that the input signal is shifted by one,

$$\underbrace{\left[\cdots, \mathbf{0}, 0, \mathbf{0}, 1, \mathbf{1}, 1, 0, 0, \mathbf{0}, \cdots \right]}_{\downarrow 2 \quad 0,0,1,0,0} \text{ vs. } \underbrace{\left[\cdots, \mathbf{0}, 0, \mathbf{1}, 1, \mathbf{1}, 0, \mathbf{0}, 0, \mathbf{0}, \cdots \right]}_{\downarrow 2 \quad 0,1,1,0,0}.$$

Consequently the wavelet and approximation coefficients differ as well. For the stationary discrete wavelet transform (SDWT) the scales are still dyadic, but the translation parameter is not down-sampled anymore (Figure 2.10.
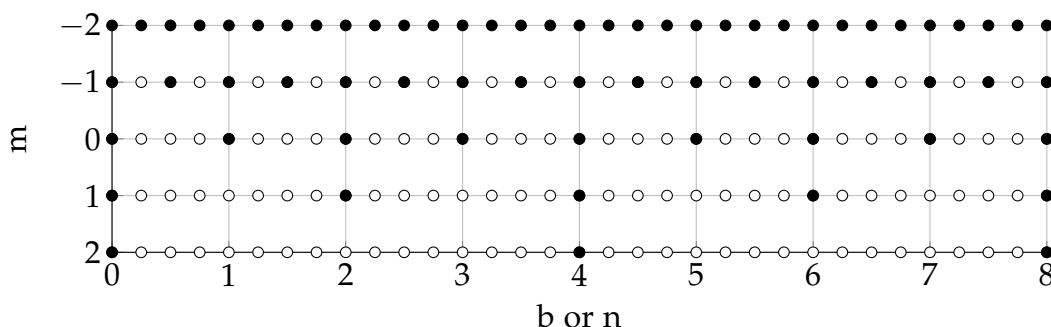
Figure 2.10.: Sub-sampling of the time-scale plane for the SDWT. White circles indicate additional points compared to the DWT.

This means that the wavelet coefficients $d_m[n]$ and the approximation coefficients $c_m[n]$ are now determined for every sample n. Instead of down-sampling the signal, as it is done for the DWT, the filter coefficients are now up-sampled as shown for the Haar wavelet in Figure 2.11. This filter-
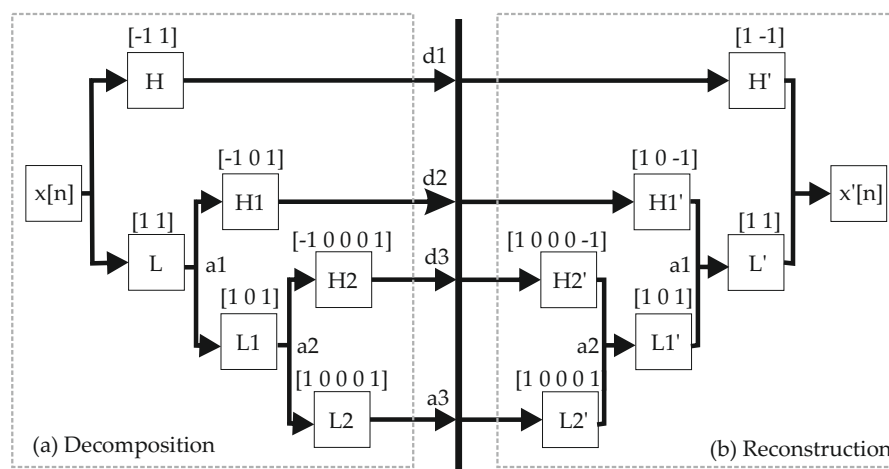
Figure 2.11.: Illustration of the SDWT for the Haar Wavelet. (a) Decomposition of the sequence $x[n]$ into its wavelet and approximation coefficients (*d*1 - *d*3, *a*3) and (b) Reconstruction of the sequence by applying the inverse transform.

bank implementation is called Algorithme à Trous[9] and also allows perfect

---

[9] À Trous is French and stands for "with holes" [14].

reconstruction as demonstrated for the Haar wavelet in Figure 2.12. We observe that all parallel paths in Figure 2.11, which are often referred to as low-pass and high-pass half-band filters, add up to an all-pass in the frequency domain.

This means, that we overcome the DWT's lack of translation invariance by adding redundant information (and destroying orthogonality).
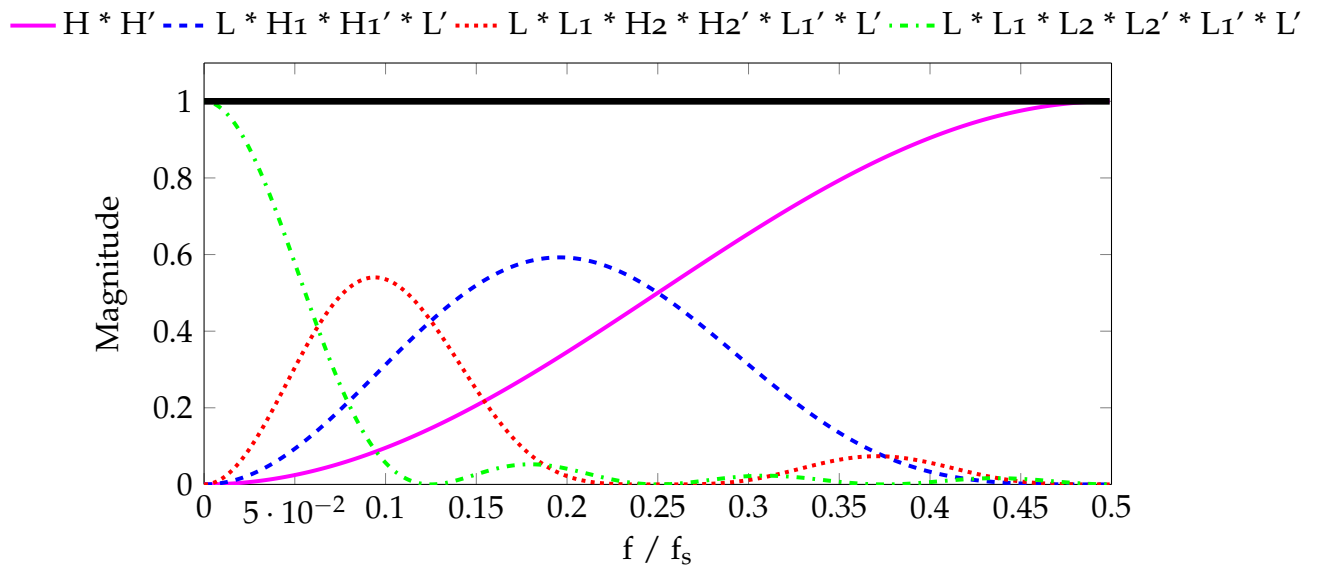

Figure 2.12.: Haar wavelet filters in the frequency domain: Adding up the magnitude responses of the parallel paths results in an all-pass illustrating the possibility of perfect reconstruction.

Although orthogonality is lost, this can lead to improved performance compared to the DWT in de-noising and compression applications as shown in [14].

3. Methods

3.1. ECG Analysis Based on the WT - A Review

For traditional analyzing methods of the ECG, such as visual inspection, the physician notes characteristic visible features within the ECG. An unusual long PR interval, e.g., indicates a conduction defect in the atria [8], or a prolongation of the QT interval might result in abnormal heart rhythm [2]. Unfortunately, for many medical issues such meaningful features cannot be identified that easily. Additionally, standard features such as the PR interval, the QRS width or the ST level are ambiguous in many cases [24,25]. As a consequence, sophisticated methods for feature extraction have been used in the literature [24–40]. These methods try to find new features which allow drawing conclusions on a patient's medical condition based on the ECG. These features can be extracted from the time domain ECG, the time-frequency domain ECG or the frequency domain ECG (Figure 3.1). Subsequently these features can then be processed via different approaches like visual inspection or machine learning algorithms. Applications for which the WT has been used successfully for extracting features from the ECG are briefly reviewed in the following.

3.1.1. Extraction of ECG Characteristic Points

Visual inspection of an ECG is usually done by evaluating the general shape of the waves and their intermediate segments, followed by measuring the characteristic features (Figure 1.1 and Table 2.1). The evaluation of the onset, peak and end of the waves can either be done manually by the physicians or automatically via an algorithm. Manual annotation is time consuming and
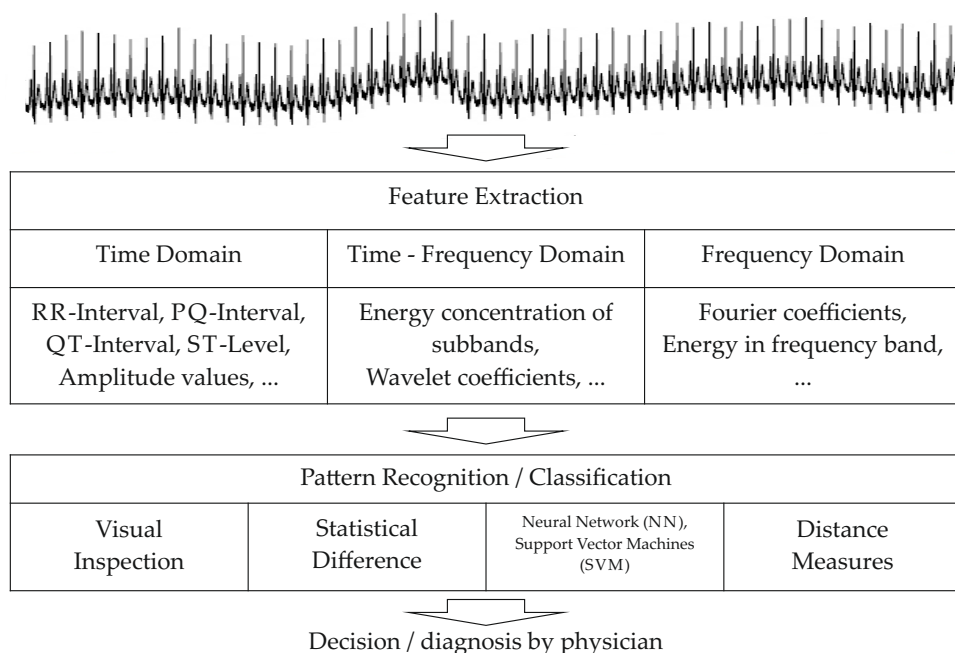
Figure 3.1.: Exemplary process for evaluating a patient's ECG.

error-prone due to possible inter-individual interpretations of the experts. Furthermore, a "golden rule" for determining the onset and end of specific waves, does not exist [4]. Thus, for a tough morphology of the ECG it often is a matter of opinion where to set the onset and end of waves, even for well-experienced experts. Although algorithms for automated extraction of ECG characteristic points do not solve this problem, they do have a considerable advantage, namely the reliable detection of relative changes. Detecting a relative prolongation of the QT interval before and after medication, e.g., could support physicians in diagnosis.

Thus, automated extraction of ECG characteristic points, called ECG delineation or ECG segmentation from now on, has been investigated intensively in literature.

There exist different approaches for QRS detection and the subsequent delineation of the single ECG beat in literature. These approaches include methods based on matched filters [26], slope criteria [27], hidden markov

models (HMM) [28], NN [29], filter-banks [30] or low-pass differentiation methods [31]. Some of the algorithms, though, are specialized on reading out only a specific interval (as e.g. the QT interval). Furthermore, most of the approaches for ECG delineation are not evaluated on standard databases (or only on subsets of a database), which makes their reproducibility and comparability difficult [4]. Moreover approaches like HMM or NN are complex and computationally expensive and often require labeled training sets. In terms of this thesis and any future work drawn from this thesis the algorithm chosen for ECG delineation (see Section 3.3), should have the following properties:

- Evaluation on complete standard databases[1] was carried out. Due to the variety of ECG beats in huge data bases, the algorithm should therefore be able to deal with many different ECG morphologies.
- The algorithm is robust against noise.
- Ability to detect all characteristic points of an ECG beat (onset, peak and end of the waves) is given.
- There is no need to train the algorithm, as it would be the case for NN.
- Implementation is as simple as possible providing the possibility of easy adaption for online delineation of ECG beats.

Li et. al. introduced a very promising method for detection of ECG characteristic points based on the Wavelet Transform [3]. This method was further investigated, improved and tested on different standard databases for ECG delineation showing impressive results in [4]. Due to this, the method was selected for ECG delineation and will be described in more detail in Section 3.3.

3.1.2. ECG Beat Classification

As explained in Section 2.1.2 electrical depolarization and repolarization of the cardiac muscle is described by a pattern of consecutive waves (P-Q-R-S-T) for the healthy heart. Any alternation of this morphological pattern or irregularity of the heart rhythm are indicators for a so called arrhythmia [9].

---

[1]MIT-BIH Arrhythmia database, QT database, European ST-T database, CSE multilead measurement database.

Arrhythmia often results from a cardiac disease and is life threatening in the worst case [32]. Thus, automatic recognition and classification of irregularly shaped beats is of great assistance for clinicians, since they can be alerted in case that suspicious beats are detected. In fact, the symptoms of those diseases may not be present all the time, which means that the ECG must be recorded for several hours in order to make a correct diagnosis [33]. One of these irregularly shaped beats indicating a cardiac arrhythmia are so called premature ventricular contractions (PVCs). An example is shown in Figure 3.2.
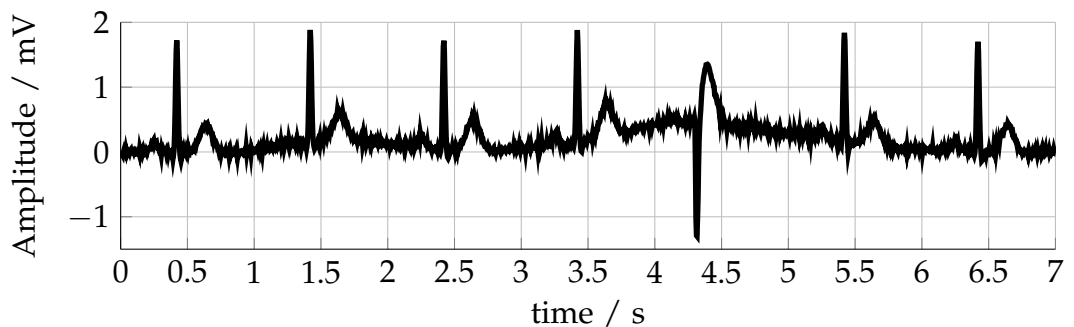

Figure 3.2.: Exemplary illustration of a premature ventricular contraction (between 4 and 5 seconds)

In 2006 Inan et al. tried to automatically detect PVC by classifying heart-beats via an NN, where they combined wavelet coefficients and timing information to obtain their feature set [34]. A general approach used for au-tomated ECG beat recognition is visualized in Figure 3.3. After optional pre-processing for noise reduction single beats are detected and subsequently used for feature extraction. Potential features are, e.g., DWT coefficients of single beats, subcomponents obtained via independent component analysis (ICA) or simply time domain features such as the RR interval. In a next step dimensionality of the feature set is reduced with the objective of only keeping the most meaningful features. As stated in [33], selecting the most informative features is a very crucial step for pattern classification, since the best classifier cannot perform well when poor features are chosen. An approach for the selection of effective features is given in [35]. Finally, a classifier, for example based on particle swarm optimization (PSO), an SVM or an NN, is trained for recognizing different types of beats.
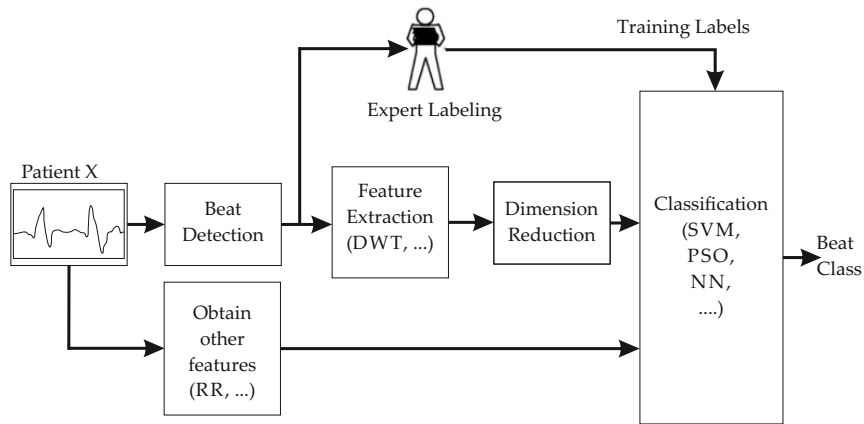
Figure 3.3.: A general approach for beat classification often used in literature.

A challenging issue for automated heart beat classification is the inter-individual variability of ECGs measured at different patients. These ECGs usually show significant variations in morphology [36]. Hence, performance of the classifier might decrease when a new patient's ECG is analyzed. Inan et al. therefore suggested to couple timing interval features with morphological features (extracted via dyadic WT) in order to improve classification accuracy. They argued that timing information, such as the RR interval ratio, is more constant among patients leading to better results [34].

Ince et al. used a similar approach for the detection of ventricular ectopic beats (VEBs) and supra-ventricular ectopic beats (SVEBs) [32]. In order to extract morphological features, SDWT using a quadratic spline wavelet of compact support was performed for the single beats. Although the DWT is non-redundant, what basically is desired for classification tasks, they claim that the redundant SDWT is better suited in this case due to the DWT's lack of time invariance and the resulting sensitivity to the alignment of the signal in time. To reduce dimensionality of morphological features principal component analysis (PCA) was applied. Additionally to SDWT coefficients, RR interval and RR interval ratio were considered. Classification was performed via an evolutionary artificial NN with a small training set and consequently a large test set. The achieved results for the proposed method are promising (for details see [32]).

Reference	Year	# Classes	Features	Wavelet	Feature Reduction	Classifier	# Beats
Jiang [37]	2006	14	DWT + ICA	Db8	Mutual Information	SVM	103898
Inan [34]	2006	3	SDWT + RR	Quadratic Spline	Predefined	NN	93281
Ince [32]	2009	5	SDWT + RR + RR ratio	Quadratic Spline	PCA	Evolutionary artificial NN	109492
Kutlu [33]	2012	5	WPD + HOS	Db6	SFSA	k - Nearest Neighbor	5887
Ye [38]	2012	5 (16)	DWT + ICA + RR	Db8	PCA	SVM	110109
Daamouch [39]	2012	6	DWT + RR ratio + RR + QRS width	Daub. + Symlets	-	SVM	40438
Chen [35]	2012	7	DWT + HOS	Symlet6 Spline	correlation based filters	NN	109492
Saha [40]	2015	6	DWT + DCT	Db4	Predefined	SVM / ELM / VVRKFA	37139

Table 3.1.: Methods for automated ECG beat recognition based on the WT. Following unknown abbreviations were used: wavelet packet transform (WPD), higher order statistics (HOS), sequential floating search algorithm (SFSA), discrete cosine transform (DCT), extreme learning machines (ELM), vector valued regularized kernel function approximation (VVRKFA)

Table 3.1 shows an overview of other promising methods for automated arrhythmia detection based on the WT within the last decade.

3.1.3. Highlighting Minor Changes in a Patient's ECG

Irregularly shaped heart beats differ significantly from normal ones in their morphology (see Figure 3.2). However, the ECG might also change in a more subtle way. These changes might not even be visible in the time domain due to the superimposition of high signal deflections or noise. Ventricular late potentials (VLPs), e.g., are low amplitude electrical oscillations of limited duration usually occurring after the QRS complex. The reason for these small electrical activities is the delayed conduction of the ventricle muscles [16]. VLPs have been used as a predictor for certain types of lethal ventricular arrhythmias [41]. Unfortunately VLPs are often masked by noise and hence not visible in the time domain.

Since both, the time- and the frequency-range of these subtle changes is of

interest, time-frequency-analysis (TFA) seems to be appropriate for detecting and highlighting the wanted information (e.g. VLPs). Among different TFA methods, the WT has shown to be well suited for this task. Addison provides an overview of the literature up until 2005, where the WT was used for detecting localized abnormalities [16].

More recently Tsutsumi et al. showed that the detection of high-frequency powers hidden within the QRS complex can improve the prediction of life threatening ventricular arrhythmias significantly [41]. They used the CWT with the Morlet wavelet to calculate time-frequency powers and subsequently determine the ratios of the peak power during the QRS complex in high-frequency bands against the peak power in the 80 Hz frequency band. After combining their features with detected VLPs, they claim to obtain significant improvement of the sensitivity for the prediction of lethal ventricular arrhythmias compared to standard cardiological measures (for details see [41]).

Another example for the detection of minor changes in a patient's ECG is given by Diery et al. in [42]. Within their work, Diery et al. investigate the morphology of the P wave, which provides information regarding the atrial conduction. Two classes are distinguished, patients with normal P wave morphology and those with abnormal morphology (atrial conduction pathology). For that reason they show that parameters derived from the CWT[2] are effective discriminators for distinguishing between the two classes. They claim that their method generally outperformed standard cardiological measures.

3.2. Graphical ECG Generator

For the verification of new developed evaluation methods it is necessary to start with well known test signals. If it is of interest whether a known pathophysiology can be quantitatively evaluated by a specific method, a proper ECG test signal containing the desired pathological information

---

[2]The wavelet used was the 2nd order derivative of the Gaussian function, since this one showed to be highly correlated with the healthy P wave.

is needed. The best case would be to have a synthetic ECG test signal containing exactly the information which is screened for and which is adjustable in any possible way in user defined, arbitrary small steps.

Therefore in this work a graphical user interface was developed, making it possible to generate any desired heartbeat morphology as well as flexible ECG time courses containing user-defined combinations of single heartbeats. The **G**raphical **E**lectro**C**ardio**G**ram **G**enerat**O**r (GECG^2O) developed in this work provides the freedom of arbitrarily adjusting a single heartbeat's morphology. This is realized in an uncomplicated, fast and easy achievable, graphical or parameterized way. The initial heart cycle is based on an artificial beat of normal morphology (Figure 3.4) generated by the method provided by McSharry et al. [43]. Additionally the designed heart cycles can be added up to an ECG time course.

There are two proposed ways of adjusting the morphology:

1. Parameterization of the single waves (P,Q,R,S,T,U)
2. Graphical drag and drop of predefined points

3.2.1. Graphical User Interface - GUI

The generator can be subdivided in 7 segments as shown in Figure 3.4: (a) Toolbar, (b) ECG Beat Panel, (c) ECG Time Course Panel, (d) Waveform Parameter Panel, (e) Signal Parameter Panel, (f) Test case Panel and (g) Information Box.

The generator produces a realistic single heart beat at startup generated by calling the freely available function *ecgsyn*[3] of McSharry et al [43]. In order to obtain typical values for the ECG beat (Table 2.2) *ecgsyn* was called with a specific parameter set[4]. This "starting heart cycle" is displayed in Figure 3.4(b) and acts as the preset for any following modifications.

---

[3]Available at http://www.physionet.org/physiotools/ecgsyn/

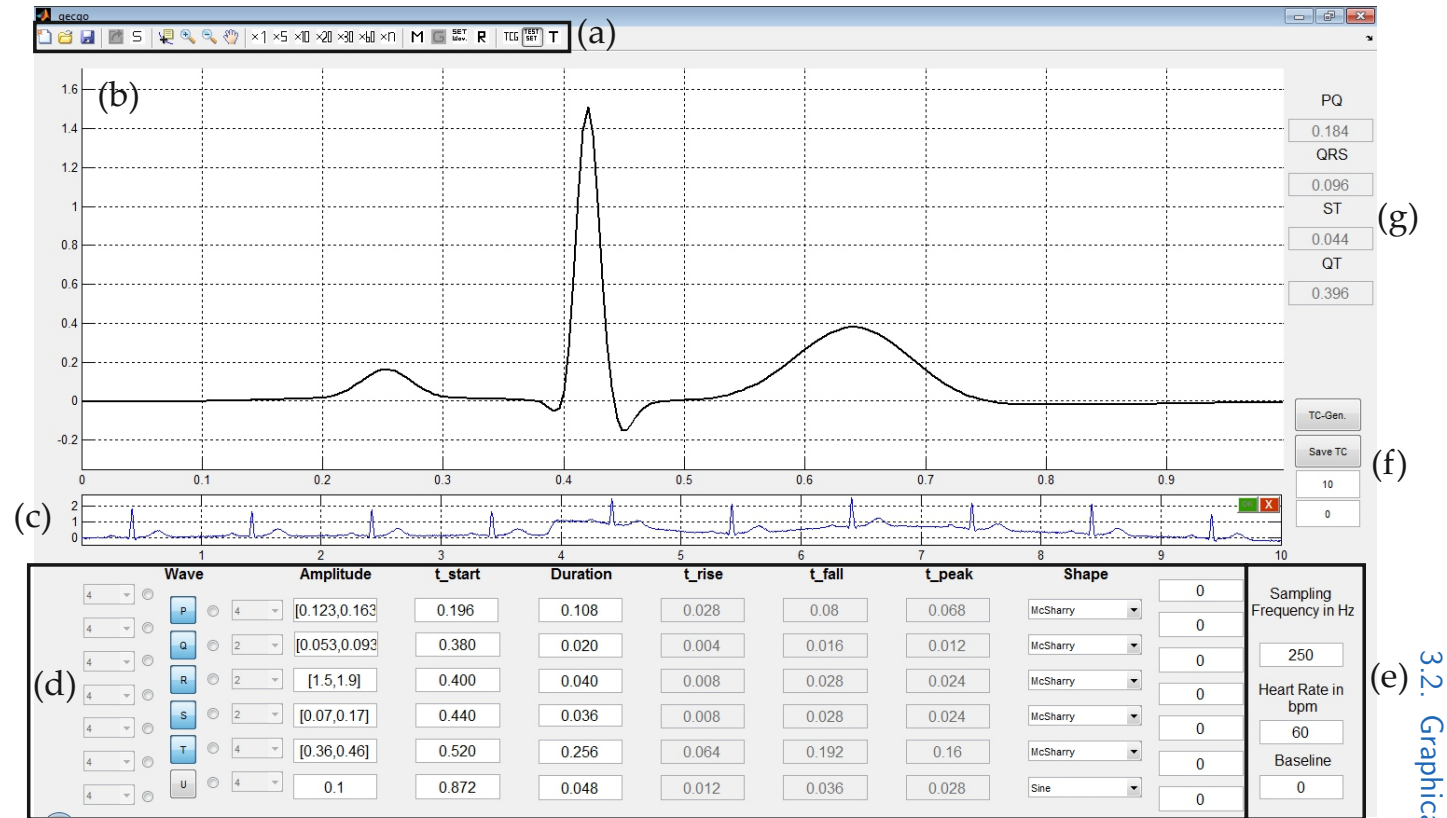[4]ecgsyn(250, 9, 0, 60, 0, 0.5, 250, [-60 -7 0 10 80], [2 -10 100 -7.5 1], [0.13 0.06 0.06 0.06 0.3])

Figure 3.4.: GECG²O Graphical User Interface for modification of the initial signal. (a) Toolbar, (b) ECG Beat Panel, (c) ECG Time Course Panel, (d) Waveform Parameter Panel, (e) Signal Parameter Panel, (f) Test Case Panel, (g) Information Box.

3.2.2. Signal and Waveform Parameters

The default sampling rate is set to 250 Hz and can be adapted to any desired value (Figure 3.4(e)). The same is true for the heart rate (HR), which is 60 beats per minute (bpm) on default. Altering the HR is realized by scaling all single waves and their intermediate segments proportionally. As a result it is possible to create a single arbitrary heart beat for morphological analysis as well as an ECG time course for, e.g., investigating the heart rate variability (HRV). However, it should be mentioned that altering all single waves and their intermediate segments proportional to the heart rate is not an optimal solution. Clifford et al. state that the single segments vary in a different manner when the heart rate changes [2]. This is not considered in the current version of the generator but will be implemented in a future release.

Basically it is possible to create any desired heart cycle consisting of maximal six waves (PQRSTU) and their intermediate segments. In order to obtain maximal variability various waveform parameters, such as magnitude, duration or shape of a single wave, can be altered. Available shapes are a sine half-wave, a (skewed) bell-shaped curve, a trapezoid as well as the default pattern generated by the algorithm of McSharry. All shapes can be parameterized in the "Waveform Parameter panel" (Figure 3.4(d)) easily and accurately by setting magnitude, onset point and duration (available for all shapes), rising and falling time of the edges (trapezoid) as well as the peak time point (skewed bell-shaped curve). An exemplary parameter setting (preset) is shown in Figure 3.4(d). Another feature of the generator is to enable or disable any single wave simply by activating or deactivating the according wave button. Disabling a wave is realized by linear interpolation between the actual on- and offset point of the wave and subsequent smoothing of the transition points. Figure 3.5 shows an exemplary heart cycle with various settings (P-wave skewed bell-shaped, altered starting time point and magnitude, R-wave sine shaped, disabled T-Wave and sine-shaped U-Wave).
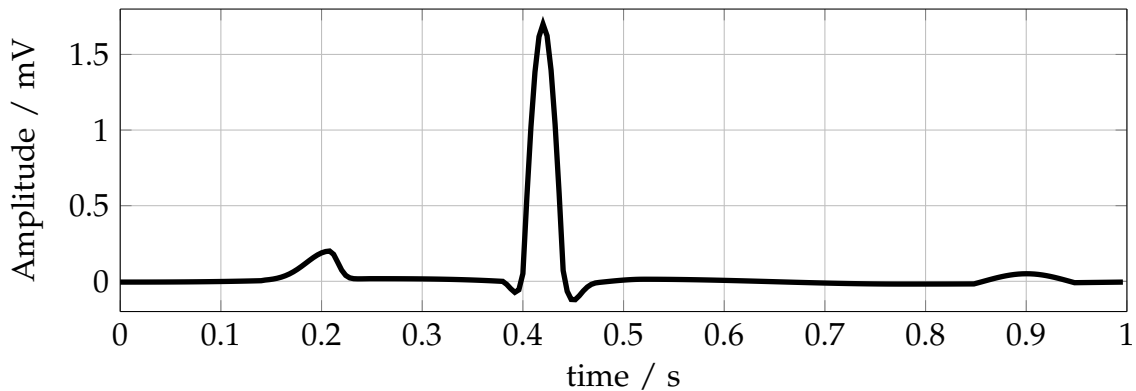
Figure 3.5.: Exemplary heart cycle with various wave parameter settings: skewed, bell-shaped P-wave adapted in onset and magnitude, sine shaped R-wave, disabled T-Wave and sine-shaped U-Wave.

3.2.3. Drag and Drop Shaping of Single Waves

A very powerful feature of this generator is the possibility to shape all single waves and their intermediate segments simply by dragging and dropping of markers (Figure 3.6). For that reason the selected segments (wave(s) and/or intermediates) are down-sampled by an adjustable factor. The resulting markers, shown for the P wave and the ST segment in Figure 3.6, can be moved arbitrarily in order to create almost any desired wave form. A piece-wise cubic Hermite interpolation is applied between the consecutive Marker points to achieve the user chosen sampling frequency.

3.2.4. ECG Time Course and Artifacts

After the construction of the single heart cycle has been completed, it can be added to an ECG time course. Thus it is possible to create any desired heart cycle series by merging single beats. Figure 3.4(c) shows such an artificial timecourse representing different morphologies with changing heart rate. To simplify the construction of long time ECGs the user is able to determine a number of n heart cycles in the Toolbar to be added to the ECG time course coming with the disadvantage that these beats all have exactly the
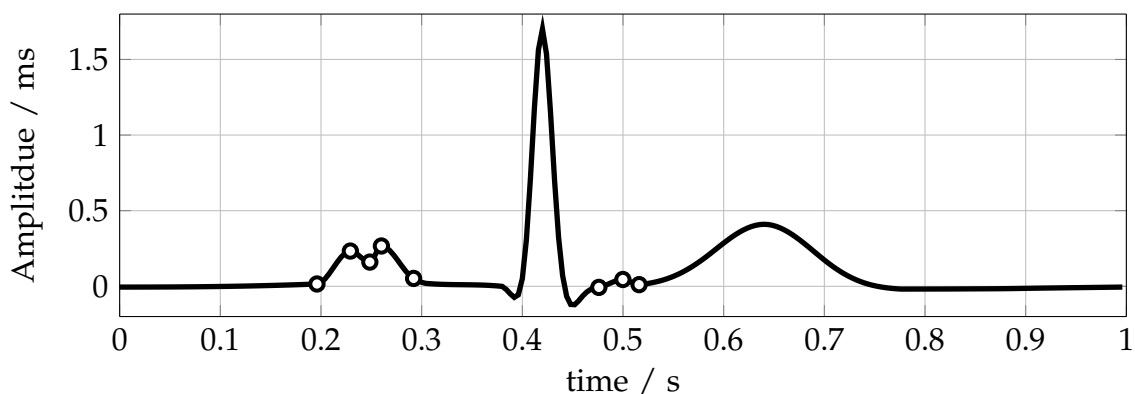
Figure 3.6.: Modifying the shape of the ECG segments by drag and drop; P-wave and ST-segment are downsampled and freely adaptable.

same morphology. If this is not desired, it is also possible to define allowed intervals for the waveform parameters. For example, one could define that the amplitude of the P wave is allowed to vary within 0.1 and 0.18 mV for the next 10 beats and create a meaningful test set in this way[5]. One could also set class labels for the specific beats for evaluating the performance of classification algorithms (Figure 3.4(f)). It should be mentioned that this generated test set can be saved in a format ready to be used with the popular machine learning software WEKA[6], however this is not part of this thesis. Furthermore white noise and motion artifacts can be applied to the series of ECG heart beats. An exemplary ECG time series superimposed with white noise and motion artifacts is shown in Figure 3.7. In a future release this could be extended by other well known noise like powerline interference or muscle artifacts.

---

[5]The test case generation follows a Gaussian distribution with mean $\mu = \frac{0.1\,\mathrm{mV} + 0.18\,\mathrm{mV}}{2} = 0.14\,\mathrm{mV}$ and standard deviation $\sigma = \frac{0.18\,\mathrm{mV} - 0.1\,\mathrm{mV}}{4} = 0.02\,\mathrm{mV}$. Thus, the interval $[0.1\,\mathrm{mV}, 0.18\,\mathrm{mV}]$ corresponds to the 95 % confidence interval.

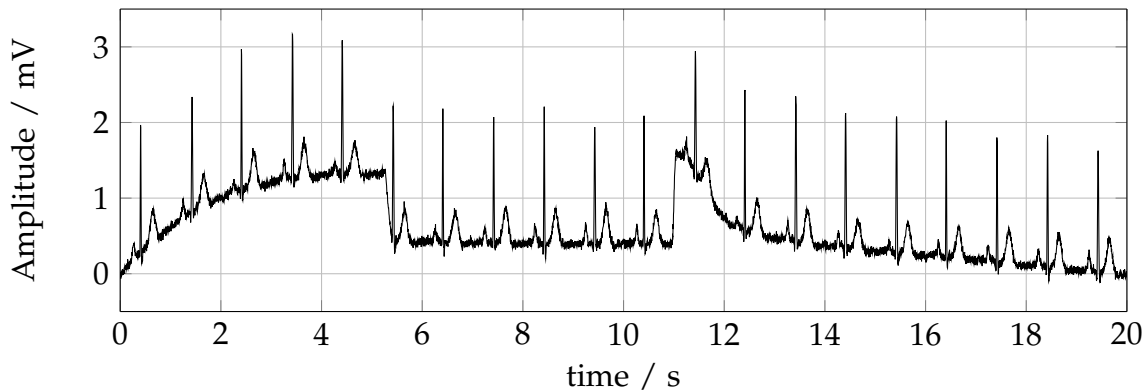[6]http://sourceforge.net/projects/weka/

Figure 3.7.: Exemplary ECG time series with superimposed white noise and motion artifacts located at 4-6 and 10-12 seconds.

3.3. ECG Delineation and Time Domain Feature Extraction

Extraction of ECG characteristic points is a crucial step for supporting physicians in making diagnosis. For that reason, clinically meaningful parameters of single beats (see Figure 1.1) are extracted automatically. The algorithm introduced in this chapter is able to read out the characteristic points shown in Figure 3.8. All other relevant time domain features, such as QRS-width, ST level or PR interval, can be derived easily from these parameters. For the beat shown in Figure 3.8 this does not seem to be very challenging. However, due to the existence of different valid P, QRS and T morphologies as well as the interference of noise (baseline wander, power-line interference, muscular noise) this has been a challenging problem for the last decades. The method chosen for ECG beat delineation is based on [3] and [4] and can be decomposed into the steps shown in Figure 3.9.

3.3.1. SDWT of the Raw ECG

As a very first step the SDWT for scales $d_1 - d_4$ of the raw ECG is determined. The mother wavelet is given by the so called biorthogonal quadratic spline
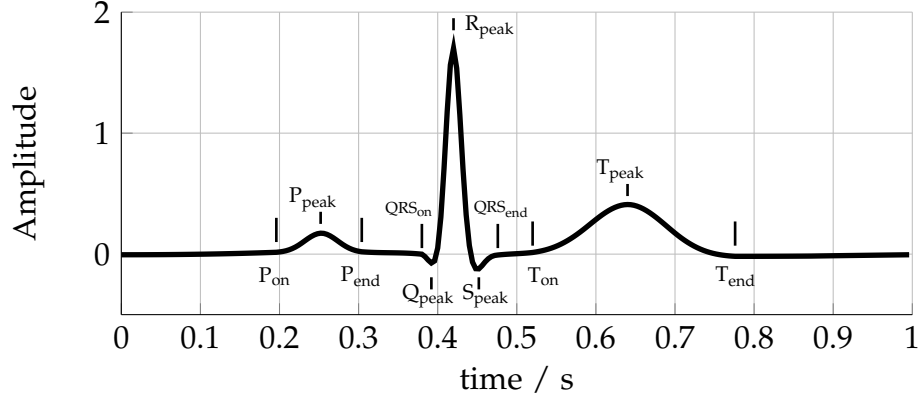
Figure 3.8.: ECG characteristic points.
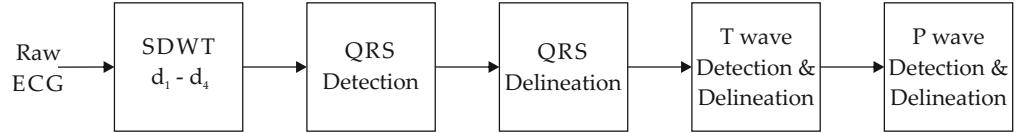
Figure 3.9.: Method used for extraction of ECG characteristic points.

wavelet $\psi(t)$, which is the derivative of its appropriate scaling function $\phi(t)$ (Figure 3.10). For this particular case it can be shown [44], that the WT at scale a is proportional to the derivative (with respect to the translation parameter b) of a smoothed version of the ECG. Smoothing is performed by the corresponding scaling filter ϕ at scale a. This means, that we are allowed to rewrite the general equation of the WT[7],

$$W(b,a) = |a|^{-\frac{1}{2}} \int_{-\infty}^{\infty} x(t)\, \psi\left(\frac{t-b}{a}\right) dt,$$

such that it corresponds to the derivative of a smoothed time-domain signal,

$$W(b,a) = -a \frac{d}{db} \int_{-\infty}^{\infty} x(t)\, \phi_a\,(t-b)\, dt, \tag{3.1}$$

---

[7]The complex conjugate is neglected here, since the mother wavelet is real valued.

where $\phi_a(t) = |a|^{-\frac{1}{2}} \phi\left(\frac{t}{a}\right)$ represents the smoothing function at a specific scale a [4].
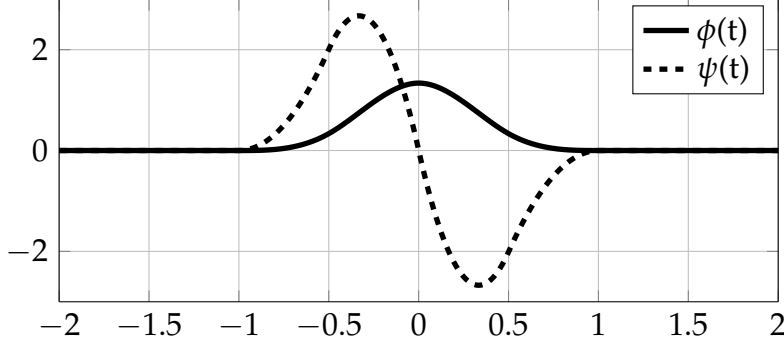

Figure 3.10.: Quadratic spline wavelet and the according scaling function.

Hence, for a particular scale a, the zero crossing at a specific translation b corresponds to a local maximum or minimum of the filtered ECG. Additionally, maxima and minima of the WT correspond to maximum positive and negative slopes. That is exactly what we are looking for, since the ECG is composed of rising and falling edges (at different frequencies) as well as local extremes.

The appropriate scaling and wavelet functions (Figure 3.10), fulfilling the desired requirements, were first derived by Mallat in 1992 [45]. The specific time-discrete realizations of $\phi(t)$ and $\psi(t)$ are given by the low-pass and high-pass decomposition filters for the biorthogonal quadratic spline wavelet, defined by the impulse responses

$$l_{\text{dec}}[n] = \frac{1}{8}\delta[n+2] + \frac{3}{8}\delta[n+1] + \frac{3}{8}\delta[n] + \frac{1}{8}\delta[n-1]$$

and

$$h_{\text{dec}}[n] = 2\,\delta[n+1] - \delta[n].$$

(3.2)

Subsequently, wavelet coefficients for scales one to four are determined via the filter-bank implementation without decimation (Algorithme à Trous), which is shown in Figure 3.11.

Figure 3.12 illustrates the frequency responses of the equivalent finite im-

3. Methods
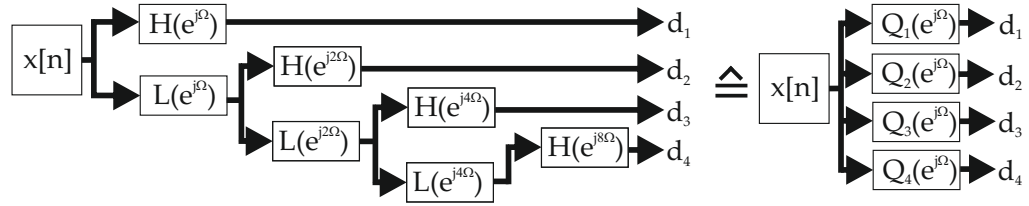
Figure 3.11.: Filter-bank implementation used for determination of the wavelet coefficients (compare to Figure 2.11).

pulse response (FIR) filters

$$Q_m(e^{j\Omega}) = \begin{cases} H(e^{j\Omega}) & \text{if } m = 1 \\ H(e^{j\,2^{m-1}\Omega}) \prod_{k=0}^{m-2} L(e^{j\,2^k\Omega}) & \text{if } m \geq 2. \end{cases} \tag{3.3}$$
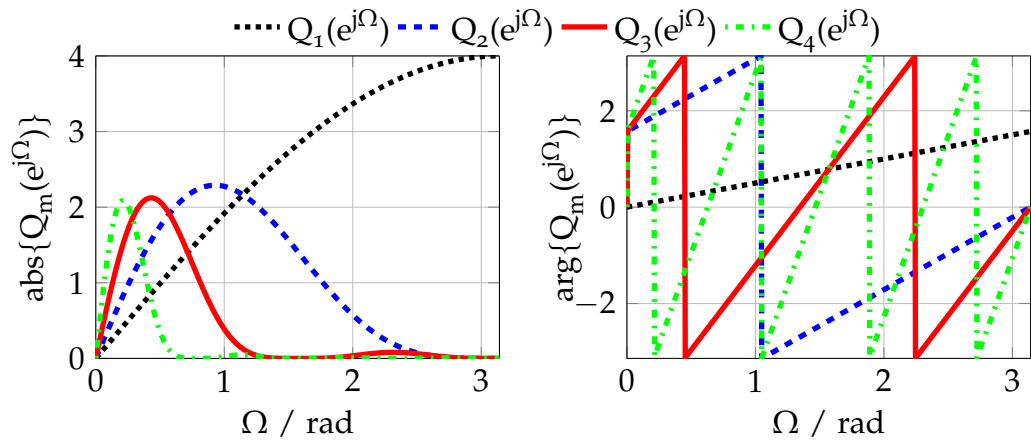
Figure 3.12.: Frequency response (magnitude and phase) of equivalent filters $Q_m(e^{j\Omega})$.

We observe, that all equivalent filters Q_m are linear phase. However, the phase lags are different for the scales one to four, i.e., $d_1 - d_4$ should be realigned in order to receive the same delay with respect to the raw ECG. The phase lag of a single scale can be calculated via the slope of the phase response, turning out to be $\frac{2^m - 1}{2}$.

The realigned wavelet coefficients $d_1 - d_4$ of a test sequence, consisting of typical P and R wave patterns, are shown in Figure 3.13.
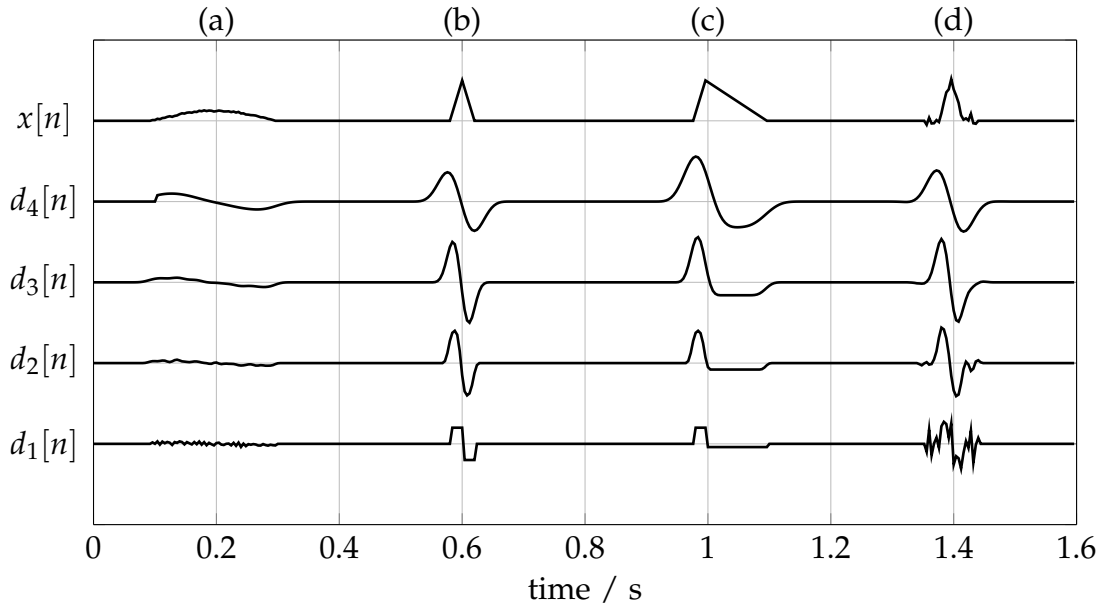
Figure 3.13.: Realigned wavelet coefficients $d_1 - d_4$ for a test sequence. (a) Typical P wave, (b) Typical R wave, (c) Asymmetric R wave, (d) R wave corrupted by noise.

The wave forms produce positive maximum - negative minimum pairs for the different scales. The zero crossings in between these pairs mark the local maxima of the accordingly smoothed test sequences. Since the P wave is generally lower frequent than the QRS complex, the main deflections can be detected in scales three and four (Figure 3.13 (a)). For a symmetric unipolar wave (Figure 3.13 (b)) Li et al. state, that all scales can be realigned, such that all zero-crossings correspond to the peak of the unipolar wave. However this is not true for asymmetric deflections, as shown in Figure 3.13 (c). The zero-crossing for the lower frequent scales do not match the local maximum exactly, i.e., we would make a mistake in these scales. For d_1, however, this mistake is zero. Unfortunately this high frequent scale is often corrupted by noise making the determination of the "right" zero crossing very difficult (Figure 3.13 (d)). Hence, we will have to find a way to find the correct zero crossing in d_1 as described in the following section.

3.3.2. R Peak Detection

The QRS complex is the most striking feature in an ECG and is therefore detected at first. For that reason we search for local positive maxima (rising edge) and negative minima (falling edge) in scales $d_1 - d_4$ (Figure 3.14). These maxima and minima are called modulus maxima (MM) from now on. Chaining the MM of the different scales, whereas the MM lying closest to each other are connected, lead to so called modulus maxima lines [19]. These MM lines are illustrated as dashed lines in Figure 3.14. Usually this is performed for the absolute values plotted in a scalogram, however we want to distinguish between positive and negative MM lines. Hence, modulus maxima lines are determined separately for positive maxima and negative minima.
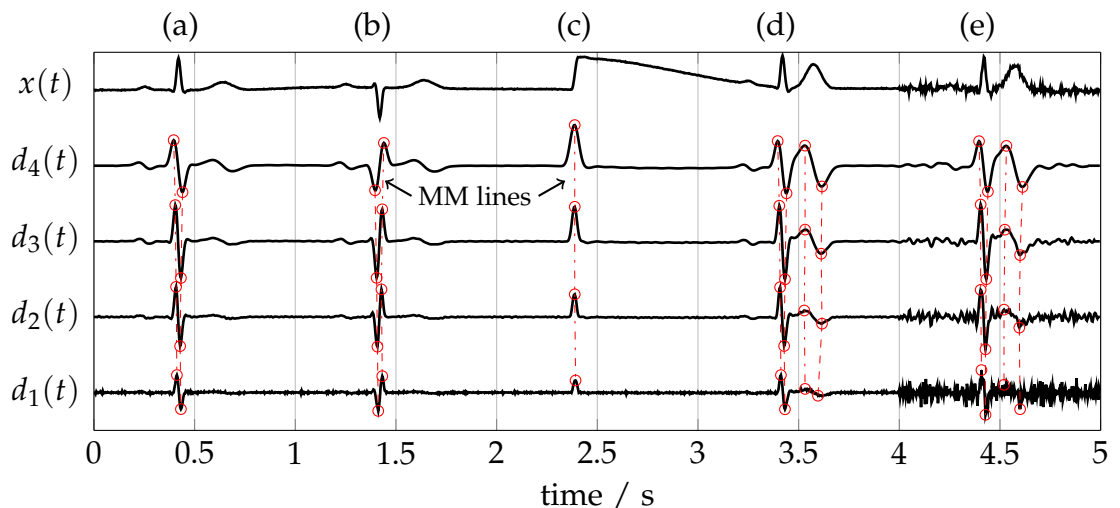
Figure 3.14.: MM higher than a specific scale dependent threshold for QRS detection. MM lines are shown as dashed lines. (a) Normal QRS complex, (b) large negative deflection (c) motion artifact, (d) unusual high T wave (e) noisy ECG with unusual high T wave.

As a first step the QRS detection algorithm determines MM lines for MM with an absolute value greater than a scale dependent threshold[8]. The search for a "valid" MM line origins at scale four, since this is the most robust scale

---

[8]In the following specific thresholds or search windows generally will not be given

regarding high frequency noise and therefore holds the lowest number of MM. Consequently all MM of level one to three, which are not within a specific neighborhood of the level 4 MM are not considered. In a next step we want to identify the correct MM of scale 3 belonging to a scale 4 MM. If there are more than one potential candidates within a neighborhood of a level 4 MM, the one best suited is determined via the following criteria:

1: $MM_{L3, best} \leftarrow$ nearest neighbor of current MM_{L4}
2: **for** all candidates in neighborhood **do**
3:     $MM_{L3} \leftarrow$ current candidate
4:     **if** value$(MM_{L3})/(2 \cdot$ distance$(MM_{L3}, MM_{L4})) >$
         $1.2 \cdot$ value$(MM_{best})/$distance(MM_{best}, MM_{L4}) **then**
5:         $MM_{L3, best} \leftarrow MM_{L3}$
6:     **end if**
7: **end for**

This prevents the algorithm from taking small local MM instead of significant MM just because the small ones are nearer to the L4 MM. Subsequently the same procedure is carried out for level 2 and level 1 MM.

By deleting all MM of scales one to three, which do not have a related MM in the next lower frequent scale, a set of potential MM lines for R peak detection is obtained (Figure 3.14 - dashed lines). However, there still might be MM lines not belonging to a QRS complex within this set. These are eliminated through the following steps:

- Delete isolated MM lines:
  A positive (negative) MM line is considered to be isolated, when there is no corresponding negative (positive) MM line within a neighborhood of 100 ms (Figure 3.14 (c)).
- Delete redundant MM lines:
  There must be a minimum distance between two positive (negative) MM lines, which is given by the maximal heart rate. In case that there are two or more positive (negative) MM lines within this minimum distance, the best suited positive (negative) MM line is determined based on the values of the MM and the distances between the positive

---

explicitly in the subsequent explanations. However, recommended values can be found in [4].

and negative MM. A possible scenario is shown in Figure 3.14 (d), where another significant MM pair is detected because of an unusual high T wave. Comparing Figure 3.14 (d) and Figure 3.15 (d), we observe that the correct MM pair is eliminated.
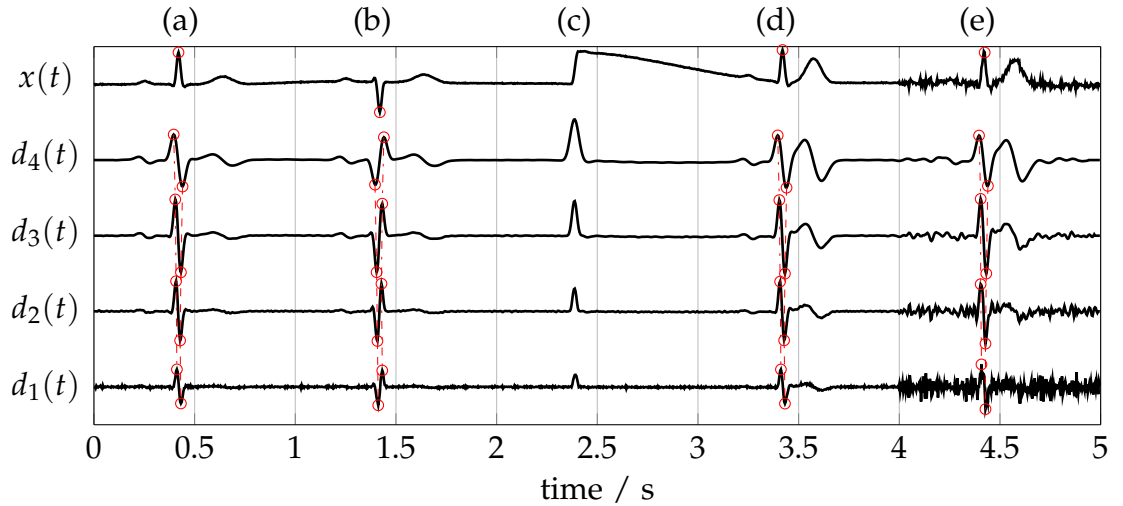
Figure 3.15.: Detection of QRS complex after eliminating isolated and redundant MM. (a) Normal QRS complex, (b) large negative deflection (c) motion artifact, (d) unusual high T wave (e) noisy ECG with unusual high T wave.

Finally the locations of the R peaks are detected by finding the zero crossings between the MM pairs for scale one, since this scale is most accurate regarding temporal information (Figure 3.15 - $x(t)$).

3.3.3. Detection of the Q and S Wave

After determining the locations of the R peaks (t_R), the algorithm continuous by detecting the peak positions of the Q and S waves (t_Q, t_S) as well as the onset and end of the QRS complex ($t_{Q_{on}}$, $t_{S_{end}}$ - Figure 3.16).

Although the typical length of the QRS complex is 110 ms, the search window starts 120 ms before t_R and ends 150 ms after t_R in order to allow untypical QRS morphologies (Figure 3.17). As stated in [4] Q and S waves
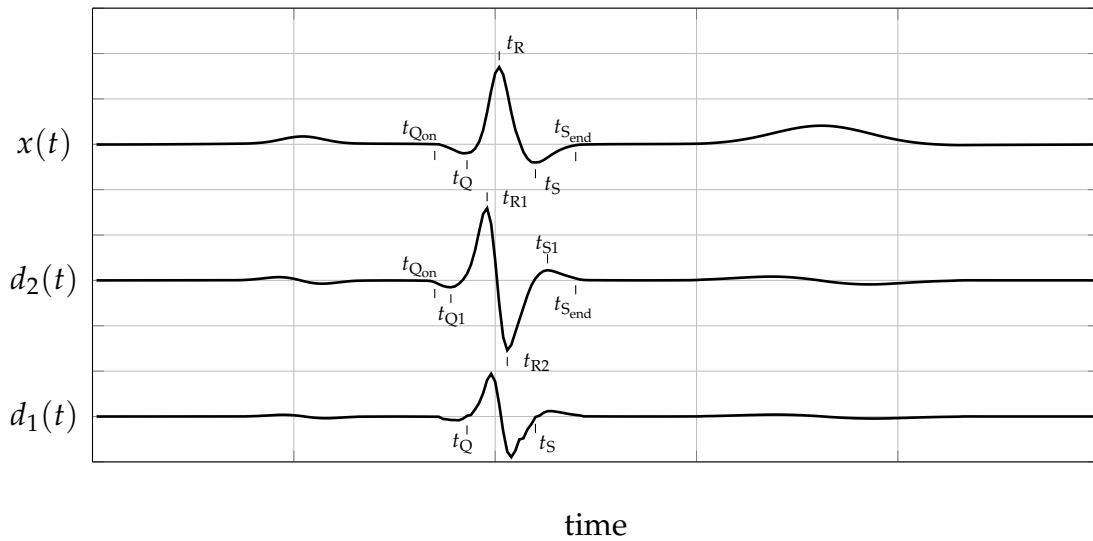
Figure 3.16.: Determining onset peak and end of the Q and S wave for the standard QRS complex.
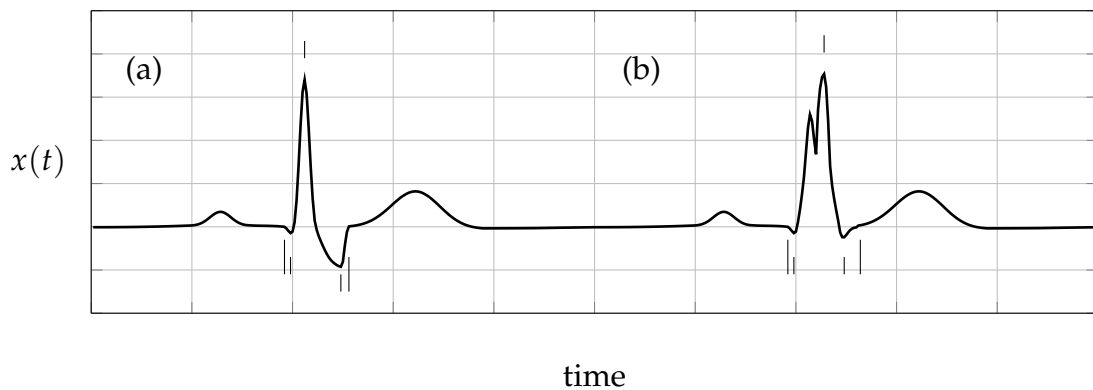
Figure 3.17.: (a) Unusual deep S wave and (b) notch in R wave.

do have their main frequency content within scale two. Hence, the search for significant MM is performed for this scale.

As shown for the standard QRS complex (Figure 3.16), the algorithm starts at t_R, which is bordered by a pair of MM (t_{R1} and t_{R2}). This pair corresponds to the maximal slopes of the R wave's rising and falling edges. We search for

significant MM before t_{R1} and after t_{R2} in order to detect the slopes of the Q and S waves (t_{Q1}, t_{S1}). If there exist more than one significant MM, the one best suited is chosen via a criterion based on the distances to t_{R1} or t_{R2} and the absolute values of the competing MM. Similarly to the determination of the R peak, the according zero crossings at scale one are then used to identify the peaks of the two waves (t_Q, t_S).

In order to determine the onset of the QRS complex, the algorithm departs from the earliest significant MM and searches to the left. Afterwards three potential candidates for the onset of the QRS complex are identified:

- Candidate 1: The absolute values of d_2 fall below a specific threshold.
- Candidate 2: A local maximum or minimum is found.
- Candidate 3: The beginning of the search window is reached.

Subsequently the candidate lying closest to the R peak (the most right one) is defined to be the onset of the QRS complex. In case that no significant MM are detected (no Q wave), the algorithm simply starts its search for the onset at t_{R1}. A similar procedure is performed for finding the end of the QRS complex (just the other way round).

Based on the presence or absence of significant MM and on their signs (positive or negative), we finally distinguish between the following cases:

- Normal QRS complex: Figure 3.18 (a)
- R complex: Figure 3.18 (b)
- qR complex: Figure 3.18 (c)
- Rs complex: Figure 3.18 (d)
- Qr complex: Figure 3.18 (e)
- rS complex: Figure 3.18 (f)
- QS complex: Figure 3.18 (g)
- rSr' complex:Figure 3.18 (h)

3.3.4. Detection of the T Wave

In contrast to the QRS complex, the T wave is a slowly varying signal. Due to this, the search for significant MM is performed at scale four. The search window starts at the end of the QRS complex and its length depends on the current RR interval. Within this search window, a set of significant MM is

time / s
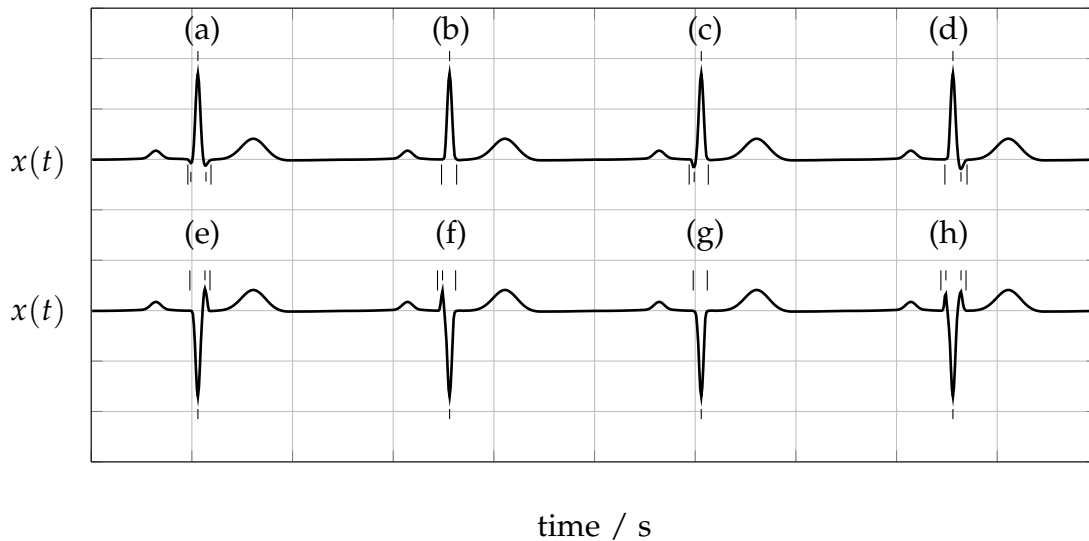
Figure 3.18.: Exemplary QRS complexes: (a) Normal QRS, (b) R, (c) qR, (d) Rs, (e) Qr, (f) rS, (g) QS and (e) rSr′ complex.

identified by extracting all MM greater than an interval dependent threshold. The simplest case would be to find one positive and one negative MM leading to the identification of a normal or inverted T wave (Figure 3.19 (a)-(b)). The zero-crossing between this pair of MM corresponds to the peak of the wave and is identified in scale three due to the better time resolution. However, there are some more valid morphological variants of the T wave which are identified by the algorithm:

- Positive biphasic T wave: Figure 3.19 (c)
- Negative biphasic T wave: Figure 3.19 (d)
- Ascending T wave: Figure 3.19 (e)
- Descending T wave: Figure 3.19 (f)

As observable in Figure 3.19 (c), a positive biphasic T wave is expressed by a significant positive MM surrounded by two significant negative MM. However, there might be invalid MM within the identified set of MM (e.g. two or more consecutive positive MM, MM caused by a discontinuity). These invalid MM are eliminated via the following strategies:

53
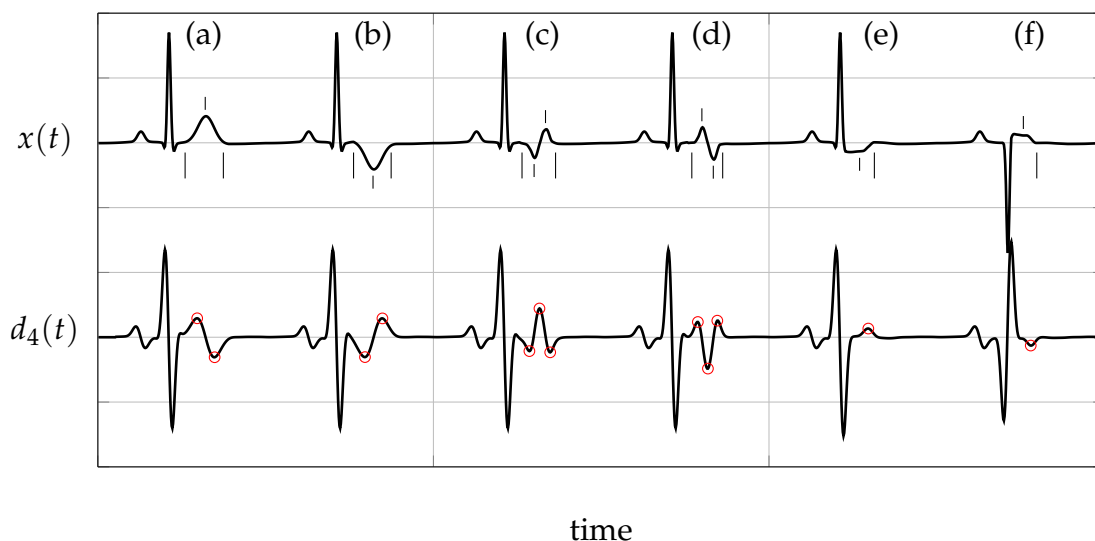
Figure 3.19.: Exemplary T waves: (a) Normal, (b) inverted, (c) positive biphasic, (d) negative biphasic, (e) ascending, and (f) descending T wave.

- MM lines with a significant MM in scale one (highest frequent scale) are eliminated since this most probably is some kind of artifact (e.g. a motion artifact).
- MM which are smaller than an eighth of the most significant positive and negative MM are considered to be irrelevant small deflections and are eliminated.
- In case of a biphasic T wave, the two surrounding MM must be approximately equal. If this is not the case, one of them is eliminated based on the distance to the center MM and the absolute values of the MM.

Finally the appropriate type of morphology is determined and onset as well as end of the T wave are defined via a similar strategy as used for the QRS complex. If desired, the algorithm also tries to identify a U wave within a specific search window following the T wave.

3.3.5. Detection of the P Wave

The detection and delineation of the P wave is very similar to the process described for the T wave. The main differences are the use of smaller thresholds and that only four different morphologies are distinguished (normal, inverted, positive and negative biphasic). The search window starts at the end of the T wave (or U wave, in case that this wave exists) and ends at the beginning of the QRS complex. All other strategies are similar to the ones described above and will not be discussed again at this point.

3.4. Data Generation

To verify the correct functionality of the segmentation algorithm, test sets were obtained via three different ways:

- Artificial ECG beats generated with $GECG^2O$.
- Real patient data from the QT database of Physionet [5].
- Real patient data from the study database of the AKh Linz.

3.4.1. Artificial ECG Beats - $GECG^2O$

The $GECG^2O$ can be used to test the algorithm's ability to recognize different morphologies and to correctly extract the corresponding ECG characteristic points for these cases. The most interesting ECG morphologies, such as biphasic waves or variations of the QRS complex, were already introduced in Section 3.3. These test cases were generated via the $GECG^2O$ and were successfully processed by the ECG delineation algorithm. Hence, the ability of the algorithm to extract ECG characteristic points for various types of ECG beats was already shown in the sections above and will not be repeated.

Instead, the suitability of the algorithm to detect minimal relative alternations in a patient's ECG before and after an event (cmp. Figure 1.2) is illustrated. For that reason the following test scenario is defined:

Minimal prolongation of the PR interval and minimal elevation of the ST segment:

The PR interval is an important clinical parameter for the assessment of conduction disturbances. A very popular example is the so called first-degree atrio-ventricular block caused by a conduction disturbance in the AV node or the bundle of His (for more details see [9]). This atrio-ventricular block results in a prolongation of the PR interval. Minimal changes of the PR interval over time might provide important information regarding the patient's state of health for the physician. Hence, it makes sense to detect minimal relative changes of the PR interval.

ST segment elevation can be an important indicator for anterior or myocardial infarction as well as for ischemic cardiac diseases (for more details see [9]). Therefore minimal relative changes of the ST level also provide important information for the physician.

In order to illustrate the algorithm's ability to detect minimal relative changes of these parameters, two data sets were created. The first simulates the patient's ECG before an specific event (normal PR interval, normal ST level) and the second simulates the ECG after a specific event (longer PR interval, ST level elevated). The combination of a prolonged PR interval and the elevation of the ST level does not have a specific medical meaning. These parameters were simply chosen since they have shown to be clinically useful for physicians. The two test ECG sequences were generated as described in Section 3.2.4, whereas lower and upper bounds for all important ECG parameters were defined. These limits do not have a specific meaning, but were chosen to be realistic. Except for the starting point of the QRS complex and the offset of the ST segment (ST level), the boundaries do not differ for the first and second data set. Table 3.2 shows the chosen parameter setting for the onset of the QRS complex (and the resulting PR interval), the level of the ST segment and the amplitude of the P wave as a representative for all other parameters. The onset of the P wave was left constant, while the onset of the QRS complex was varied as shown in Table 3.2 in order to achieve the desired variation of the PR interval. The lower and the upper limits were defined via the $GECG^2O$, while mean and standard deviation of the parameters were calculated as described in Section 3.2.4.

We then created 500 ECG beats (approximately 10 minutes) covered in Gaussian noise with SNR = 30 dB for each set. All ECG characteristic points were

	Dataset 1: Beats $1-500$				Dataset 2: Beats $501-1000$			
	LL	UL	μ	σ	LL	UL	μ	σ
QRS_{on} in ms	360	376	368	4	380	396	388	4
PR interval in ms	164	180	172	4	184	200	192	4
ST offset in mV	-20	20	0	10	10	50	30	10
P_{amp} in mV	146	170	158	6	146	170	158	6

Table 3.2.: Lower and upper limits (LL, UL) for onset of the QRS complex, ST offset and amplitude of the P wave defined via GECG^{2}O. The limits for the PR interval result from QRS_{on} and a constant $P_{on} = 196\,$mV.

extracted by applying the ECG delineation algorithm. Figure 3.20 shows a set of randomly picked beats of every set, whereas we observe that there is no obvious difference between these sequences at first glance. The zoom level of the ECG series shown in Figure 3.20 should be approximately equal to the zoom level of common ECG monitors in hospitals.

The extracted ECG characteristic points were compared via estimated probability density functions (pdf) and a two-sample t-Test[9]. The results are shown in Section 4.1.

3.4.2. The QT Database

The QT database (QTDB) provides more than 3000 manually annotated ECG beats designed for the evaluation of segmentation algorithms and includes a broad variety of QRS and ST-T morphologies [5]. Hence, this database is suited to assess the robustness of our algorithm with regard to the inter-variety of different patient's ECGs.

All beats, which were manually annotated by one expert, are extracted and compared to the results provided by the algorithm. For every ECG characteristic point labeled by the expert, the difference between the expert label and the time instant determined by the algorithm was calculated. In a next step mean (μ) and standard deviation (σ) for all differences was

---

[9]Simply said, the two-sample t-test is used to determine if the two means of the samples are equal. In our case we want to find out, whether the means of the PR interval and the ST level are equal for data set one and two. For more information on the t-test see e.g. [46].

(a)

$x_1(t)$

time

(b)

$x_2(t)$

time
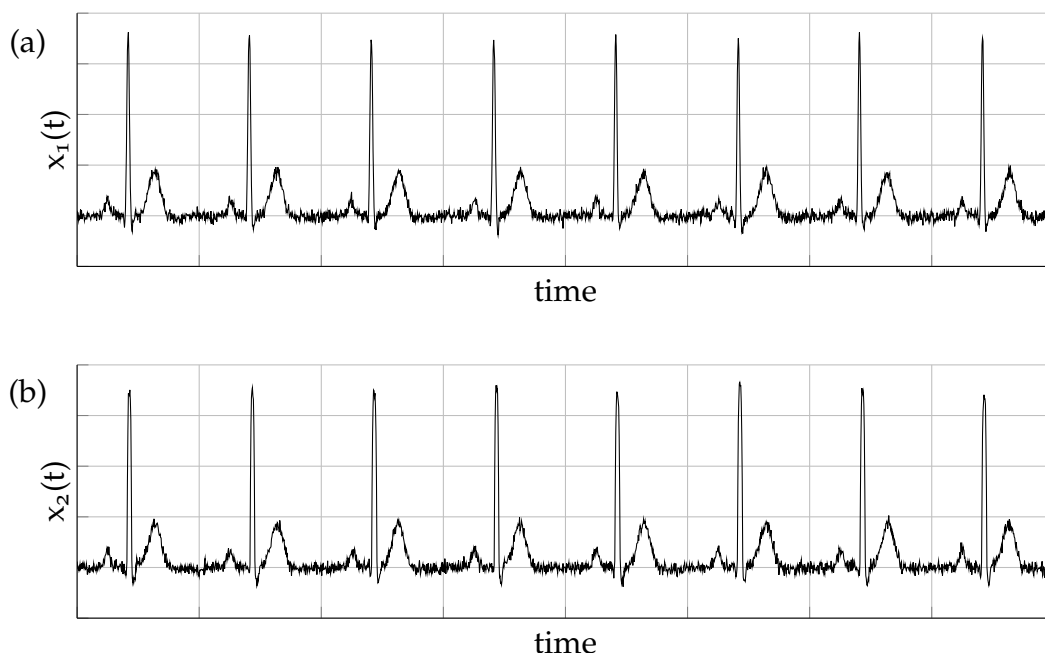
Figure 3.20.: Artificially generated noisy ECG with no obvious difference at first glance. (a) Normal PR interval, normal ST level and (b) prolonged PR interval and ST elevation.

determined. Every patient record consists of two leads, which both were visible for the expert when annotation was carried out [5]. Thus, both leads were processed by the algorithm and the relevant differences for calculating μ and σ were determined by taking the minimum distances between the expert labels and the algorithm labels. Sometimes it is more difficult to identify a specific characteristic point in one lead than in the other one (Figure 3.21). For the P wave the expert obviously preferred the first lead available (Figure 3.21 (a)). In contrast, the peak of the T wave is easier to identify in the second lead available (Figure 3.21 (b)). Looking only at the first lead, we might also think of a normal T wave and subsequently would be far away from the second lead's labels of the T wave. Since the algorithm is not able to deal with both leads simultaneously we used the strategy described above and suggested by [4] to receive a reasonable result for the mean and standard deviation of the error. This might make our results slightly better

than they really are, but for this evaluation we wanted to compare our results with another ECG beat segmentation algorithm [31]. Annotations for this algorithm are provided on Physionet as well and were therefore used for comparison. We used exactly the same strategy to determine μ and σ of the differences as we did for the algorithm implemented within this thesis. The algorithm's ability to detect P and T waves as well as the QRS complex is expressed by calculating the sensitivity (Se). This characteristic value was determined by dividing all true positive (TP), i.e., all waves which were correctly detected by the algorithm, by the total number of existing waves in the according data set,

$$Se = \frac{\text{true positive}}{\text{true positive} + \text{false negative}}$$

$$Se = \frac{\text{TP}}{\text{TP} + \text{FN}}.$$

(3.4)

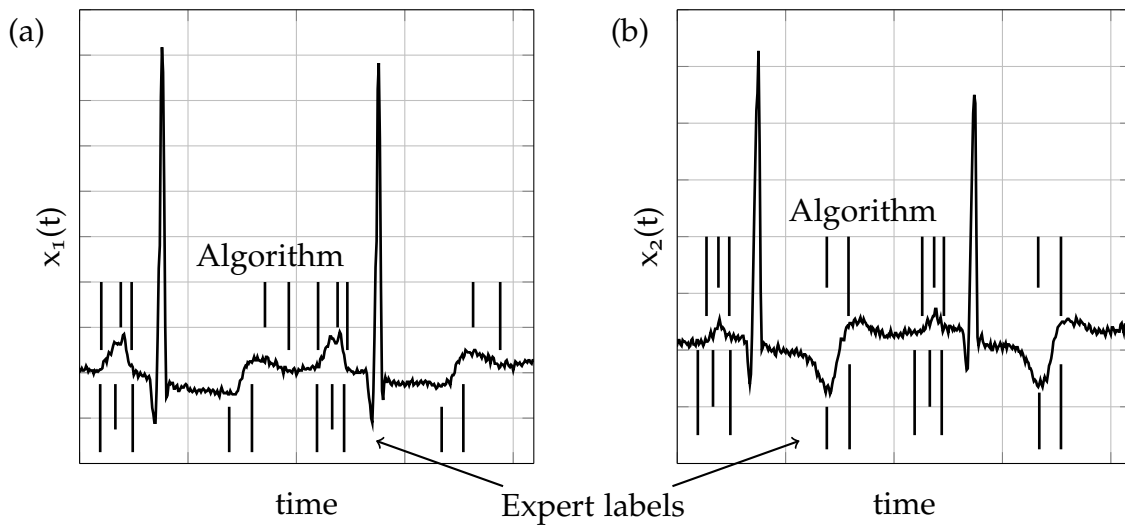Figure 3.21.: Expert and algorithm labels for the two available leads. For the P wave the expert labels fit very well for the first lead (a), but do not fit that well for the second lead (b). The correct T wave is easier to identify in the second lead (b).

In our case the true positive correspond to the waves detected by the algorithm and the expert, while the false negative are formed by the waves

only detected by the expert. A small set of patient records was excluded from evaluation due to the author's opinion that these data sets are of little relevance. A so called prominent U wave (Figure 3.22), e.g., is not identified correctly by the algorithm as done by the expert. This is a limitation of the algorithm, since a tall T wave is detected instead. However, this kind of limitation is not of any relevance for our future studies and is therefore tolerated. All other excluded sets are similar to this case and are summarized in Table 3.3.
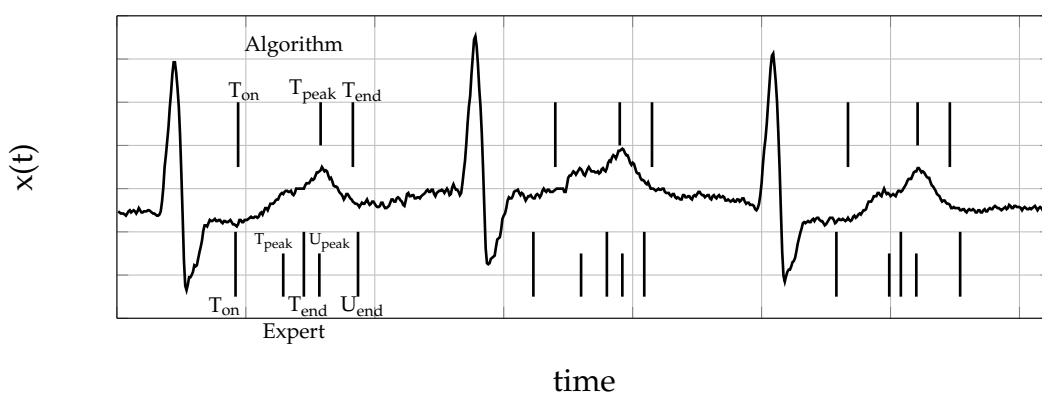
Figure 3.22.: Excluded data set sel36: A prominent U wave (U amplitude higher than T amplitude) was identified by the expert. This is a limitation of the algorithm, which would simply detect a T wave. The labels for the second and third beat have the same sequence than the first one.

Expert markers were automatically extracted from Physionet via a Matlab$^{\circledR}$ script and then compared to the algorithm's result. Table 4.1 in Section 4.2 presents the results for the algorithm implemented within this work and the algorithm based on LPD [31].

3.4.3. Study Database of the AKh Linz

A set of 26 morphological interesting heart beats of 15 different patients was selected by a senior physician (Figure 3.23). These beats were taken

Record	Number of beats	Reason for exclusion
sele0409	30	Morphology of T wave not relevant
sel36	31	Morphology of T and U wave not relevant
sel31	30	Morphology of T wave not relevant
sel38	30	Insignificant P wave
sel40	30	Insignificant P wave
sel45	30	Morphology of T and U wave not relevant
sel47	30	Morphology of T and U wave not relevant
sel50	32	Morphology of T and U wave not relevant

Table 3.3.: Data sets excluded from evaluation of the ECG beat segmentation algorithm.

from the study database of the AKh Linz[10], and were labeled by 18 experts (assistant as well as senior physicians).

To allow efficient and fast labeling, a Matlab$^{\circledR}$ graphical user interface (GUI) for setting onset, peak and end of P, Q, R, S as well as T wave was implemented within this thesis (Figure 3.24). The Matlab$^{\circledR}$ standalone provides the possibility to set 13 labels per beat at maximum[11]. Furthermore other features like the possibility to label waves as "not present", an automatic zoomed view or the possibility to scroll through the ECG sequence were implemented as well but are not discussed in detail here.

Subsequently, box-plots showing the interquartile range (IQR) and the whiskers[12] of our expert labels for all beats and characteristic points were created. An example is shown in Figure 3.25, the results for all other beats are presented in Section 4.3. For better visualization, the median of the current data set was subtracted from the according expert labels, such that all medians of the resulting distributions are equal to zero. Based on these estimated distributions available for every beat and every characteristic point, an exclusion criterion was defined. If the IQR of the expert labels

---

[10]Released by the ethics committee of Upper Austria in the course of the project "Herzfrequenzvariabilität und EKG Morphologie bei Intensivpatienten."

[11]P_{on}, P_{peak}, P_{end}, QRS_{on}, Q_{peak}, $Q_{end} = R_{on}$, R_{peak}, $R_{end} = S_{on}$, S_{peak}, QRS_{end}, T_{on}, T_{peak}, T_{end}.

[12]For more information see e.g. http://de.mathworks.com/help/stats/boxplot.html.

for a specific characteristic point is higher than the typical duration of the according wave (Table 2.2), this characteristic point is excluded from the evaluation of the algorithm. The reason for that is, that we would not receive a reliable value of the difference between the median of the expert labels and the algorithm label for such a wide scattering of the expert labels. Fortunately only 5 characteristic points needed to be excluded (Table 3.4).
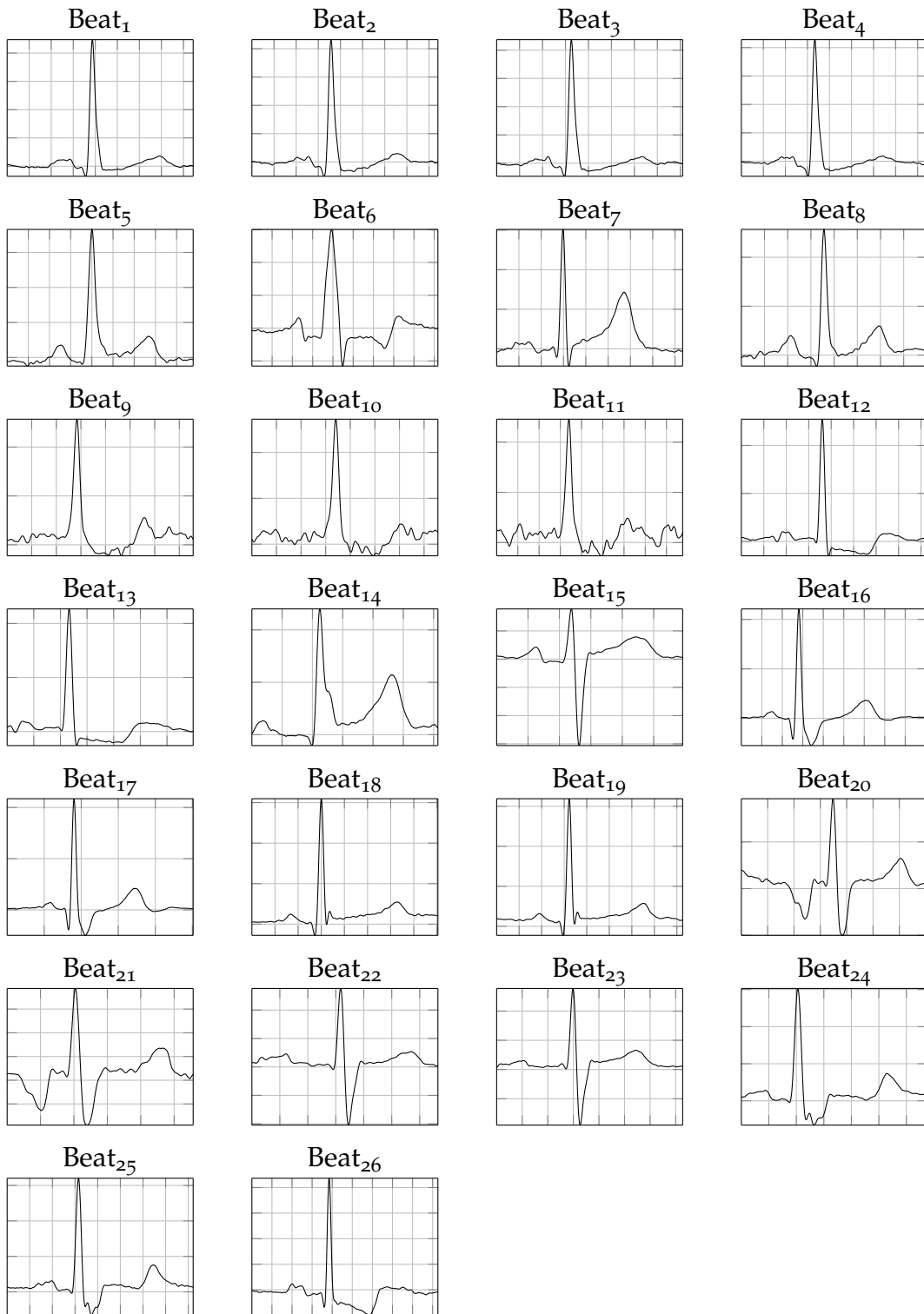
Figure 3.23.: Set of 26 beats selected for evaluation of the algorithm.
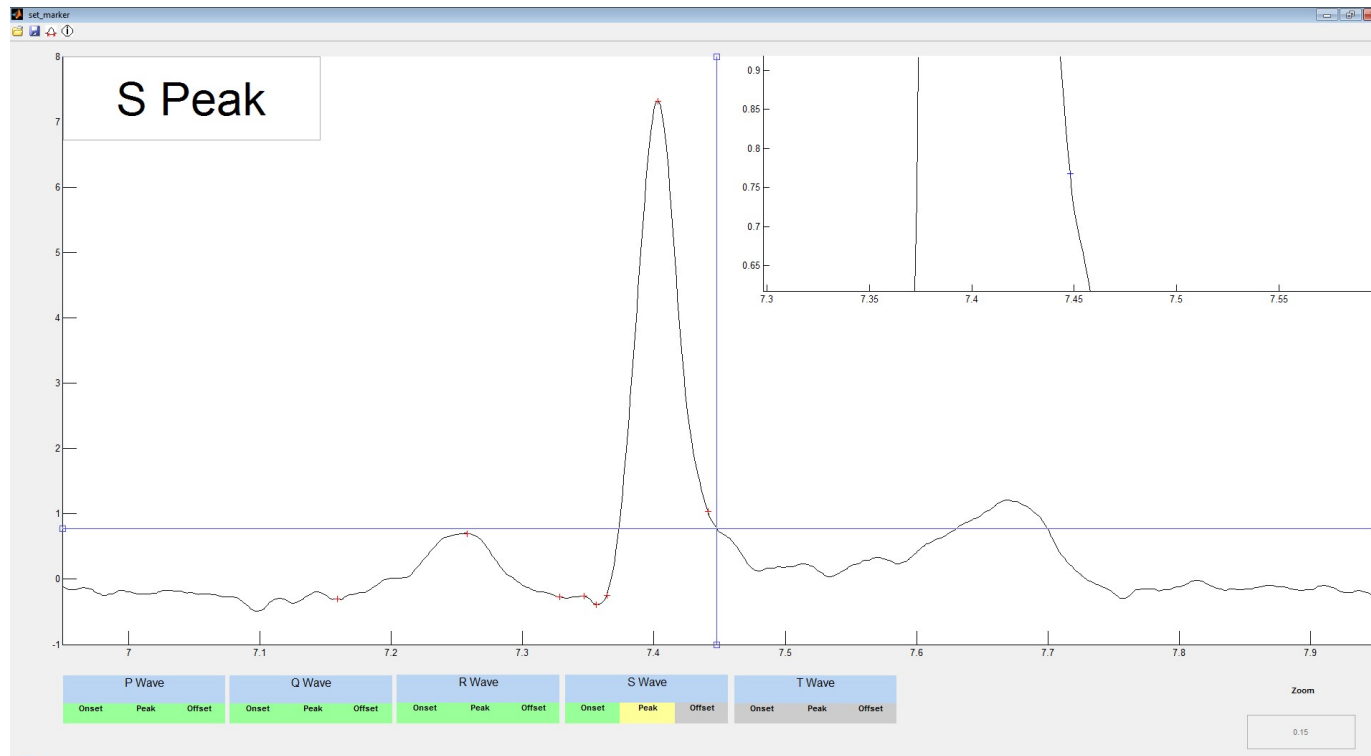
Figure 3.24.: GUI for labeling ECG characteristic points.
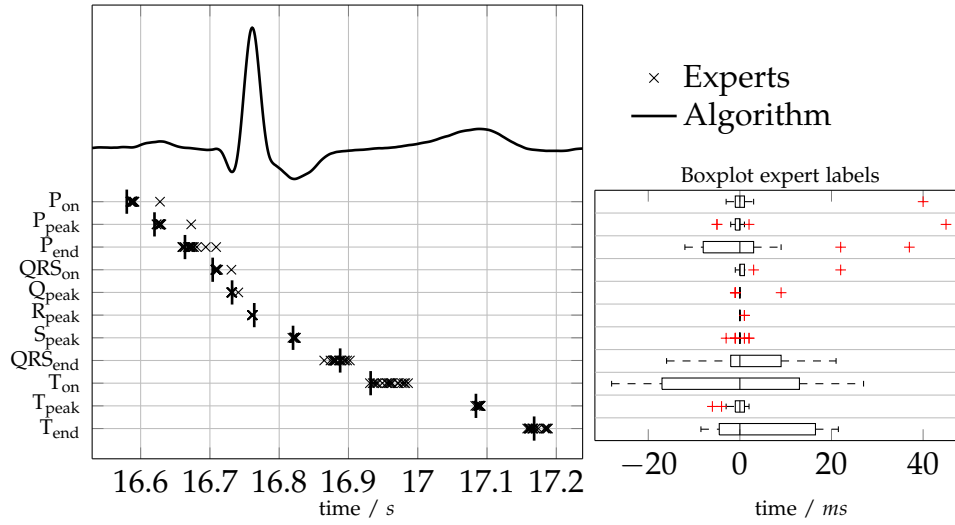
Figure 3.25.: Labels set by experts and by the algorithm for beat 17 and the according box-plot.

Beat	11	11	11	11	12
Characteristic Point	P_{on}	P_{peak}	P_{end}	QRS_{on}	QRS_{end}
IQR / ms	180	154	150	21	30

Table 3.4.: Characteristic points excluded for evaluation of the segmentation algorithm.

Finally, the median of the differences between the median of the expert labels and the algorithm label was determined. The result is again visualized via a box-plot and can be found in Section 4.3 (Figure 4.5).

4. Results

4.1. Artificial ECG Beats - GECG^{2}O

Figure 4.1.: Comparison of ECG characteristic points before and after an event for noisy ECG. (a) PR interval, (b) ST level and (c) P wave amplitude.

Figure 4.1 shows the estimated pdfs of three ECG characteristic points before and after a specific event, e.g. an intervention by a physician. We observe that the pdfs of the extracted PR intervals (Figure 4.1 (a)) and the ST levels (Figure 4.1 (b)) significantly differ before and after the event. This is not true for the amplitude of the P wave, which represents an ECG characteristic point which did not change significantly over time. As a result, the relative prolongation of the PR interval and the elevation of the QT interval are detected successfully.

For comparison we show the estimated pdfs based on the extracted ECG characteristic points for the clean ECG (Figure 4.2). Comparing Figure 4.1

and Figure 4.2 we observe that the standard deviations of the distribution are significantly influenced by the noise. However for the noisy ECG it is still possible to reliably detect relative changes of the ECG characteristic points.

This is also verified by the results of the two-sample t-test performed for the noisy ECGs. For the PR interval and the ST level we can reject the so called null hypothesis that test set one (before event) and test set two (after event) come from a single normal distribution with the same mean and unknown variance at the 5 % significance level. This means that we do have a statistically significant difference between the PR intervals (ST levels) before and after the event. For the P amplitude we cannot reject the null hypothesis at the 5 % significance level, i.e., we cannot claim that there is a statistical significant difference between the P amplitude values of the two data sets.
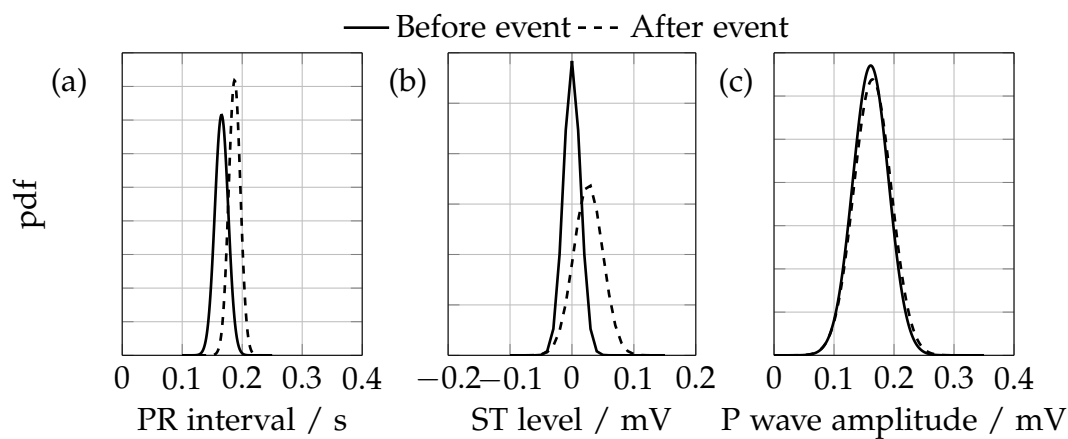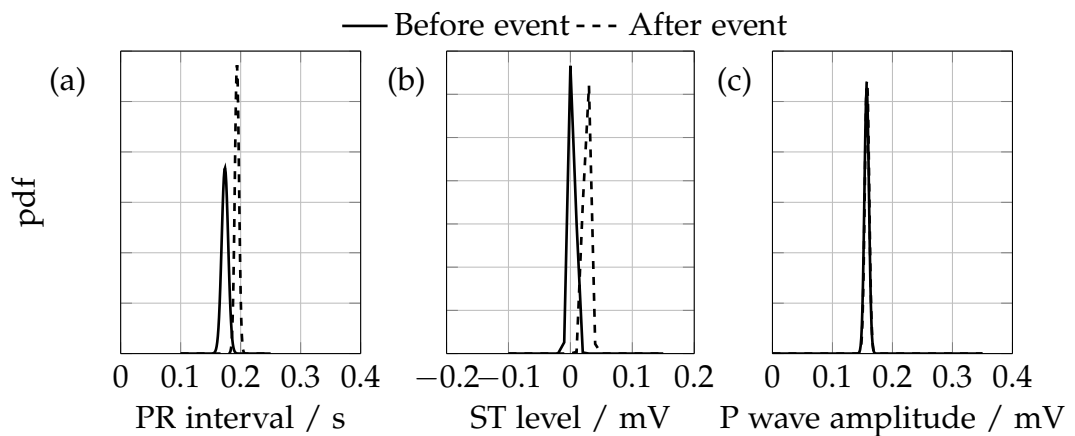

Figure 4.2.: Comparison of ECG characteristic points before and after an event for clean ECG. (a) PR interval, (b) ST level and (c) P wave amplitude.

4.2. The QT Database

Table 4.1 shows mean and standard deviation of the differences between expert labels and the labels determined by the segmentation algorithm

implemented within this work. For comparison the same is illustrated for the work of Laguna et al. [31].

Sensitivity lies between 98 % and 100 % and is very similar for both algorithms. While the values for the mean difference seem to be a bit smaller for the work based on LPD, the standard deviations of the differences tend to be higher than in this work. In total, for the segmentation algorithm, the mean deviations from the expert labels are below 12 ms. The standard deviation usually lies between 9 ms and 23 ms, except for the onset of the T wave, where it is significantly higher (38.5 ms).

| | Annotations | WT | | | LPD | | |
| | | Se | μ | σ | Se | μ | σ |
	-	%	ms	ms	%	ms	ms
P_{on}	2959	98.77	−11.21	16.10	98.30	−10.32	23.49
P_{peak}	2959	98.77	−2.49	13.42	98.30	−0.73	20.54
P_{end}	2959	98.77	3.67	19.83	98.30	4.15	17.57
QRS_{on}	3380	99.91	−6.28	9.67	99.91	3.70	11.51
R_{peak}	3380	99.91	1.15	9.60	99.91	3.34	11.82
QRS_{end}	3380	99.91	−3.41	13.13	99.91	0.63	11.79
T_{on}	1112	98.32	4.76	38.52	97.96	−11.96	39.33
T_{peak}	3253	98.61	−2.43	19.08	98.70	1.41	21.82
T_{end}	3253	98.61	1.38	22.58	98.70	−4.36	36.86

Table 4.1.: Performance comparison between this work (WT) and the work based on LPD [31].

4.3. Study database of the AKh Linz

Figure 4.3 and Figure 4.4 show the expert labels and the algorithm labels for every characteristic point. Additionally the distribution of the expert labels is estimated and visualized via a box-blot. Results for all other beats are shown in Appendix A.1.

We can make the following observations:

- Figure 4.3 (a) - Beat$_3$:
  The algorithm detects most characteristic points with sufficient precision when compared with the expert labels. The peak of the S wave is not labeled by the algorithm, since this wave is too small to be detected by the algorithm and consequently is assumed not to be present.
- Figure 4.3 (b) - Beat$_5$:
  This beat represents an ST elevation. Due to the fact that the Q wave is very small, the algorithm does not identify its peak. We also observe a higher discrepancy for the onset of the T wave. All other observations are similar to the case described above.
- Figure 4.3 (c) - Beat$_6$:
  The expert labels for T$_{peak}$ and T$_{end}$ can be divided into two groups (inverted T wave and biphasic T wave). Due to this the scattering of the expert labels is quite broad. The algorithm detected a biphasic T wave and therefore 2 peaks are labeled. However the option of setting two T peaks was not provided for the experts.
- Figure 4.3 (d) - Beat$_{11}$:
  This beat shows high discrepancies between the expert labes for the P wave and the onset of the QRS complex. As mentioned in Section 3.4.3, these characteristic points are excluded from the subsequent evaluation of the algorithm. However all other distributions show acceptable scattering of the expert labels and hence are considered for evaluation.
- Figure 4.4 (a) - Beat$_{16}$:
  In this case we do have an interesting QRS morphology. According to the majority of the expert labels, this should be an rS complex (compare to Figure 3.18 (f)). This type of QRS complex is also correctly identified and labeled by the algorithm.
- Figure 4.4 (b) - Beat$_{18}$:
  This beat illustrates the algorithm's ability to recognize unusual long and deep S waves.
- Figure 4.4 (c) and (d) - Beat$_{21}$ and Beat$_{25}$:
  These cases show two more interesting and difficult morphologies the algorithm is able to deal with.
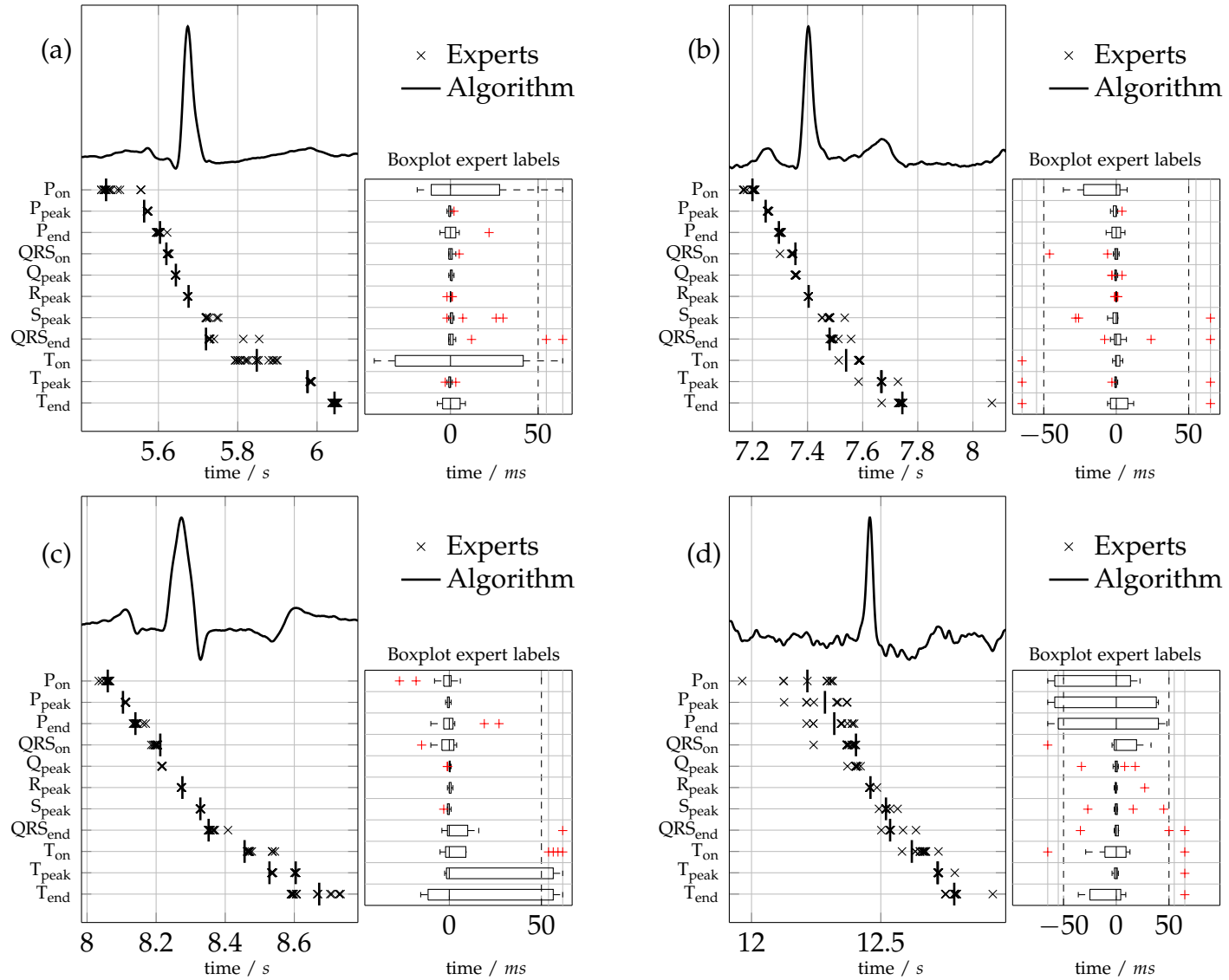
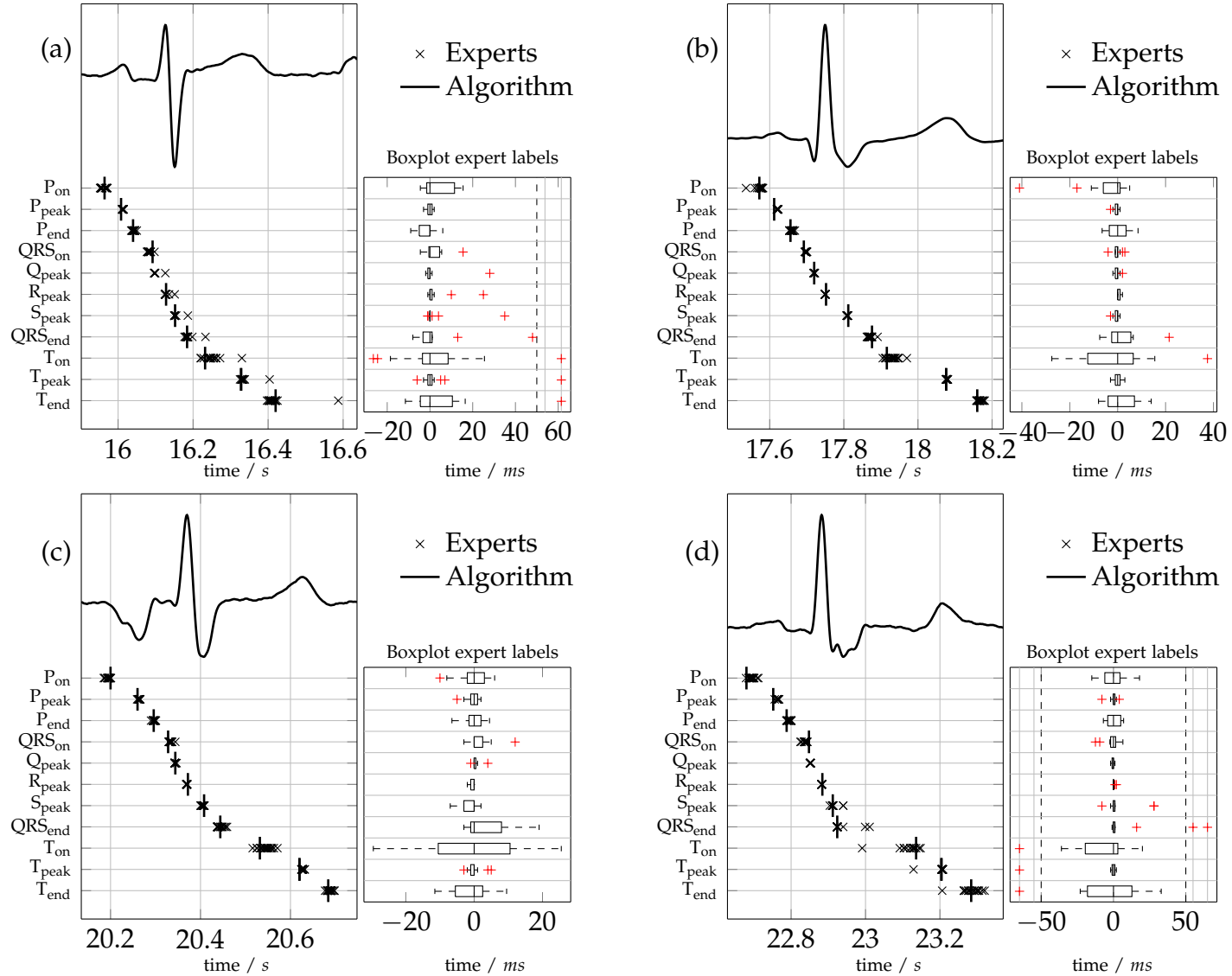Figure 4.3.: Expert and algorithm labels for beat (a) 3, (b) 5, (c) 6 and (d) 11.

Figure 4.4.: Expert and algorithm labels for beat (a) 16, (b) 18, (c) 21 and (d) 25.

In a next step the deviations of the algorithm labels from the median of the expert markers were calculated for every beat and characteristic point (Appendix Table A.1). These results are summarized and visualized via a box-plot for every ECG characteristic point in Figure 4.5.

- P_{on}: The onset of the P wave is detected with sufficient precision. The whiskers are within $-10\,ms$ and $14\,ms$, while two differences are a little higher ($18\,ms$ - $Beat_2$, $22\,ms$ - $Beat_8$). However these values are still tolerable for P_{on}.
- P_{peak}: For the peak of the P wave the algorithm tends to label the P peak a bit earlier than the experts. The whiskers ($-1\,ms$ and $13\,ms$) are narrow enough. The high outlier ($-34.5\,ms$) belongs to $Beat_{10}$, which shows a broad scattering of the expert labels as well. Due to this, the high discrepancy is acceptable. The other one is due to its small value $-6.5\,ms$ - $Beat_{13}$ still satisfactory.
- P_{end}: This characteristic point does not show any outlier with whiskers between $-7\,ms$ and $13\,ms$ leading to a satisfying result.
- QRS_{on}: The same is true for the onset of the QRS complex with whiskers between $-11\,ms$ and $7\,ms$.
- Q_{peak}: As expected the whiskers are very narrow for the peak of the Q wave ($-2\,ms, 2\,ms$). This has two reasons. First, a smaller set of beats (18) was considered since the Q wave was not always present (or not considered to be present by the algorithm). Second, in case that the Q wave is present, the peak usually is unambiguous.
- R_{peak}: The R peak shows very narrow whiskers as well ($-4\,ms, 0\,ms$).
- S_{peak}: The peak of the S wave illustrates very similar results like the Q and the R peak (whiskers $-2\,ms, 2\,ms$). However there are two outliers, which show the same characteristic. For beat $Beat_{12}$ and $Beat_{26}$ the first rising edge after the falling edge of the R wave is too small for the algorithm to be considered as S wave. Due to this, the algorithm sets the S_{peak} a bit later than the majority of the experts did. However it should be mentioned that little differences of the expert's opinion are noticeable for this characteristic point and beat as well.
- QRS_{end}: The end of the QRS complex shows whiskers between $-13\,ms$ and $17\,ms$. Additionally two outliers are observable, whereas the one belonging to $Beat_{26}$ was already described for S_{peak}. For the second one ($Beat_7$) the algorithm does not detect an S wave at all and sets

the end of the QRS complex to the end of the R wave. Due to this we observe this high discrepancy.

- T_{on}: For the onset of the T wave a very broad scattering is observable (whiskers $-48.5\,ms, 49.5\,ms$). However, for this characteristic point the expert labels in general show wide scattering as well.
- T_{peak}: In contrast to T_{on}, this characteristic point shows very narrow whiskers ($1\,ms, 10\,ms$).
- T_{end}: The scattering for this point is a bit wider (whiskers $-22.5\,ms, 20\,ms$) but still tolerable. However there are three obvious outliers. Two of them ($Beat_6$, $Beat_7$) are due to the fact, that the algorithm detected a biphasic T wave for these two cases. Consequently the end of this wave shows a high discrepancy, since the majority of the experts defined the wave to be inverted. Concerning the positive outlier, belonging to $Beat_{12}$, it should be mentioned that the scattering of the expert labels was high as well for this characteristic point.
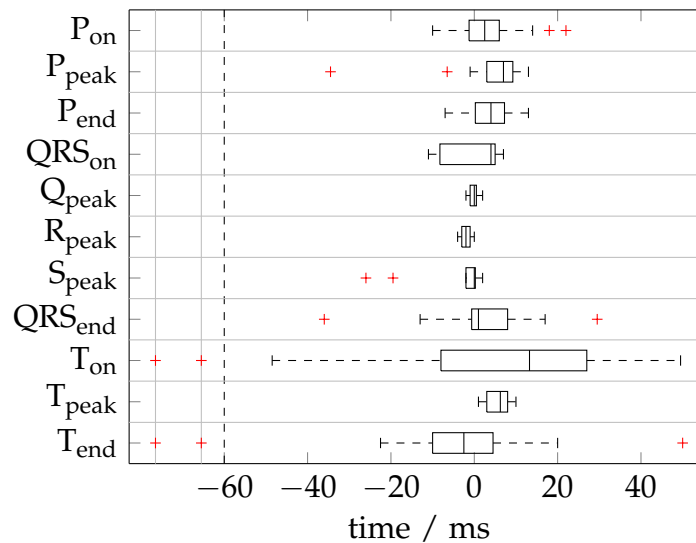

Figure 4.5.: Difference between median of expert labels and the algorithm label. Points lying outside the interval $[-60\,ms, 60\,ms]$ are compressed.

5. Discussion and Conclusion

5.1. ECG Analysis Based on the WT in General

In the following the literature introduced in Section 3.1 is briefly discussed with regard to potential fields of application and scientific issues for the AKh Linz GmbH.

Automated ECG Beat Classification:
Automated ECG Beat Classification based on the DWT or variations of the DWT (SDWT, ...) has shown promising results for detecting and identifying normal as well as pathological heart beats. As explained in Section 3.1.2, the identification of irregularly shaped beats within several hours of ECG recordings is inevitable for cardiac disease detection, e.g. cardiac arrhythmia, at medical departments like the operative intensive care unit. Additionally, neurologists at the AKh Linz GmbH are working on the evaluation of the autonomic nervous system based on heart rate variability analysis, which is a completely different field of application for ECG analysis, however, using the same raw signal. For this particular case, contractions of the heart which are not triggered by the sinoatrial node, are considered to be artifacts[1] (for more details see [47]). Manual elimination of these artifacts is very time consuming, especially for long-term ECG. Hence, a system for the automatic detection and/or elimination of distinct beat morphologies or undesired heart beats would lead to a significant improvement of the whole analysis in different medical subject areas. In contrast to the literature introduced

---

[1] For the assessment of the autonomous nervous system only the impact of the sinoatrial node is of relevance. Heartbeats like supraventricular extrasystoles derive from an irregular action-potential in the atria instead from the sinoatrial node. Thus they are not dedicated to the autonomous regulatory system and must be excluded from analysis.

in Section 3.1.2, other potential and probably more intuitive features than wavelet coefficients, such as the ECG characteristic points extracted within this work, should be considered for the automated classification of heart beats as well. If it is possible to reliably distinguish between artifacts and normal heart beats only using ECG characteristic points, an evaluation system should not become unnecessarily complex by adding non-transparent features such as DWT coefficients.

Highlighting Minor Transient Changes in a Patient's ECG:

As introduced in Section 3.1.3, the WT or more generally TFA can be used to detect transient oscillations of low amplitude, which are superimposed by high signal deflections in the ECG (e.g. VLP occurring after the QRS complex). This extracted information can be used as an additional predictor in order to increase discriminatory power for open medical issues.

A big issue for these considerations is the way the ECG is pre-processed. In many cases the ECG is automatically band-pass filtered by ECG monitors. Hence, it is possible that the information we are actually interested in, is already canceled by the ECG monitor. Due to this, for future studies at the AKh Linz GmbH, two ECGs will be acquired and analyzed in parallel. Additionally to the ECG sampled at $f_s = 240\,\mathrm{Hz}$, which is usually obtained for all patients at the operative intensive care unit of the AKh Linz GmbH, a long term ECG sampled at $f_s = 1000\,\mathrm{Hz}$ will be acquired as well. The latter one is, in contrast to the 240 Hz ECG, recorded as raw ECG, i.e., without performing any pre-processing. This allows a TFA for frequencies up to maximal 500 Hz.

Concluding this section, there of course exist other methods for illustrating the development of the signal spectrum over time than the WT. However, the WT is one of the most popular among these time frequency distributions (TFD) for analyzing physiological signals like the ECG. The most common reasons for using the WT are its suitability to analyze non-stationary signals and that signal-activities at different time-scales can be resolved simultaneously. The STFT, in contrast, implicitly selects a time-scale by defining a specific window length. The ECG is composed of P wave, QRS complex and T wave, all having slightly different typical duration and consequently slightly different time scales. The RR interval, usually in the range of one second, is located on another time scale. Assuming that higher frequent

oscillations of short duration are present as well, we add another time scale to our considerations. For slow varying signals, like the heart rate ($\frac{60}{RR}$), the exact value of the heart rate (frequency) is more important than the precise time when the heart rate changes. In contrast, concerning our higher frequent oscillations, we are more interested in the time instant when the oscillation occurs (e.g. after QRS) than in the exact frequency of the oscillation. These changes of the TFD over more scales might therefore provide important diagnostic information. For this scenario the WT should be highly suitable and probably outperforms techniques like the STFT. [16]

5.2. ECG Beat Segmentation

In Section 3.4.1 and Section 4.1 we illustrated a possible application scenario for the segmentation algorithm. The algorithm was evaluated on noisy synthetic data, however the characteristics of the noise and the ECG did not change over time. Although the algorithm is able to deal with different morphologies, noise and artifacts, the ECG and the noise should not change their characteristics too significantly over time in order to allow a meaningful analysis of the relative changes. For the case that we want to compare the ECG before and after a specific event, like a medical treatment or induction, it is possible that one of the ECG sequences (before or after the event) is superimposed by serious noise, e.g., caused by muscle shivering. One then has to make sure that detected changes in the ECG are not due to the noise, but due to changes of the ECG itself.

The algorithm's ability to detect relative changes was shown using data generated via the GECG^{2}O while the segmentation capability was tested successfully on a large set of real patient data (QTDB). However, because the algorithm has not been tested on real patient ECG data containing different pathophysiologies, the algorithm might behave not optimally for a scenario shown in Figure 5.1. For the second beat in Figure 5.1 the segmentation algorithm detects the wrong end of the T wave, since the U wave is not as dominant as it is for the other beats. This result would have a significant negative influence in case that we want to track relative changes of the QT interval. Considering the second beat separately, the detected T_{end} seems to be plausible. However, if we include the other beats to our considerations,

we notice that this must be the wrong T_{end}. As a result, in a future version the segmentation algorithm could use information of previous beats in order to select the correct MM in a more intelligent way and consequently the correct ECG characteristic points.
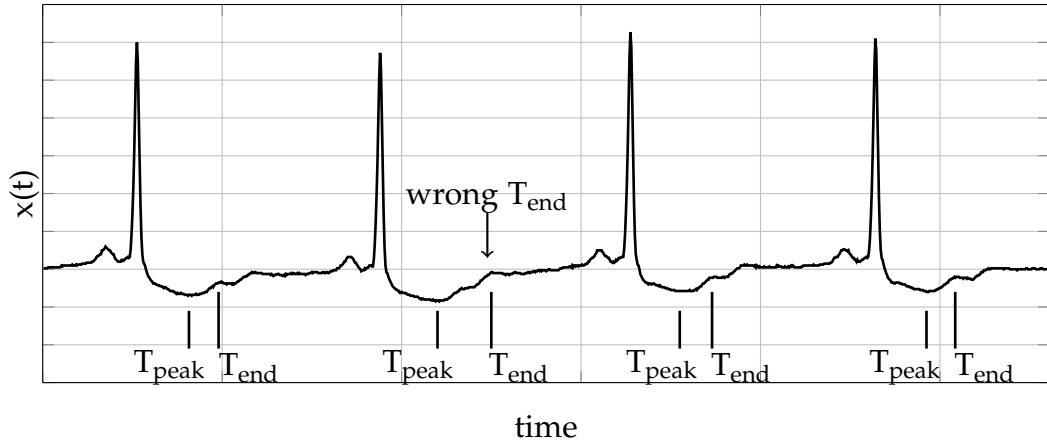
Figure 5.1.: Imperfect behavior of the segmentation algorithm for detecting the end of the T wave.

Concerning the results of the study database (Section 4.3) we can draw the following conclusion:

For most of the cases, the segmentation algorithm's deviation from the median of the expert markers is satisfactory small. However, there are some exceptions for which the algorithm significantly differs from the majority of the expert labels. The onset of the T wave, e.g., differs strongly from the median of the experts (Figure 4.5). For this characteristic point a high deviation between algorithm and expert labels is also observable for the evaluation on the QTDB database (Table 4.1). Hence, the determination of T_{on} cannot be done reliably. Figure 4.3 (a) shows one of the reasons for this. The T wave rises only very slow, making the determination of the onset very difficult in this case. This is also confirmed by the expert labels, which show a very broad scattering.

Due to the fact that the algorithm strongly relies on thresholds, the author believes that the results in general can be improved significantly by allowing individual thresholds for different morphologies or patients. Although this

requires interaction with an expert, we believe that this is of great advantage for cases like untypically small or large waves.

5.3. Conclusion and Outlook

This thesis is seen as a foundation for future research in the fields of ECG signal analysis, especially for detecting minimal changes within a patient's ECG. The brief description of the WT and what it can be used for, should help future project members to get started. Furthermore, a first version of a framework for ECG data analysis has been developed. This framework mainly consists of the GECG^{2}O, which is seen as a tool for evaluation and verification of potential ECG analysis methods, and an ECG beat segmentation algorithm in order to allow the detection of relative changes of ECG characteristic points. These tools are of great value for scientific issues regarding ECG analysis and for the consecutive development of future diagnostic medical devices in form of analysis routines.
Building on this work the following research topics or work packages are identified:

Extending the GECG^{2}O:
The GECG^{2}O should be extended by providing a library of artificial and real ECG beats in order to introduce variable morphologies. These beats will be available as initial beats, which then can be adjusted and parameterized as it is possible for the synthetic ECG beat used in the current version. As a first step the set of 26 real patient ECG beats, selected and labeled by experts within this work, will be provided.
Another extension could be to combine the segmentation algorithm and the GECG^{2}O. This allows to import real patient data, automatically detect single beats and determine their characteristic points as well as the subsequent free adjustment and parametrization of the single beats.
Additionally to the possibilities to encode information given in the current version of the generator, in a future release it should be possible to add meaningful transient events to the ECG beat, e.g. VLPs. One scenario is to start with real patient ECG data, add (simulated) VLPs on purpose and

5. Discussion and Conclusion

consequently evaluate different ECG analysis methods with respect to their suitability to extract this specific information, which was hidden in the ECG time course before. In order to evaluate a method's robustness against noise and artifacts, muscle shivering, power-line interference or motion artifacts can be added to the ECG before analyzing it.

Detecting minimal changes of the ECG before and after volume loading:

Considering medical inductions like operative blood transfusion it is of great relevance whether there are minimal differences in the ECG before and after volume loading. Obvious changes of the ECG usually are not observed for this case. However, there is evidence to detect minimal alternations of the ECG before and after this event [24]. For that reason we define the following steps:

- Recording of the ECG for patients[2] before and after volume loading.
- Trying to find intra-patient patterns for changes of the ECG characteristic points (PR, QT interval, ST level) or other intuitive measurements (e.g. changes of the signal energy per beat). For that reason we plan to distinguish between two "classes", namely `before the event` and `after the event`. Depending on whether the classes can be separated linearly or not, pattern recognition shall be carried out using simpler methods, e.g., linear discriminant analysis, or more sophisticated ones such as NN.
- In case that the discriminatory power of the features described above is not satisfactory, we additionally could include features extracted from time-frequency distributions, such as the WT.
- Following, investigations whether the detected intra-patient patterns can be generalized to inter-patient patterns should be carried out.

Provided that the approach explained above leads to scientifically valuable results, other open medical issues could be analyzed with the same strategy.

---

[2]In the course of the project "Herzfrequenzvariabilität und EKG Morphologie bei Intensivpatienten."

Appendix

Appendix A.

ECG Segmentation Algorithm

A.1. Study Database of the AKh Linz GmbH - Additional Results

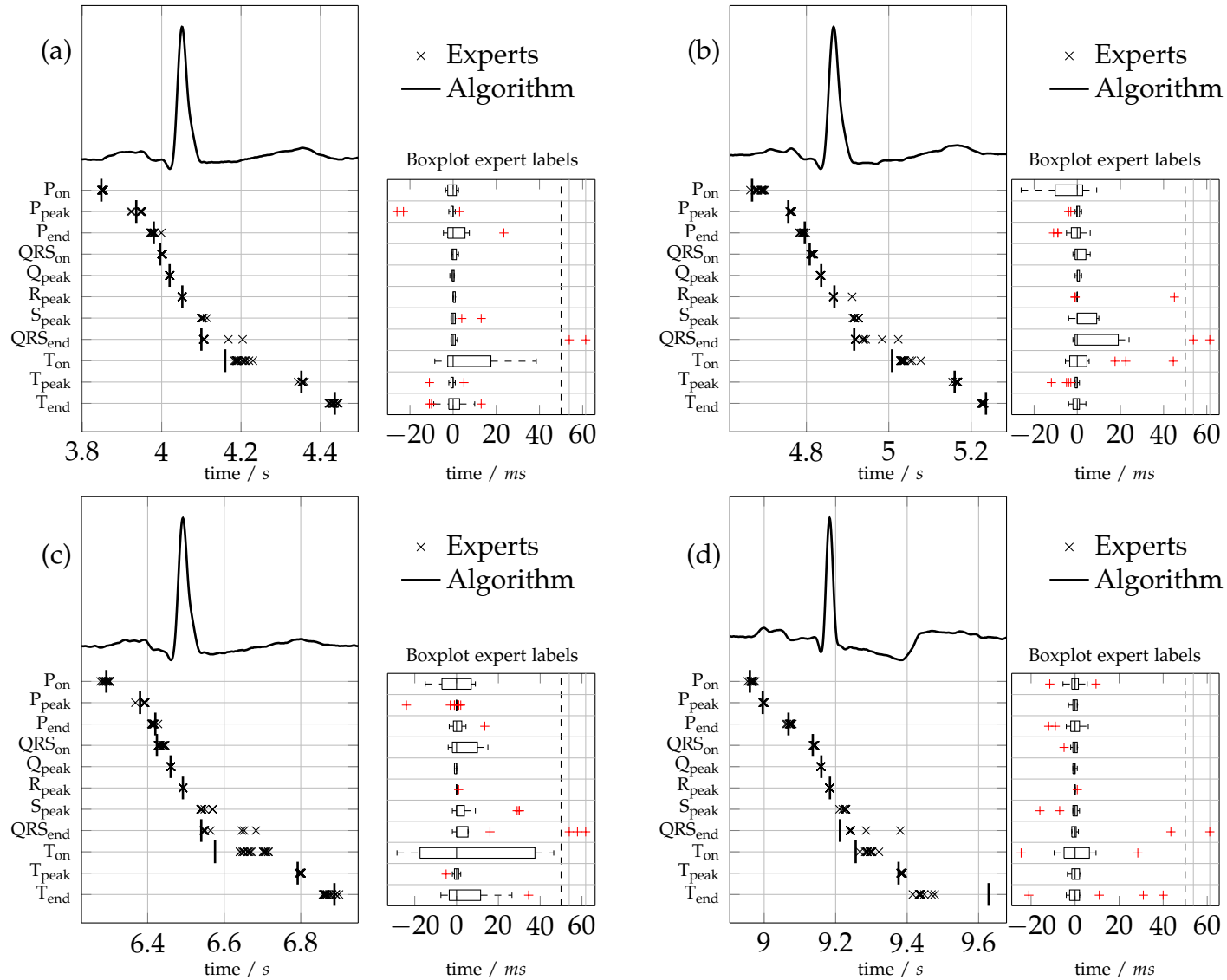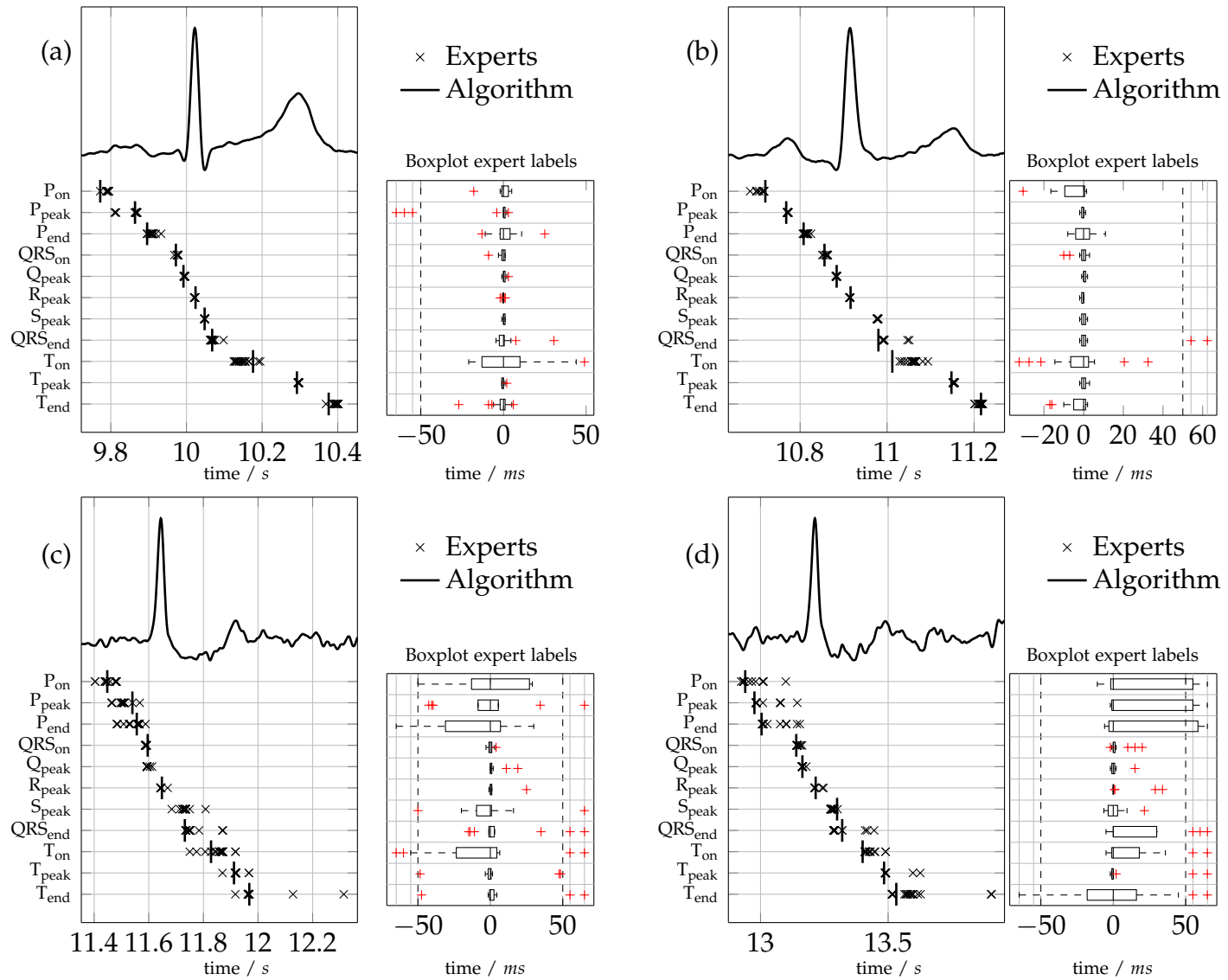Figure A.1.: Expert and algorithm labels for beat (a) 1, (b) 2, (c) 4 and (d) 7.

Figure A.2.: Expert and algorithm labels for beat (a) 8, (b) 9, (c) 10 and (d) 12.
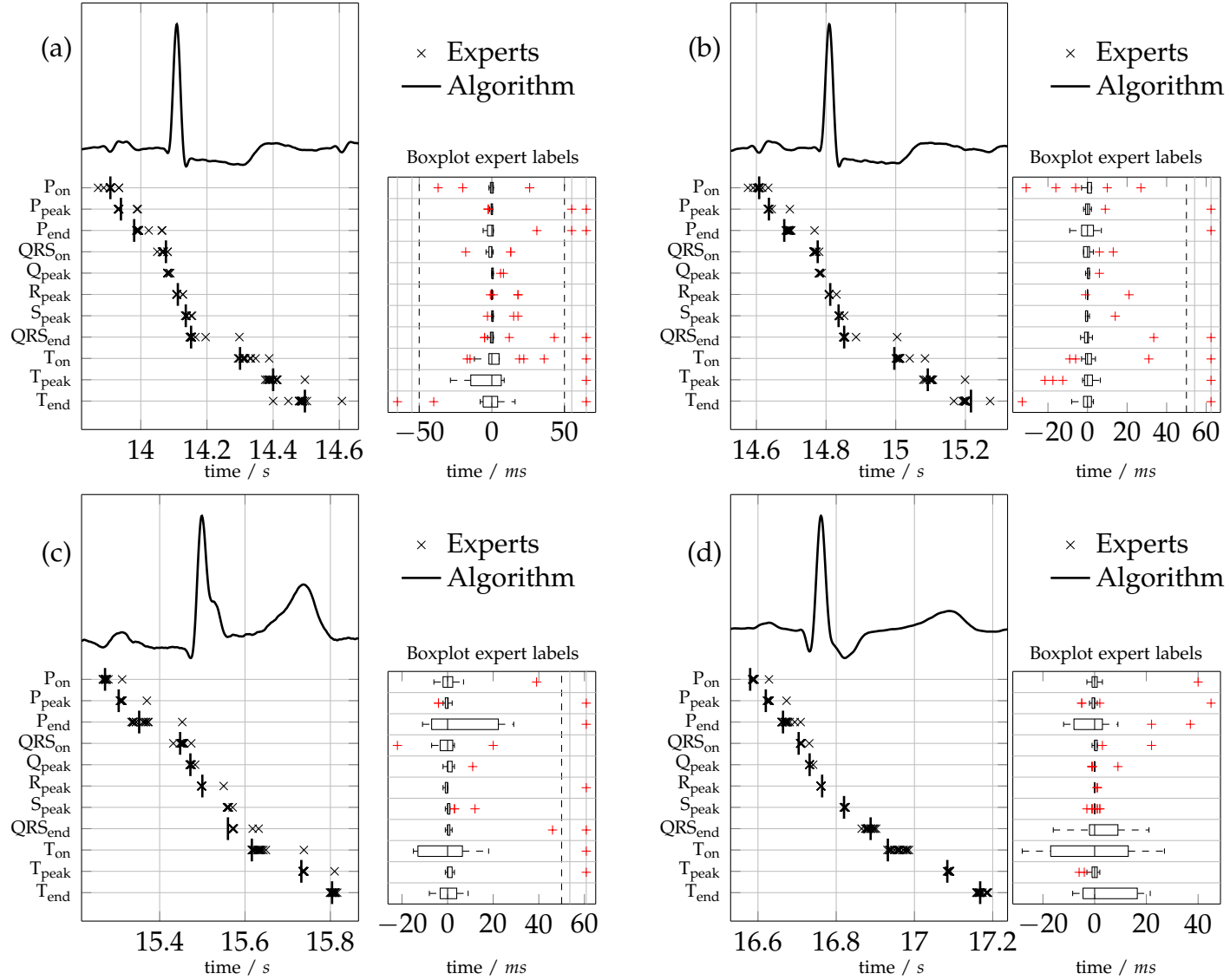
Figure A.3.: Expert and algorithm labels for beat (a) 13, (b) 14, (c) 15 and (d) 17.
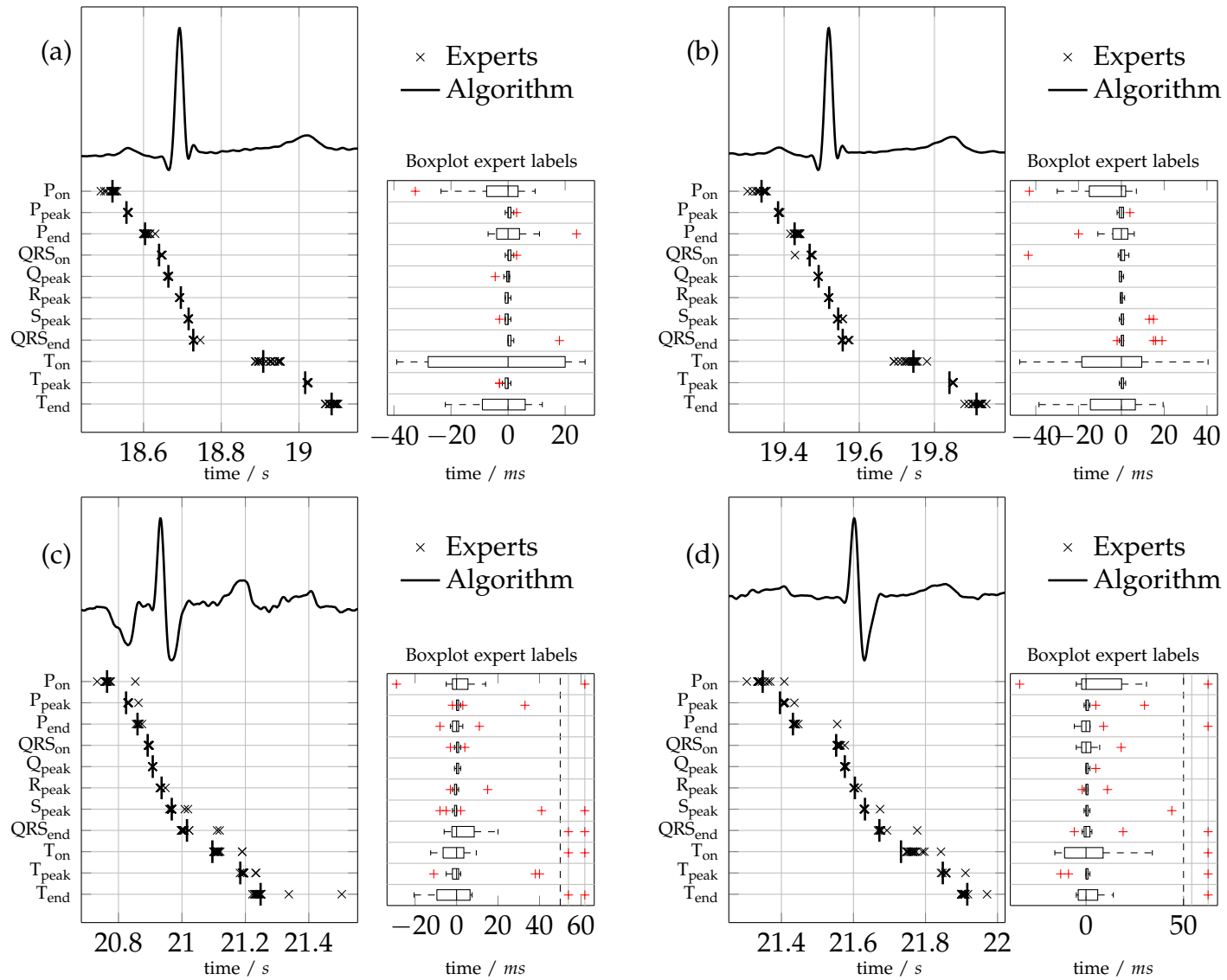
Figure A.4.: Expert and algorithm labels for beat (a) 19, (b) 20, (c) 22 and (d) 23.
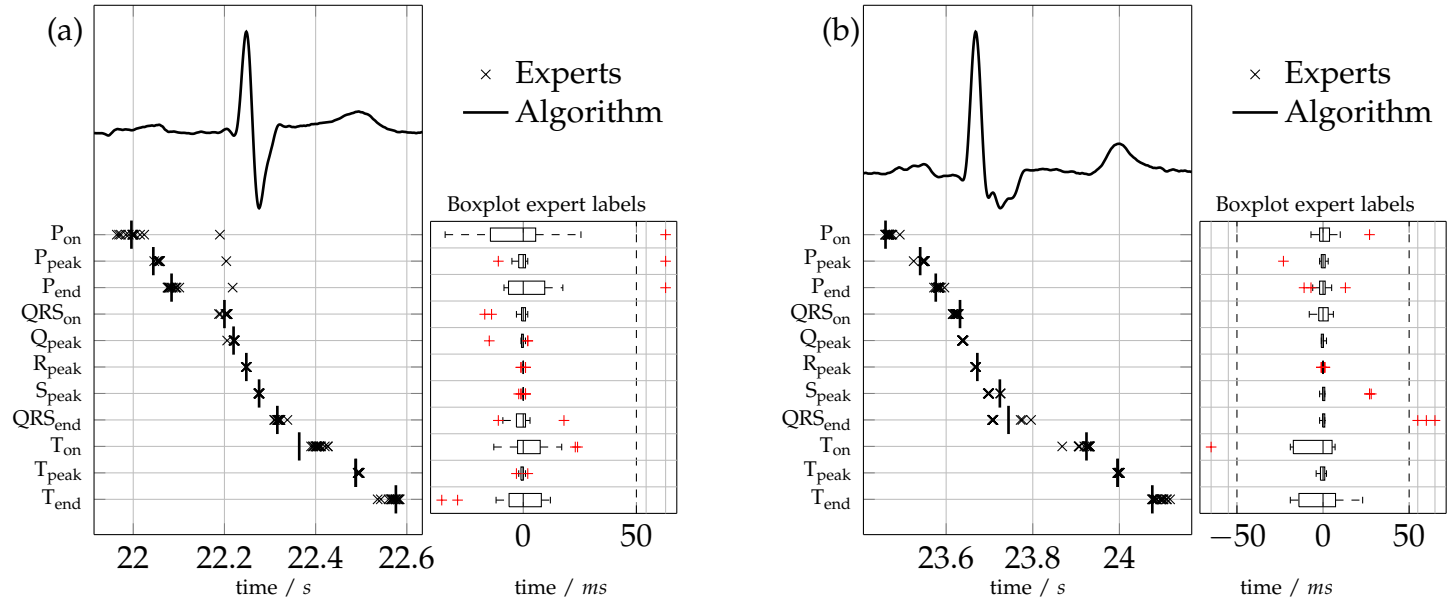
Figure A.5.: Expert and algorithm labels for beat (a) 24, (b) 26.

	P_{on}		P_{peak}		P_{end}		QRS_{on}		Q_{peak}		R_{peak}		S_{peak}		QRS_{end}		T_{on}		T_{peak}		T_{end}	
	N	E-A	N	E-A	N	E-A	N	E-A	N	E-A	N	E-A	N	E-A	N	E-A	N	E-A	N	E-A	N	E-A
B_1	18	3.5	18	12.0	18	-4.5	18	4.5	18	0.5	18	-1.0	18	-	15	6.0	18	-48.5	18	3.0	18	-4.0
B_2	17	22.0	17	7.0	17	-3.0	18	4.0	18	-2.0	18	-2.0	18	-	15	4.0	18	-62.5	18	7.0	18	-8.0
B_3	18	7.0	18	9.0	18	-4.0	18	3.0	18	-1.0	18	-2.0	18	-	17	8.0	18	-11.5	18	8.0	18	0.5
B_4	18	0.0	18	12.0	18	-6.5	18	7.0	18	1.0	18	0.0	18	-	17	8.0	18	-74.5	18	8.0	18	-22.5
B_5	18	2.5	18	9.0	18	4.0	18	-10.0	18	-	18	-1.0	18	-	17	8.0	18	46.5	18	1.0	18	-9.0
B_6	18	1.0	18	8.0	18	3.0	16	-11.0	16	-	18	-3.0	18	1.0	18	2.0	18	12.0	18	8.5	18	-66.5
B_7	18	5.5	18	3.0	18	5.0	18	5.0	18	-1.0	18	-1.0	18	-	18	29.5	16	-35.5	16	8.5	16	-191.0
B_8	18	18.0	18	3.0	18	12.0	18	5.0	18	2.0	18	-2.0	18	0.0	18	-0.5	18	-30.0	18	4.0	18	20.0
B_9	18	-4.5	18	4.0	18	6.0	18	5.0	18	-1.0	18	-1.0	18	-	17	12.0	18	49.5	18	5.0	18	2.0
B_{10}	14	5.0	14	-34.5	14	2.0	15	-7.0	15	-	18	-4.0	18	-	15	17.0	18	37.5	18	6.5	18	-3.5
B_{11}	10	-	10	-	10	-	17	-	17	-	18	-2.0	16	-0.0	16	-0.0	15	42.0	15	3.0	15	1.0
B_{12}	15	-5.0	15	7.0	15	8.0	17	3.0	17	-0.0	18	-3.0	16	-19.5	16	-	18	13.0	18	6.0	18	50.0
B_{13}	18	-0.0	18	-6.5	18	13.0	18	-8.0	18	-	18	-3.0	18	1.0	18	1.0	18	11.0	18	4.5	18	-10.0
B_{14}	18	-1.0	18	-1.0	18	-1.0	18	-9.0	18	-	18	-3.0	18	2.0	18	0.5	18	13.0	18	8.5	18	-16.0
B_{15}	17	1.0	17	7.0	17	-7.0	17	6.0	17	-0.0	17	-1.0	17	-	14	12.0	17	15.0	17	4.0	17	3.0
B_{16}	18	-7.5	18	5.0	18	4.0	14	-10.5	14	-	18	-2.0	17	-1.0	17	1.0	18	14.5	18	3.0	18	-11.5
B_{17}	18	8.0	18	8.0	18	8.0	18	5.0	18	0.0	18	-3.0	18	2.0	18	-7.0	18	27.0	18	5.0	18	-1.5
B_{18}	18	5.0	18	10.0	18	3.5	18	6.0	18	0.0	18	-3.0	18	-2.0	18	-6.5	18	16.5	18	2.0	18	6.0
B_{19}	18	2.5	18	3.0	18	2.0	18	6.0	18	0.5	18	-3.0	17	-0.0	17	-0.0	18	18.0	18	7.0	18	5.0
B_{20}	18	6.0	18	2.0	18	9.0	18	4.5	18	-1.0	18	-1.5	17	-2.0	17	-1.0	18	-4.5	18	9.0	18	6.5
B_{21}	16	-5.0	16	4.0	16	0.5	16	4.0	16	-1.0	17	-2.0	18	-1.0	18	-4.0	18	13.5	18	7.0	18	4.5
B_{22}	17	-2.0	17	6.0	17	3.0	16	3.0	16	-1.0	17	-3.0	17	-0.0	17	-13.0	18	15.5	18	10.0	18	-5.5
B_{23}	13	-10.0	13	10.0	13	6.0	17	6.0	17	-1.0	17	-2.0	17	-2.0	17	2.0	17	31.0	17	8.0	17	-12.0
B_{24}	14	2.5	14	13.0	14	-0.5	15	5.0	15	1.0	17	-0.0	17	-0.0	17	4.0	17	39.0	17	7.0	17	-4.0
B_{25}	17	14.0	17	12.0	17	6.0	16	-10.5	16	-	17	-2.0	17	0.0	17	-0.0	17	-8.0	17	2.0	17	3.0
B_{26}	17	6.0	17	8.0	17	7.0	17	-9.0	17	-	17	-4.0	17	-26.0	17	-36.0	17	1.0	17	3.0	17	18.0

Table A.1.: Deviations of the algorithm labels from the median of the expert markers for every beat and characteristic point. N: number of experts, who labeled this beat. E-A: Label of the algorithm subtracted from the median of the expert labels. The cells including a dash are either characteristic points which were excluded for this evaluation or it was not possible to calculate the difference because the segmentation algorithm did not detect this characteristic point (only relevant for Q_{peak} and S_{peak}).

Bibliography

[1] Statistik Austria, "Demographische Prognosen," http://www.statistik.at/web_de/statistiken/bevoelkerung/demographische_prognosen/index.html, 2013.

[2] G. D. Clifford, F. Azuaje, and P. McSharry, *Advanced Methods And Tools for ECG Data Analysis*. Norwood, MA, USA: Artech House, Inc., 2006.

[3] C. Li, C. Zheng, and C. Tai, "Detection of ECG characteristic points using wavelet transforms," In *IEEE Transactions on Biomedical Engineering*, Vol. 42, No. 1, pp. 21–28, January 1995.

[4] J. Martinez, R. Almeida, S. Olmos, A. Rocha, and P. Laguna, "A wavelet-based ECG delineator: evaluation on standard databases," In *IEEE Transactions on Biomedical Engineering*, Vol. 51, No. 4, pp. 570–581, April 2004.

[5] P. Laguna, R. G. Mark, A. Goldberg, and G. B. Moody, "A database for evaluation of algorithms for measurement of QT and other waveform intervals in the ECG," In Proceedings of the *Computers in Cardiology (CinC 1997)*. IEEE, 1997, pp. 673–676.

[6] A. L. Goldberger, L. A. Amaral, L. Glass, J. M. Hausdorff, P. C. Ivanov, R. G. Mark, J. E. Mietus, G. B. Moody, C.-K. Peng, and H. E. Stanley, "Physiobank, physiotoolkit, and physionet components of a new research resource for complex physiologic signals," In *Circulation*, Vol. 101, No. 23, pp. e215–e220, 2000.

[7] E. A. Ashley and J. Niebauer, *Cardiology explained*. Remedica, 2004.

[8] F. Freytag, *EKG im Rettungs-und Notdienst*. Schattauer Verlag, 2010.

[9] M. S. Thaler, *The only EKG book you'll ever need*. Lippincott Williams & Wilkins, 2015.

[10] J. Wasilewski and L. Poloński, "An Introduction to ECG Interpretation," In *ECG Signal Processing, Classification and Interpretation*, A. Gacek and W. Pedrycz, Eds.   Springer London, 2012, pp. 1–20.

[11] H.-P. Schuster and H.-J. Trappe, *EKG-Kurs für Isabel*.   Georg Thieme Verlag, 2005.

[12] M. Huemer, "Anwendung von Wavelets in der Automatisierungstechnik," Master's thesis, Johannes Kepler Universität, Austria, 1995.

[13] A. Mertins, *Signaltheorie: Grundlagen der Signalbeschreibung, Filterbänke, Wavelets, Zeit-Frequenz-Analyse, Parameter-und Signalschätzung*.   Wiesbaden: Springer Vieweg, 2013.

[14] D. L. Fugal, *Conceptual wavelets in digital signal processing: an in-depth, practical approach for the non-mathematician*.   Space & Signals Technical Pub., 2009.

[15] A. Teolis, *Computational signal processing with wavelets*.   Springer Science & Business Media, 2012.

[16] P. S. Addison, "Wavelet transforms and the ECG: a review," In *Physiological Measurement*, Vol. 26, No. 5, p. R155, 2005.

[17] S. G. Mallat, "Multiresolution approximations and wavelet orthonormal bases of $L_2(\mathbb{R})$," In *Transactions of the American Mathematical Society*, Vol. 315, No. 1, pp. 69–87, 1989.

[18] ——, "A theory for multiresolution signal decomposition: the wavelet representation," In *Pattern Analysis and Machine Intelligence, IEEE Transactions on*, Vol. 11, No. 7, pp. 674–693, July 1989.

[19] ——, *A wavelet tour of signal processing: the sparse way*.   Academic press, 2008.

[20] G. Strang and T. Nguyen, *Wavelets and filter banks*.   SIAM, 1996.

[21] W. Sweldens and R. Piessens, "Wavelet sampling techniques," In Proceedings of the *Statistical Computing Section*, 1993, pp. 20–29.

[22] S. G. Mallat, "Multifrequency channel decompositions of images and wavelet models," In *IEEE Transactions on Acoustics, Speech and Signal Processing*, Vol. 37, No. 12, pp. 2091–2110, December 1989.

[23] W. Bäni, *Wavelets: eine Einführung für Ingenieure*. Oldenbourg Verlag, 2005.

[24] B. Scheller, G. Pipa, H. Kertscho, P. Lauscher, J. Ehrlich, O. Habler, K. Zacharowski, and J. Meier, "Low hemoglobin levels during normovolemia are associated with electrocardiographic changes in pigs," In *Shock*, Vol. 35, No. 4, pp. 375–381, 2011.

[25] B. Gramatikov, J. Brinker, S. Yi-Chun, and N. V. Thakor, "Wavelet analysis and time-frequency distributions of the body surface ECG before and after angioplasty," In *Computer Methods and Programs in Biomedicine*, Vol. 62, pp. 87–98, 2000.

[26] A. Koeleman, H. Ros, and T. Van den Akker, "Beat-to-beat interval measurement in the electrocardiogram," In *Medical and Biological Engineering and Computing*, Vol. 23, No. 3, pp. 213–219, 1985.

[27] E. Mazomenos, T. Chen, A. Acharyya, A. Bhattacharya, J. Rosengarten, and K. Maharatna, "A Time-Domain Morphology and Gradient based algorithm for ECG feature extraction," In Proceedings of the *IEEE International Conference on Industrial Technology (ICIT'2012)*, March 2012, pp. 117–122.

[28] R. Andreao, B. Dorizzi, and J. Boudy, "ECG signal analysis through hidden Markov models," In *IEEE Transactions on Biomedical Engineering*, Vol. 53, No. 8, pp. 1541–1549, August 2006.

[29] Z. Dokur, T. Ölmez, E. Yazgan, and O. K. Ersoy, "Detection of ECG waveforms by neural networks," In *Medical engineering & physics*, Vol. 19, No. 8, pp. 738–741, 1997.

[30] V. Afonso, W. J. Tompkins, T. Nguyen, and S. Luo, "ECG beat detection using filter banks," In *IEEE Transactions on Biomedical Engineering*, Vol. 46, No. 2, pp. 192–202, February 1999.

[31] P. Laguna, R. Jané, and P. Caminal, "Automatic detection of wave boundaries in multilead ECG signals: validation with the CSE database," In *Computers and biomedical research*, Vol. 27, No. 1, pp. 45–60, 1994.

[32] T. Ince, S. Kiranyaz, and M. Gabbouj, "A Generic and Robust System for Automated Patient-Specific Classification of ECG Signals," In *IEEE Transactions on Biomedical Engineering*, Vol. 56, No. 5, pp. 1415–1426, May 2009.

[33] Y. Kutlu and D. Kuntalp, "Feature extraction for ECG heartbeats using higher order statistics of WPD coefficients," In *Computer methods and programs in biomedicine*, Vol. 105, No. 3, pp. 257–267, 2012.

[34] O. Inan, L. Giovangrandi, and G. Kovacs, "Robust Neural-Network-Based Classification of Premature Ventricular Contractions Using Wavelet Transform and Timing Interval Features," In *IEEE Transactions on Biomedical Engineering*, Vol. 53, No. 12, pp. 2507–2515, December 2006.

[35] Y.-H. Chen and S.-N. Yu, "Selection of effective features for ECG beat recognition based on nonlinear correlations," In *Artificial intelligence in medicine*, Vol. 54, No. 1, pp. 43–52, 2012.

[36] R. Hoekema, G. J. Uijen, and A. van Oosterom, "Geometrical aspects of the interindividual variability of multilead ECG recordings," In *IEEE Transactions on Biomedical Engineering*, Vol. 48, No. 5, pp. 551–559, May 2001.

[37] X. Jiang, L. Zhang, Q. Zhao, and S. Albayrak, "ECG Arrhythmias Recognition System Based on Independent Component Analysis Feature Extraction," In Proceedings of the *IEEE TENCON 2006*, November 2006, pp. 1–4.

[38] C. Ye, B. Kumar, and M. Coimbra, "Heartbeat Classification Using Morphological and Dynamic Features of ECG Signals," In *IEEE Transactions on Biomedical Engineering*, Vol. 59, No. 10, pp. 2930–2941, October 2012.

[39] A. Daamouche, L. Hamami, N. Alajlan, and F. Melgani, "A wavelet optimization approach for ECG signal classification," In *Biomedical Signal Processing and Control*, Vol. 7, No. 4, pp. 342–349, 2012.

[40] S. Saha and S. Ghorai, "Effect of feature fusion for discrimination of cardiac pathology," In Proceedings of the *IEEE Third International Conference on Computer, Communication, Control and Information Technology (C3IT'2015)*, February 2015, pp. 1–6.

[41] T. Tsutsumi, N. Takano, N. Matsuyama, Y. Higashi, K. Iwasawa, and T. Nakajima, "High-frequency powers hidden within QRS complex as an additional predictor of lethal ventricular arrhythmias to ventricular late potential in post–myocardial infarction patients," In *Heart Rhythm*, Vol. 8, No. 10, pp. 1509–1515, 2011.

[42] A. Diery, D. Rowlands, T. R. Cutmore, and D. James, "Automated ECG diagnostic P-wave analysis using wavelets," In *Computer methods and programs in biomedicine*, Vol. 101, No. 1, pp. 33–43, 2011.

[43] P. McSharry, G. Clifford, L. Tarassenko, and L. Smith, "A dynamical model for generating synthetic electrocardiogram signals," In *IEEE Transactions on Biomedical Engineering*, Vol. 50, No. 3, pp. 289–294, March 2003.

[44] J. Sahambi, S. Tandon, and R. Bhatt, "Wavelet based ST-segment analysis," In *Medical and Biological Engineering and Computing*, Vol. 36, No. 5, pp. 568–572, 1998.

[45] S. Mallat and S. Zhong, "Characterization of signals from multiscale edges," In *IEEE Transactions on Pattern Analysis & Machine Intelligence*, No. 7, pp. 710–732, 1992.

[46] M. G. Bulmer, *Principles of statistics.* Courier Corporation, 2012.

[47] W. Struhal, A. Javor, C. Brunner, T. Benesch, V. Schmidt, M. R. Vosko, and G. Ransmayr, "The phoenix from the ashes: cardiovascular autonomic dysfunction in behavioral variant of frontotemporal dementia." In *Journal of Alzheimer's disease: JAD*, Vol. 42, No. 3, pp. 1041–1046, 2014.